


Cranial and postcranial anatomy of a juvenile baurusuchid (Notosuchia, Crocodylomorpha) and the taxonomical implications of ontogeny

Daniel Martins dos Santos¹  | Joyce Celerino de Carvalho² |
 Carlos Eduardo Maia de Oliveira³ | Marco Brandalise de Andrade⁴ |
 Rodrigo Miloni Santucci²

¹Zoology Graduate Program, Institute of Biological Sciences, University of Brasília, Brasília, Brazil

²University of Brasília, Planaltina Campus (FUP), Brasília, Brazil

³Federal Institute of Education, Science and Technology of São Paulo, Votuporanga Campus (IFSP), Sao Paulo, Brazil

⁴Pontifical Catholic University of Rio Grande do Sul, Porto Alegre, Brazil

Correspondence

Daniel Martins dos Santos, Zoology Graduate Program, Institute of Biological Sciences, University of Brasília, Brasília, Brazil.
 Email: danielmartinsantos@hotmail.com

Abstract

Baurusuchidae comprises a clade of top-tier terrestrial predators and are among the most abundant crocodyliforms found in the Adamantina Formation, Bauru Basin, Brazil (Campanian-Maastrichtian). Here, we provide a detailed description of the cranial and postcranial osteology and myology of the most complete juvenile baurusuchid found to date. Although the preservation of juvenile individuals is somewhat rare, previously reported occurrences of baurusuchid egg clutches, a yearling individual, and larger, but skeletally immature specimens, comprise a unique opportunity to track anatomical changes throughout their ontogenetic series. Its cranial anatomy was resolved with the aid of a three-dimensional model generated by the acquisition of computed tomography data, and its inferred adductor mandibular musculature was compared to that of mature specimens in order to assess possible ontogenetic shifts. A subsequent phylogenetic analysis included the scoring of *Gondwanasuchus scabrosus*, the smallest baurusuchid species known to date, to evaluate its

Abbreviations: 4th dt, fourth hypertrophied dentary tooth; ac, articulation channel; ah, anterior hollow; an, angular; ana, axial neural arch; ang, angular; anp, angular pathology; aoc, articular surface for the occipital condyle; aop, articular surface for odontoid process; ap fs, anterior palpebral frontal suture; ap, ascending process; ar, anterior ridge; art, articular bone; ast, astragalar trochlea; atl, astragalar tarsale ligament pit; ax, axis vertebra; bo, basioccipital; bs, basisphenoid; capic, intercentrum capitular process; cc, cnemial crest; cif, crest for the insertion of M. iliofemoralis; cp, calcaneal peg; cs, choanal septum; cv, cervical vertebrae; d, dentary; dca, distal carina; dh, distal hook of fibula; dia, diapophysis; dmp, depression for insertion of M. pterygoideus; dv, dorsal vertebrae; ect, ectopterygoid; emf, external mandibular fenestra; euf, eustachian foramina; exo, exoccipital; ext, distal extensors; f, frontal; fac, fibular articular facet of the femur; ff, fibular facet; fsc, frontal's saggital crest; fsn1, spinal nerve foramen; fsn2, spinal nerve foramen 2; gst, gastralia; gt, great trochanter; hu, humerus; hy, hypapophysis; ic, intercentrum; icc, intercentrum cotyle; if, foramen incisivum; il, ilium; ior, infraorbital ridge; itf, infraorbital fenestra; itf, infratemporal fenestra; j, jugal; jpr, jugal posterior ramus; jtld, jugal triangular lateral depression; l, lacrimal; lell, external lateral ligament; m, maxilla; maf, mandibular adductor fossa; md, medial depression; mdr, medial distal roller; mr, mandibular ramus; mssl, medial scapulosternal ligament; msy, mandibular symphysis; mx, maxilla; n, nasal naas, articular surface for the neural arches; nc, neural canal; ncs, neurocentral suture; nd, nasal depression; ns, neural spine; nsp, nasal septum; nvf, neurovascular foramen; ofb, olfactory bulb; op, odontoid process; orb, orbit; pa, parapophysis; pap, preacetabular process; pat, proatlas; pc, pneumatic cavity; pchd, parachoanal depression of pterygoid wings; pf, prefrontal; pfp, prefrontal pillars; pl, palatines; pl, pars laterale; plcpalatine medial constriction; pm, pars mediale; pm, premaxillae; pm-mn, premaxillary-maxillary notch; pmx, premaxilla; pmx.t, premaxillary tooth; pns, proatlas neural spine; poz, postzygapophysis; pp pos, posterior palpebral postorbital suture; prep, postacetabular process; prz, prezygapophysis; pt + v, pterygoid and vomer; pt, pterygoids; ptap, pterygoid aponeurosis; pu, pubis; q, quadrate; qj, quadratojugal; qld, quadrate's lateral depression; rp, retroarticular process; sa, surangular; sac, supracetabular crest; sb, scapular buttress; scs, scapulocoracoid suture; sk, sagittal keel; sof, supraorbital fenestra; spl, splenials; sps, spalled surface; sq, squamosals; stf, supratemporal fenestra; syp, symphyseal peg; sys, mandibular symphysis; tal, tibial-astragalar ligament pit; tbf, tibial articular facet; vap, ventral articular process.

Funding information

Coordenação de Aperfeiçoamento de Pessoal de Nível Superior; Conselho Nacional de Desenvolvimento Científico e Tecnológico

phylogenetic relations relative to a known juvenile. We find considerable differences between juveniles and adults concerning skull ornamentation and muscle development, which might indicate ontogenetic niche partitioning, and also anatomical and phylogenetic evidence that *G. scabrosus* corresponds to a young semaphoront lacking mature cranial features.

KEYWORDS

anatomy, Baurusuchidae, myology, Notosuchia, ontogeny

1 | INTRODUCTION

Baurusuchidae Price, 1945 is a group of medium-sized and predatory terrestrial crocodyliforms from Gondwana (Gasparini, 1971). Among other characters, these forms are commonly characterized by the following synapomorphies: (1) oreinirostral skulls with transversely expanded temporal regions (Riff & Kellner, 2011); (2) reduction in the number of teeth (Riff, 2003); (3) ziphodont dentition (Nascimento, 2014); (4) vertically high quadrates (Nascimento & Zaher, 2010; Riff, 2003); (5) medial approximation of the prefrontals (Godoy et al., 2014; Montefeltro et al., 2011); (6) triangular, fan-like depression on the lateral surface of the anterior ramus of the jugal (Riff, 2003). In the past decade, several research efforts were directed toward their osteology, phylogeny, neuroanatomy, and paleoecology, drawing from abundant fossil materials including cranial and postcranial remains, egg clutches and nesting sites, as well as coprolites (Cardia et al., 2018; de Oliveira et al., 2021; Dumont Jr et al., 2020; Montefeltro et al., 2020; Nascimento & Zaher, 2010; Oliveira et al., 2011).

Although most fossil finds are concentrated in the Campanian-Maastrichtian Adamantina Formation of the Bauru Basin, southeastern Brazil, fragmentary baurusuchid remains have also been recovered from both Argentina and Pakistan (Gasparini, 1972; Martinelli & Pais, 2008; Wilson et al., 2001). Currently, there are a total of 10 valid species described from the Bauru Basin alone, that is, *Baurusuchus pachecoi* Price, 1945; *Baurusuchus salgadoensis* Carvalho et al., 2005; *Stratiotosuchus maxhechti* Campos, 2001; *Baurusuchus albertoi* Nascimento & Zaher, 2010; *Pissarrachampsia sera* Montefeltro et al., 2011; *Campinasuchus dinizi* Carvalho et al., 2011; *Gondwanasuchus scabrosus* Marinho et al., 2013; *Aplestosuchus sordidus* Godoy et al., 2014; *Aphaurosuchus escharafacies* Darlim, Carvalho, et al., 2021; Darlim, Montefeltro, & Langer, 2021; and *Aphaurosuchus kaiju* Martins et al., 2023. Curiously, despite its relatively high diversity, the Bauru Basin baurusuchids share a high degree of morphological similarity in cranial and postcranial anatomy and dentition. Species differentiation is based mostly on subtle traits, instead of clear-cut

characteristics. On the other hand, *G. scabrosus* stands alone in displaying clear differences regarding teeth ornamentation, with conspicuous apicobasal sulci.

Despite recent descriptions of postcranial materials (Cotts et al., 2017; Godoy et al., 2016; Nascimento & Zaher, 2010), some well-known semi-complete skeletons still remain undescribed (e.g., UFRJ DG 285-R, Vasconcellos & Carvalho, 2010), and more data are needed to increase overall anatomical knowledge beyond cranial features, with the potential to improve cladistic resolution. Moreover, important sources of morphological variation that could be mistakenly perceived as autapomorphies, such as sexual dimorphism, teratogenesis, ontogeny, and taphonomic deformation, have not been assessed among the baurusuchid holotypes.

Ever since the onset of modern studies into animal development, ontogeny was recognized as crucial for a comprehensive grasp of a species ecology and phylogeny (Gould, 1985). Several archosaurian fossil lineages, including crocodyliforms, have been shown to undergo substantial morphological shifts throughout ontogeny, (Carr, 2020; Drumheller et al., 2021; Otero et al., 2019; Woodruff et al., 2018). Once better understood, these changes were important to understand the past diversity of these groups, potentially identifying recently erected taxa as semaphoronts of previously described species (Horner & Goodwin, 2006; Horner & Goodwin, 2009; Scannella & Horner, 2010; Woodward et al., 2020). Hennig (1966), in his efforts to introduce useful and strictly defined nomenclature to phylogenetic systematics, conceived the “character-bearing semaphoront” as an organism, or individual, at any given point or stage along its ontogeny (Assis, 2016; Rieppel, 2003). Consequently, the definition of term highlights the importance of using corresponding semaphoronts as basis to establish monophyletic groups, as treating different ontogenetic stages as terminals is problematic, especially in paleontology (Sharma et al., 2017).

The current work presents, for the first time, a detailed osteological description of a semi-complete baurusuchid juvenile (IFSP-VTP/PALEO-0003), the most complete notosuchian juvenile known to date. We provide a three-

dimensional reconstruction of its skull utilizing computed tomography (CT) imagery, compare it to other baurusuchid specimens of different sizes, and perform an exploratory phylogenetic analysis with the inclusion of *G. scabrosus* and IFSP-VTP/PALEO 0003 in Martinelli et al.'s (2018) data matrix to evaluate and contrast their placement. These analyses allowed the identification of several ontogenetic changes, which can be used as guides to identify skeletally immature baurusuchid individuals among known and undescribed specimens. The identification of ontogenetic shifts in morphology provides a framework for future anatomical descriptions and rationale for an assessment of specimen age, leading to more robust phylogenetic hypotheses.

2 | GEOLOGICAL SETTING

Baurusuchids, as well as a myriad of other notosuchian forms, are very abundant in the Bauru Basin (Figure 1a), a Late Cretaceous pelitic/psammitic sedimentary sequence, known from the southeastern part of Brazil. It has an estimated outcropping area of roughly 370.000 km², covering the states of Goiás, Mato Grosso, Mato Grosso do Sul, Minas Gerais, Paraná and São Paulo (Fernandes, 2004). The Bauru Basin is divided into the Caiuá and Bauru Groups, which included the red sandstones of the Rio Paraná, Goio Erê, and Santo Anastácio Formations, with paleoenvironments interpreted as semiarid to arid and rare fossil sites (Batezelli, 2010; de Souza et al., 2021; Fernandes & Coimbra, 1996; Kellner et al., 2019; Manzig et al., 2014).

The Bauru Group, in turn, is highly fossiliferous, and classically composed of the Araçatuba Formation, marked by lacustrine, thinly laminated mudstones and siltstones; the Adamantina Formation, with its braided fluvial sandstones; and the high-energy alluvial fan sandstones and conglomerates of the Uberaba and Marília Formations (Batezelli, 2010; Batezelli et al., 1999; Soares et al., 1980). Former age estimates have ranged between Coniacian and Maastrichtian (Bertini, 1993; Dias-Brito et al., 2001; Goldberg & Garcia, 2000), whereas recent efforts with radioisotopic methods have yielded ages toward the end of that range, between the Campanian-Maastrichtian (Castro et al., 2018; Dias et al., 2021). This is also supported by recently described Campanian palynomorphs from Araçatuba Formation deposits (Arai & Fernandes, 2023).

The specimen herein described was collected in 2006, in Adamantina Formation outcrops in the vicinities of Fernandópolis, São Paulo (Figure 1a). It was embedded in oxidized, massive red sandstones (which may still be seen in the specimen, serving as its substrate after preparation) typical of the aforementioned unit, and, curiously,

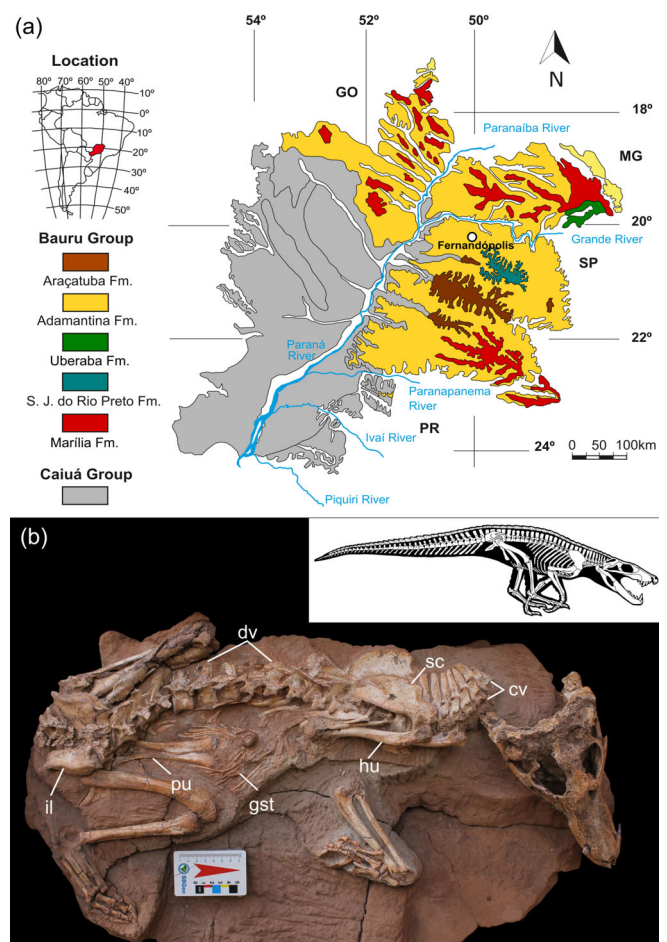


FIGURE 1 (a) Location of Bauru Basin within South America and its geological map. The Caiuá sequence is homogenized in gray, whereas stratigraphic units belonging the Bauru Group are highlighted in color. The specimen was collected in the vicinities of Fernandópolis-SP municipality, marked in white. (b) IFSP-VTP/PALEO-0003 specimen in dorsolateral view. All but the caudal series is preserved as shown by the skeletal reconstruction on the top right corner (by Felipe Alves Elias). cv, cervical vertebrae; dv, dorsal vertebrae; gst, gastralia; hu, humerus; il, ilium; pu, pubis. Scale bar in (b) = 1 m.

was also in close lateral proximity with a mostly complete but undescribed skeletally mature individual, which will be the target of future publications.

3 | MATERIALS AND METHODS

Articulated cranial and postcranial remains were collected utilizing a combination of electrical and hand tools, later being transported from the field to the laboratory within a plaster jacket. Preparation employed a series of pneumatized Paleo Tools hand jacks. The specimen is deposited in the vertebrate paleontology collection of the Federal Institute of Education, Science and

TABLE 1 Abbreviation list of myological nomenclature with respective source references.

Abbreviations	Muscle	References
<i>Cranial adductors</i>		
mAMEP	<i>M. adductor mandibulae externus profundus</i>	Holliday and Witmer (2007); Tsai and Holliday (2011); Sellers et al. (2022)
mAMES	<i>M. adductor mandibulae externus superficialis</i>	
mAMP	<i>M. adductor mandibulae posterior</i>	
mIRA	<i>M. intramandibularis</i>	
mPTd	<i>M. pterygoideus dorsalis</i>	
mPTv	<i>M. pterygoideus ventralis</i>	
<i>Appendicular musculature</i>		
add 1 + 2	<i>M. adductor femoris 1 and 2</i>	Romer (1923); Meers (2003); Turner (2006); Sertich and Groenke (2010); Godoy et al. (2016)
bb	<i>M. biceps branchii</i>	
cbb	<i>M. coracobrachialis brevis</i>	
cbv	<i>M. coracobrachialis brevis ventralis</i>	
ds	<i>M. deltoideus scapularis</i>	
ecrb	<i>M. extensor carpi radialis brevis</i>	
edc	<i>M. extensor digitorum communis</i>	
ext	<i>Distal extensors</i>	
fdl	<i>M. flexor digitorum longus</i>	
fmte	<i>M. femorotibialis externus</i>	
fti	<i>M. flexor tibialis internus</i>	
fu	<i>M. flexor ulnaris</i>	
gc	<i>M. gastrocnemius</i>	
if	<i>M. iliofemoralis</i>	
ilfb	<i>M. iliofibularis</i>	
it	<i>M. iliotibialis</i>	
ls + t	<i>M. levator scapulae and M. trapezius</i>	
p + sc	<i>M. pectoralis and M. supracoracoideus</i>	
pifi 1 + 2	<i>M. puboischiofemoralis internus 1 + 2</i>	
pq	<i>M. pronator quadratus</i>	
pt	<i>M. pronator teres</i>	
sc	<i>M. supracoracoideus</i>	
sp	<i>M. supinator</i>	
svt	<i>M. serratus ventralis thoracis</i>	
tbb	<i>M. triceps branchii</i>	
tbl	<i>M. triceps branchii caput laterale</i>	
tbm	<i>M. triceps branchii caput mediale</i>	

Technology of São Paulo (Votuporanga, São Paulo, Brazil), under the number IFSP-VTP/PALEO-0003. Given the varied myological nomenclature utilized in previous works, the anatomical descriptions and muscular reconstructions employ the most used terms in the literature. A list of abbreviations and their respective source references is provided in Table 1. Discussions about the cranial material are focused on ontogeny, comparing it to

adult forms. A list of taxa and specimens used for these comparisons is also provided in Table 2.

3.1 | CT and image processing

After mechanical preparation, the skull was separated from the skeleton for CT image acquisition using a Revolution

TABLE 2 List of taxa and specimens mentioned in osteological and myological comparisons as well as their respective sources. Holotypes were utilized when not otherwise stated (other type specimens are highlighted in bold).

Taxon and specimens	Source
<i>Baurusuchus</i> sp. FEF-PV-R-1/9 IFSP-VTP/PALEO 0002	Dumont Jr et al. (2020)
<i>Baurusuchus pachecoi</i>	Price (1945)
<i>Baurusuchus salgadoensis</i>	Carvalho et al. (2005)
<i>Baurusuchus albertoi</i>	Nascimento and Zaher (2010) and Nascimento (2014)
<i>Stratiosuchus maxhechti</i>	Campos (2001) and Riff (2003)
<i>Gondwanasuchus scabrosus</i>	Marinho et al. (2013)
<i>Aplestosuchus sordidus</i>	Godoy et al. (2014)
<i>Aphaurosuchus escharafacies</i>	Darlim, Carvalho, et al., 2021 and Darlim, Montefeltro, and Langer, 2021
<i>Campinasuchus dinizi</i> CPPLIP 1237 CPPLIP 1360	Carvalho et al. (2011)
<i>Pissarrachampsia sera</i> LPRP/USP 0049	Godoy et al. (2018)
<i>Sebecus icaeorhinus</i>	Molnar (2010) and Pol et al. (2012)
<i>Mariliasuchus amarali</i>	Nobre and Carvalho (2013)
<i>Araripesuchus tsangtsangana</i>	Turner, 2006
<i>Simosuchus clarki</i>	Georgi and Krause (2010), Kley et al., 2010, and Sertich and Groenke (2010)
<i>Alligator mississippiensis</i>	Romer (1923) and Witmer and Ridgely (2008)
<i>Melanosuchus niger</i>	Vieira et al. (2018) and Vieira et al. (2019)

EVO model at IMEB (Imagens Médicas de Brasília-DF), resulting in 392, 593, and 692 slices, respectively, of 0.50 mm each, with resolution of 512 × 512 pixels, 140 kV, and 240 mA. Data were processed in the freely available software InVesalius (Amorim et al., 2015), where manual segmentation and three-dimensional modeling of each skull bone was conducted. A yet undescribed adult baurusuchid skull, FEF-PV-R-1/9, has been scanned and modeled under the same conditions described above, and is employed below for myological reconstructions and comparisons.

3.2 | Phylogenetic analysis

Despite controversial (dos Santos et al., 2021), the inclusion of juveniles in phylogenetic analysis is conducted here in an exploratory manner, in order to compare the position of IFSP-VTP/PALEO-0003 in relation to adult specimens and, therefore, we must keep in mind that its position in the tree may not reflect its true evolutionary relationships as the material is an immature specimen. IFSP-VTP/PALEO-0003 was codified into the Martinelli et al. (2018) matrix, which is expanded upon and a more recent version of Pol et al. (2012, 2014) and Fiorelli et al. (2016), comprising 440 characters and 115 taxa. *G. scabrosus*, the smallest known baurusuchid, was also included in the analysis in order to compare its position relative to that of the juvenile herein described. Previously, this taxon had only been included in matrices encompassing solely baurusuchids (Darlim, Montefeltro, & Langer, 2021; Godoy et al., 2014; Montefeltro et al., 2011). The following series of 43 ordered characters were maintained from the work of Fiorelli et al. (2016): 1, 3, 6, 10, 23, 37, 43, 44, 45, 49, 65, 67, 69, 71, 73, 77, 79, 86, 90, 91, 96, 97, 105, 116, 126, 140, 142, 143, 149, 167, 182, 187, 193, 197, 226, 228, 279, 339, 356, 357, and 364. The remaining characters were treated as unordered; characters were treated as unweighted.

The analyses utilized TNT software (Goloboff et al., 2008) and were run in two consecutive rounds to obtain the most parsimonious trees (MPTs). A heuristic search was conducted with 10,000 replicates, using random addition sequence to avoid local optima. The tree bisection reconnection (TBR) option was used as swapping algorithm, saving 10 trees per round. The resulting trees retrieved in memory went through a final round of TBR branch swap. Similarly to previous works that employed versions of this data matrix, an attempt to run the analyses including all 115 taxa produced poorly resolved topologies, making necessary the testing and pruning of a specific set of five species based on fragmentary materials (described below). The first round of analyses resulted in 170 trees, followed by a second round that yielded 5568 MPTs, from which the strict consensus was obtained as a working hypothesis. Attempts utilizing the “new technology” algorithm produced identical results.

4 | RESULTS

4.1 | Systematic paleontology

Crocodyliformes Hay, 1930, sensu Benton & JamesM, 1988.

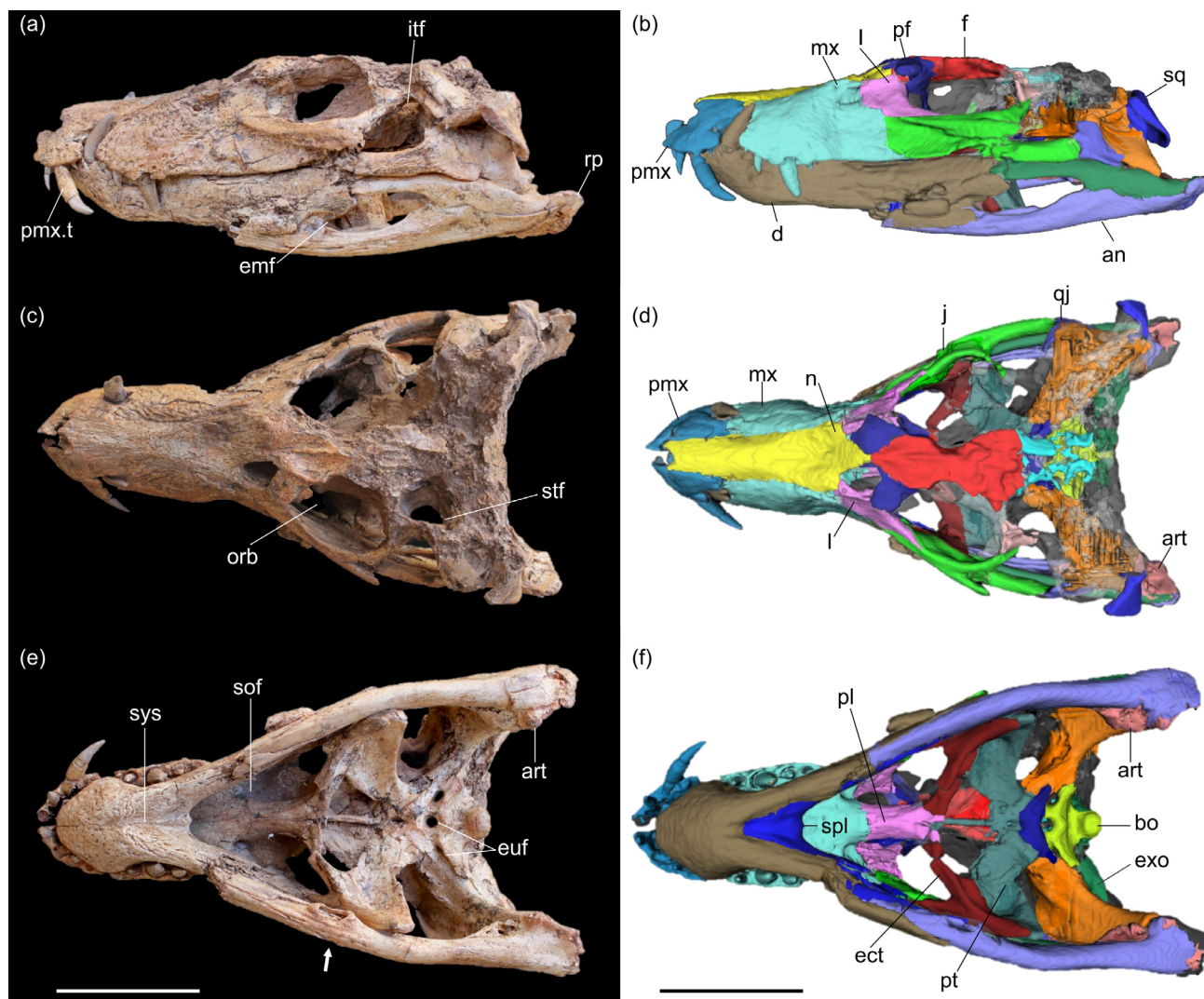


FIGURE 2 The complete, articulated cranium of IFSP-VTP/PALEO 0003. Photographs (a, c, e) and three dimensional, computed tomography reconstruction of the skull and mandibles (b, d, f) in left lateral (a, b), dorsal (c, d), and ventral (e, f) views. Most bones were individually reconstructed and colored, except for damaged elements of the basicranium and skull table. White arrow in (e) points to pathology on the ventromedial surface of the right angular bone. an, angular; art, articular; bo, basioccipital; d, dentary; ect, ectopterygoid; emf, external mandibular fenestra; euf, eustachian foramina; exo, exoccipital; f, frontal; itf, infratemporal fenestra; j, jugal; l, lacrimal; mx, maxilla; n, nasals; pf, prefrontal; orb, orbit; pl, palatines; pmx, premaxilla; pmx.t, premaxillary tooth; pt, pterygoids; q, quadrate; qj, quadratojugal; rp, retroarticular process; sa, surangular; sof, suborbital fenestra; spl, splenials; sq, squamosals; stf, supratemporal fenestra; sys, mandibular symphysis. Scale bars = 5 cm.

Mesoeucrocodylia Whetstone & Whybrow, 1983.

Notosuchia de Gasparini, 1971.

Baurusuchidae Price, 1945.

Baurusuchinae Montefeltro et al., 2011.

IFSP-VTP/PALEO-0003.

4.2 | State of preservation and taphonomy

The specimen consists of a semi-complete skeleton, including the skull, cervico-dorsal series with three

preserved dorsal osteoderms, sacrum, shoulder and pelvic girdles, as well as appendicular elements, lacking only the tail. Most of the bones were found articulated and in life position, with zygapophyses still connected up to the 13th dorsal vertebra, glenohumeral condyle still attached to the scapular glenoid and femoral head within the acetabulum (Figure 1b, see skeletal reconstruction in detail). The right coracoid and humerus were displaced and preserved parallel to one another. Posteriorly, the pelvic girdle displays a surprising level of articulation, with not only the three sacral vertebrae still in place, but also the ischia and pubes. The latter remain articulated medially along the pubic symphysis

and maintain contact posteriorly with the ischium along the pubic peduncle.

The skull preserves the left–right symmetry when seen in both dorsal and palatal views, indicated by similar orbit size in addition to symmetrical pterygoid and choanal morphology (Figure 2). Considerable erosional damage removed most of the dorsal surface of the skull table, substantially affecting the frontal, postorbitals, parietals, and squamosals. Fortunately, the left supratemporal fossa and fenestra were preserved. Sculpturing patterns of dermal bones are fully visible, most conspicuously on the rostrum and symphyseal portion of the dentary. There is evidence of dorsoventral flattening of the skull in the form of a fracture that extends ventroposteriorly through the dentary and infratemporal fenestra, displacing the anterior ramus of the jugal in relation to the posterior one, and also of the partial collapse of the temporal bar. The choanal septum and medial and lateral eustachian foramina are both preserved with minimum distortion.

Postcranial elements also display evidence of dorsoventral flattening. The femora, for instance, are more laterally projected than expected, given that notosuchians (including baurusuchids) are suggested to have had a parasagittal gait (Riff & Kellner, 2011; Tavares et al., 2017). The ischia seem also to have been compressed, given that their distal blades are not ventromedially joined. A clear torsion of the axial skeleton can be observed starting at the 14th dorsal vertebra. Their positions vary from being laid on their left sides to a more vertical position, in addition to a decreasing level of rib articulation, possibly reflecting the disarticulation of these elements whereas still embedded in soft tissues during decay. Finally, all appendicular bones, with minor exceptions, could be identified, including anterior and posterior stylopodial, zygopodial, and autopodial elements.

4.3 | Skull and mandibles

The skull of IFSP-VTP/PALEO 0003 concentrates the most conspicuous ontogenetic differences in relation to adult individuals. It is marked by relatively large orbits (Figure 2a,c), which roughly divides it into two subequal preorbital and postorbital portions, shallower mandibular symphysis, more posterior-projecting retroarticular processes (Figure 2a), and incipient sculpturing of dermal bones relative to adult forms. Most of its external surface is well preserved, except for the skull table (frontal, parietal, postorbitals, and squamosals) (Figure 2a,c,e). The acquisition of computerized tomography data allowed for the individual reconstruction of most bones (Figure 2b,d,f), but unfortunately the internal structures of the

basicranium are heavily distorted and/or fragmented, preventing modeling beyond their external profiles.

This specimen can be confidently assigned to Baurusuchidae by the presence of a combination of commonly cited characters (Figures 2, 3 and 6): a lateromedially compressed rostrum (oreinostry) with reduced number of ziphodont teeth, verticalized distal portion of the quadrates, anteroposteriorly large ectopterygoids, a depression on the lateral facet of the quadrate (Carvalho et al., 2004; Carvalho et al., 2005; Price, 1945; Riff, 2003); premaxillary-maxillary contact internalized into a ventrally-opened notch that encompasses a hypertrophied fourth dentary tooth, a transverse suture between the maxilla and the palatines, an anterior extension of the palatines that does not reach the anterior margin of the suborbital fenestra and posteroventral depressions of the mandibular symphysis (Darlim, Carvalho, et al., 2021; Darlim, Montefeltro, & Langer, 2021; Godoy et al., 2014; Martins et al., 2023; Montefeltro et al., 2011).

The presence of a ridged ventral surface of the choanal septum, a quadrate fenestra internalized into the otic notch and, most conspicuously, the simplified morphology of the choanae, lacking parachoanal fossae on a solid ectopterygoid-ptyergoid ventral surface, place this specimen into the Baurusuchinae subclade within Baurusuchidae (Figures 2e,f and 5d,e) (Darlim, Carvalho, et al., 2021; Darlim, Montefeltro, & Langer, 2021; Montefeltro et al., 2011; Nascimento, 2014).

Other taxonomically relevant features are the limited medial approximation of the prefrontals at a single point (Figures 2c,d and 5c), a character originally assigned to *Pissarrachampsinae*, but also seen in the Baurusuchinae *A. sordidus* (Godoy et al., 2014), a somewhat sharp sagittal crest within a frontal depression (Figure 2c), similar to the autapomorphies supporting the recently described *A. kaiju* (Martins et al., 2023) and a posterodorsal depression on the nasal, a feature of *Aphaurosuchus* spp. also found in some *Pissarrachampsinae* specimens (Darlim, Carvalho, et al., 2021; Darlim, Montefeltro, & Langer, 2021; Martins et al., 2023). The latter characters and proximity of collection sites suggest that IFSP-VTP/PALEO 0003 could be a juvenile *Aphaurosuchus*. A not yet seen pathology, in the form of an eruption-like bone recess on the ventromedial edge of the right angular (Figure 2e), is also visible in this specimen and will be the object of future investigations.

4.3.1 | Premaxilla

These are paired elements that comprise the anteriormost portion of the rostrum, anteroposteriorly longer than wide or tall, and possessing four teeth. The premaxillae encircle the anteriorly facing external nares, contacting the nasals dorsally and the maxillae posteroventrally (Figure 3 a₁, b, c).

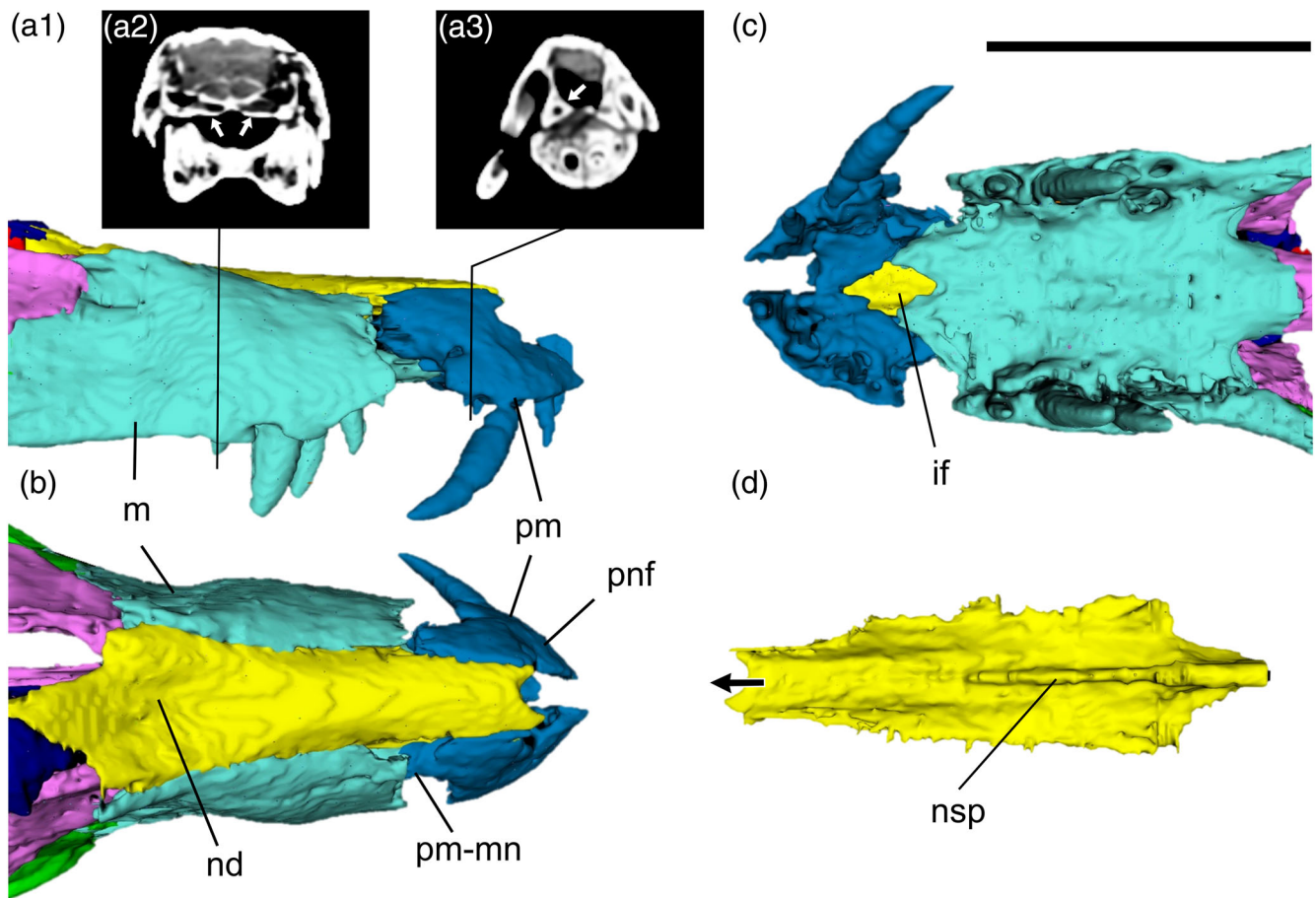


FIGURE 3 Three-dimensional rostrum model of IFSP-VTP/PALEO 0003, highlighting individual bone morphology. (a1) Left-lateral view (reversed), showing premaxillary and maxillary alveolar margins and posterior (a2) and anterior (a3) transverse cross sections. White arrows indicate pneumatic recesses. (b) Rostrum in dorsal view. Note the posterior constrictions of the nasal and its wide depression. (c) Palatal view where a rhomboidal-shaped incisive foramen is observed. (d) Fused nasals in ventral view with well-developed nasal septum that reaches mid-length. Scale bar = 5 cm. if, *foramen incisivum*; m, maxilla; nd, nasal depression; nsp, nasal septum; pm, premaxillae; pm-mn, premaxillary-maxillary notch.

They display a trapezoidal outline in lateral view, marked by a vertical anteromedial margin, where counterparts meet collaterally, a straight dorsal edge contacting the nasals, and a convex ventrolateral alveolar border. In both dorsal and ventral views, the bone has a more triangular shape. Anteriorly, as left, and right elements contact, the premaxillae form an ascending, posterodorsal tubular process, which, as in other baurusuchids, contributes to the formation of the internarial bar. This is fragmented at its base, leaving a non-bisected open naris, which is considered a taphonomic artifact. Nasals also contribute to the internarial bar, but their contribution is also incomplete.

External nares are ellipsoidal in anterior view, with a posterolateral major axis, and are surrounded by conspicuous semicircular shallow depressions, the perinasal fossae (Figure 3b). In lateral aspect, the premaxillae meet the nasals and the maxillae posteriorly along a tapering ascending process, resulting in a wedge-like triple contact between

these bones. Its posterior border is concave due to the presence of a well-defined notch between the premaxilla and maxilla bones for the insertion of a fourth, hypertrophied dentary tooth. The presence of the notch also obscures the premaxilla-maxilla suture, precluding a correct assessment of its conformation. Ventrolaterally, the premaxillae have shelves that emerge from the medial alveolar margins and are sutured to one another along the sagittal line, helping to form the anterior portion of the palate. Curiously, with the aid of computerized imagery, it was possible to determine that cross-sectional shape of the premaxillary shelves is triangular, with clear, pneumatic tubular foramina extending anteroposteriorly (Figure 3 a₁ and a₂). The premaxillary palatal surface is marked anteriorly by the *foramen incisivum*, a relatively large rhomboidal-shaped opening, in addition to circular, alveolar-like fossae, between the first and second premaxillary teeth diastema, for the placement of the first procumbent dentary teeth.

Sculpturing is more pronounced dorsally, closer to the more heavily ornamented nasals, consisting of generally antero-posteriorly directed, elongated, and shallow grooves, becoming smoother ventrally. Three small, circular neurovascular foramina can be seen above the lateral alveolar margins of tooth two, three and four on the left side, whereas only two are present on the opposing side. A distinctive feature of these premaxillae, in comparison with those of more mature individuals, is the fact they mostly overhang the dentary symphysis anteriorly, resulting in the first two premaxillary teeth not contacting the anterolateral surface of the dentary.

The premaxillae contain a total of four teeth set in a single wave, increasing in size up to the third tooth and then decreasing abruptly at the fourth alveolus. All teeth display mesio-distal serrated carinae, with homogeneous denticles. The first premaxillary incisiviform tooth is marked by a somewhat symmetrical D-like cross section (Hendrickx et al., 2015), with transversely-shifted serrated carinae, whereas more posterior teeth are more labio-lingually compressed with an elliptical sectional outline, a pattern that continues on the maxillary teeth.

4.3.2 | Maxilla

Comprising the majority of the lateral aspect of the rostrum, the maxilla displays a complex morphology, defined by a lateral process, which is lateromedially compressed and nearly vertically oriented, contributing to the conspicuous oreinirostry of baurusuchids (Price, 1945; Riff & Kellner, 2011), as well as a palatal shelf, that meets medially with its counterpart to form an extensive portion of the secondary palate (Figures 2 and 3a–c). The maxilla contacts the premaxilla anteriorly, the nasals dorsally, the lacrimals posterodorsally, the jugal posteriorly, and the ascending process of the pterygoid ventrally.

In lateral view, the maxilla possesses a trapezoidal profile that tapers anteriorly and forms the posterior margin of the premaxillary-maxillary notch, within which the fourth hypertrophied dentary tooth is allocated. Its ventral margin is marked by an anterior concavity, following the maxillary tooth row, transitioning to a straighter aspect posteriorly toward the jugal (Figure 3a,b). As mentioned above, the lateral surface of the maxilla is more verticalized in comparison with other crocodylomorphs. This condition differs substantially from that of sebecids, where the maxilla and nasals meet to form a triangular cross section of the rostrum, with a somewhat sharp dorsal end. Instead, in baurusuchids, the rostrum is rounder in shape dorsolaterally (Figure 3a a₁).

The internal anatomy of the palatal shelf could only be assessed with the aid of computerized tomography, and the axial slices were particularly revealing (Figure 3 a₁). The images show the palatal shelf in an orthogonal angle with the lateral process of the maxilla, forming a thick, vertical wall, that corresponds to the medial margins of the alveoli, and then extending medially as a transverse platform. The latter has a triangular cross section, dorsoventrally thicker close to alveoli and tapering to a bony slate at the sagittal plane. Throughout its length, the maxilla displays a highly pneumatized palatal shelf, with most of its internal volume filled by recesses (Figure 3a). These openings occur in similar positions and might be homologous to the maxillary sinuses described for the extant crocodylians, such as *Alligator mississippiensis* (Witmer & Ridgely, 2008), and recently observed in adult *C. dinizi* (Fonseca et al., 2020). Due to taphonomic dorsoventral compression, some intricate bony laminae within the palatal recesses collapsed, precluding a clear assessment of its morphological complexity, although some portions of the recesses were multichambered.

Dorsally, the internal surface of the palatal shelf is concave, and is subtly bisected by a sharp protuberance, defining left and right portions, as well as the ventral and lateral limits of the nasopharyngeal duct (sensu Witmer & Ridgely, 2008). Anteriorly, the duct is formed by the palatal shelf and nasal bones only, whereas posteriorly, as the maxilla deflects laterally, it is capped by the anterodorsal extension of the pterygoid, shaping a sigmoidal cavity.

Given the ziphodonty of baurusuchids, the slightly lateromedially-compressed alveoli have elliptical outlines. Moreover, these are separated by more conspicuous spaces in comparison with adult forms, the alveoli of which are often confluent. Maxillary teeth, as shown by tomography data (Figure 3), are deeply rooted within the bone, reaching its dorsal region, and thus creating visible bulges on its lateral surface. These are organized into a single size wave, in which the third tooth is the largest, and like posterior premaxillary teeth have serrated carinae and display further labiolingual compression. Ontogenetically, the teeth become more robust and the aforementioned bulges become more marked. The dorsolateral surface of the maxilla is more heavily ornamented than the lateral alveolar margin, with vermiform grooves and pits, whereas the latter bears four neurovascular foramina along the third, fourth, and fifth maxillary teeth. In palatal view, it is possible to see incipient sculpturing around the raised alveolar margins.

4.3.3 | Nasal

The nasals are fused into a single bone making up the entire dorsal length of the rostrum (Figure 3a,b). It contacts the premaxilla anteriorly, the maxilla laterally, the

prefrontal/frontal posteriorly, and the lacrimal postero-laterally. It is dorsoventrally flattened, with an elongated profile in dorsal view, where its length vastly exceeds its width. Anteriorly, the nasal forms a triple wedge-like junction with the premaxilla and the maxilla, dorsomedial to the fourth dentary tooth notch, lateral to which the bone is mostly overlapped by the maxilla (Figure 3). Unfortunately, the perinarial region of the nasal has been broken off, precluding the preservation of the internarial bar.

In dorsal view, the nasal shows relatively straight, parallel margins in its anterior half, posterior to which it is slightly concave laterally, before it expands transversely as it approaches the prefrontals and the frontal. Also, the bone is mostly flat above the premaxilla, presenting a moderate concavity with a somewhat rhombic cross section at the mid length of the rostrum, finally forming a wide depression anterior to the frontal suture. As it widens posteriorly, the nasal takes part in the anterior palpebral attachment surface, an anteroposteriorly long facet that reaches the anterodorsal rim of the orbits. Ventrally, along its posterior half, the bone possesses a crude septum that divides the nasal cavity into left–right portions (Figure 3d). Dorsal ornamentation consists of straight grooves closer to the external nares and more randomly placed, vermiform grooves posteriorly. Minute rounded pits, that are common on the nasals of adult forms, are absent.

4.3.4 | Jugal

The jugals of IFSP-VTP/PALEO-0003, as in most crocodyli-forms, make up the lateral cheek region of the skull and contact the maxillae anteriorly, the lacrimals anterodorsally, the ectopterygoids ventrally, the postorbitals posterodorsally and the quadratojugals posteriorly (Figure 2a,b). The right element has been substantially affected by erosion. They are lateromedially flattened bones, substantially longer than tall, and their medial surfaces are concave, thus resulting in their anterior and posterior ends curving slightly inward. In lateral view, the jugals have a tri-radial architecture, marked by subequal anterior and posterior rami, in addition to an ascending posterodorsal process that, alongside the postorbitals, form the postorbital bar (Figure 4a–c). The anterior ramus is a dorsoventrally expanded contributing to the ventral margin of the orbits. This border is gently concave along its length. It also contains a conspicuous infraorbital crest on its dorsolateral surface that tapers anteriorly, reaching the jugal-maxilla contact, and thickens posteriorly, merging with the posterior ramus. Ventral to the crest, a triangular depression is seen, a common feature also observed in adult forms and a previously

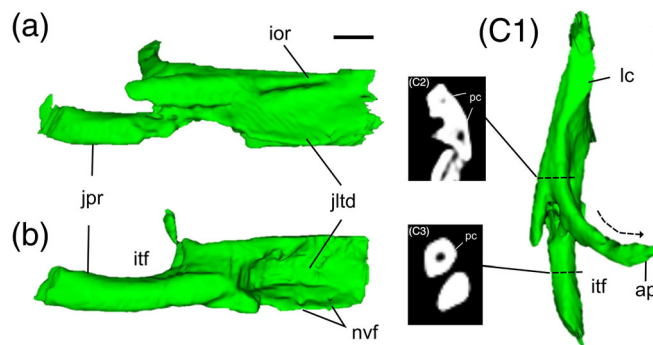


FIGURE 4 Isolated (a) left (flipped) and (b) right jugals of IFSP-VTP/PALEO 0003. (c1) Left jugal in dorsal aspect showing a posteromedially inclined ascending process. (c2 and c3) Pneumatic cavities present in both anterior and posterior portions of the jugal (not to scale). The latter contributes to the postorbital bar. ap, ascending process; itf, infraorbital fenestra; ior, infraorbital ridge; jpr, jugal posterior ramus; jlt, jugal triangular lateral depression; nvf, neurovascular foramina; pc, pneumatic cavity. Scale bar = 1 cm.

cited baurusuchid character (Montefeltro et al., 2011) (Figure 4a,b).

The posterior ramus is rod-like (roughly circular in cross-section) that meets the quadratojugal along a vertical, sutured contact. Furthermore, its dorsal surface forms the ventral border of the infratemporal fenestra. Internally, the jugals are pneumatized. Along the posterior ramus, a tubular-like recess extends to the anterior region, as revealed by CT scan slices (Figure 4 c₁, c₂, and c₃), which, in addition to the presence of neurovascular foramina, suggests that the recess might connect with the jugal external surface. The ascending process adjoins with the postorbital descending equivalent in a planar contact, contributing to roughly half of the postorbital bar, also forming the anterior border of the infratemporal fenestra.

Sculpturing varies over the jugal surface, with anteroventrally-inclined grooves more common on the lateral triangular depression, alongside local foramina, whereas vermiform horizontal grooves are present more posteriorly, especially close to the jugal-quadratojugal contact. The medial surface is mostly smooth, with the exception of neurovascular foramina that emerge close to its mid-length, near the transition between anterior and posterior rami. The maxilla-jugal contact is marked by a sheet-like lateral overlap of the jugal over the maxilla, which is lateromedially thicker. Ventrally, these also constitute a triple contact with the ectopterygoid platform.

4.3.5 | Quadrate

Temporal and braincase bones display a substantial degree of fragmentation and erosion. The quadrates, in

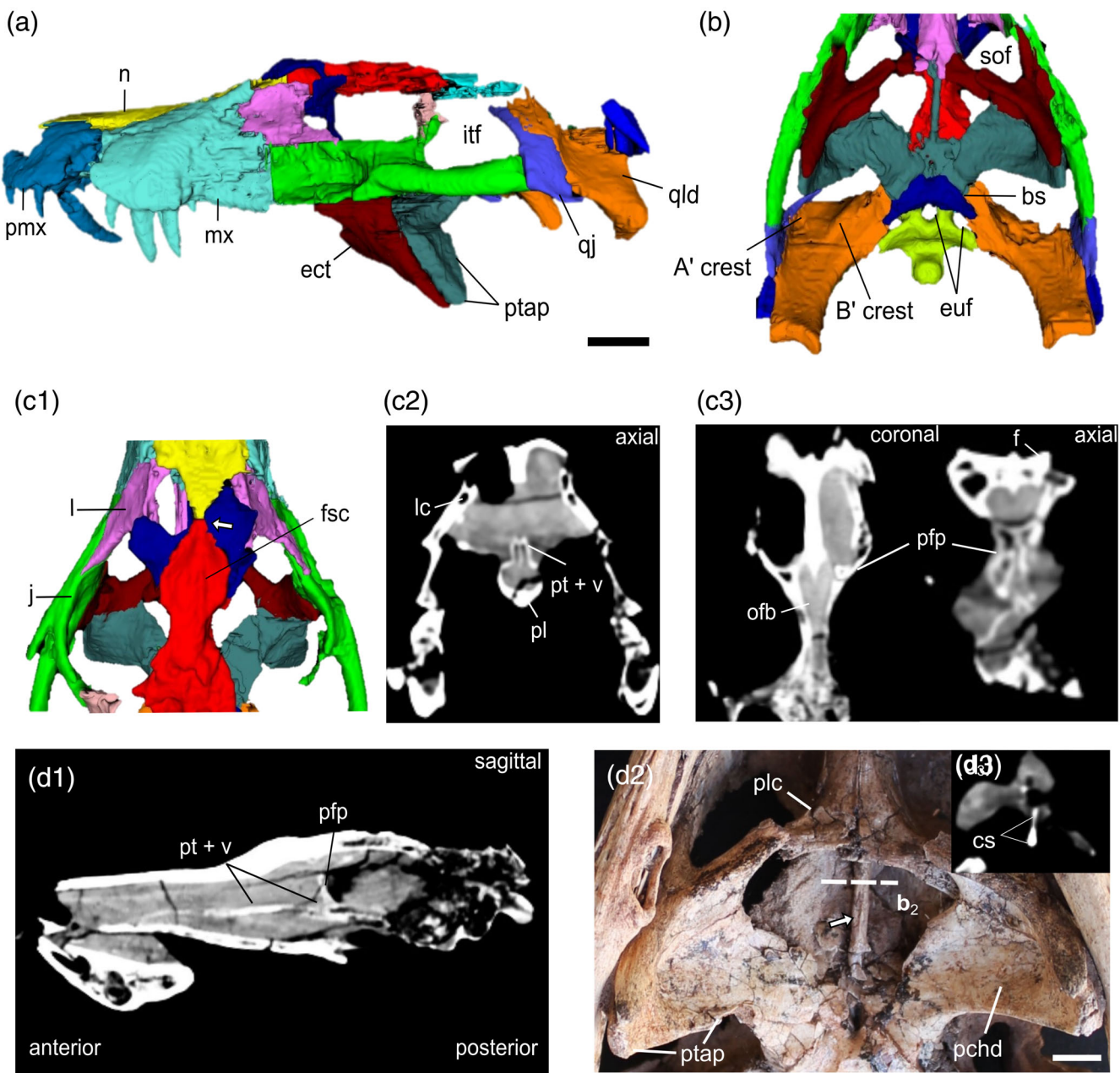


FIGURE 5 Digitally reconstructed skull highlighting the frontal, prefrontals, lacrimals, quadrates, quadratojugals, and the ectopterygoid-ptyergoid complex in lateral (a), ventral (b), and (c1) dorsal views. (c1) shows in detail the medial approximation of the prefrontals at a single point (white arrow), which does not prevent the contact between tapering nasal and frontal processes, as well as coronal and axial slices focusing on the prefrontal pillar structure. (c2) highlights an axial CT slice showing putative lacrimal ducts. (c3) Descending prefrontal pillars in axial cross section. (d1) Sagittal slice showing anterior extension of the pterygoids and vomer closing the nasopharyngeal passage dorsally (full rostral-occipital length shown) (d2) Photograph of the ectopterygoid-ptyergoid complex in ventroposterior view. Undevloped sagittal keel on choanal septum shown by white arrow. Note the relatively large and septate losangular choanae and the dorsal extension of the choanal septum (d3). bs, basisphenoid; cs, choanal septum; ect, ectopterygoid; euf, eustachian foramina; fsc, frontal's sagittal crest; itf, infratemporal fenestra; j, jugal; l, lacrimal; mx, maxilla; n, nasal; ofb, olfactory bulb; pchd, parchoanal depression of pterygoid wings; pfp, prefrontal pillars; plc, palatine medial constriction; pmx, premaxilla; ptap, pterygoid aponeurosis; pt + v, pterygoid and vomer; qj, quadratojugal; qld, quadrate's lateral depression; sof, suborbital fenestra. Scale bars, (a, b and c) = 2 cm; (d2) = 1 cm.

particular, have been affected by vertical compression, collapsing their dorsal process almost completely, including the otic cavity, and hampering an assessment of its

relations with braincase elements. Distally, however, they are well-preserved, displaying ventroposteriorly-oriented mandibular condyles (Figure 5a,b). As in other

crocodyliforms, the quadrate and quadratojugal are anterodorsally inclined, sharing a long contact with similar orientation. Its lateral surface bears a wide and shallow semicircular depression, synapomorphic for baurusuchids (Riff, 2003), that reaches the borders of the otic cavity and the posterior margin of the quadratojugal. Posteriorly, it contacts the squamosals along their posteroverventral processes, which extend laterally. In occipital view, this suture forms an acute, crest-like feature that divides the quadrate into lateral and medial surfaces.

The mandibular condyles are transversely-oriented (perpendicular to the rostral-occipital axis) and well separated by a medial sulcus. The lateral hemicondyle is more robust and placed more dorsally than the medial, whereas the latter is considerably more ventrally developed and narrower, thus generating a medially sloping condylar plane, following the superficial inclination of the articular. The quadrate ventral surface is also moderately well-preserved, revealing a dorsomedial curvature as it sutures with the ventral braincase elements, including the basioccipital, basisphenoid, and pterygoids. This ventral facet is slightly concave and displays two tendon attachment crests that composed the quadrate aponeurosis (Figure 5b). The first is lower, bordering the quadrate-quadratojugal suture and, consequently, the internal infratemporal fenestra, whereas the other is more medially dislocated, robust, and sinuous, curving toward the basisphenoid at a diverging angle from the former. These are, respectively, interpreted as homologous to crests A and B of modern crocodylians, and associated with the origins of mAMP and mAMES muscle groups (Holliday & Witmer, 2007; Iordansky, 2000).

4.3.6 | Quadratojugal

It consists of an L-shaped, lateromedially thin bone, marked by anterior and dorsal processes, making up the anterior infratemporal region of the skull (Figure 5a,b). The former is short and thicker than other portions of the bone and firmly sutured to the posterior ramus of the jugal along a vertical irregular contact close to the ventroposterior edge of the infratemporal fenestra. The dorsal process is a thin, anteroposteriorly short bony wall that ascends toward the temporal bar, forming most of the posterior limits of the aforementioned fenestra. Moreover, its dorsal end is slightly anterodorsally deflected but was not preserved enough for an assessment of its contacts. Posteriorly, it contacts the quadrate along an extensive suture that probably reached the ventral surface of the temporal bar. Its base is considerably longer

anteroposteriorly than its apical region, forming a larger surface area that contributes to the lateral semicircular depression of the quadrate. Its ventral border is convex up to the jugal contact, where a small gap between the skull and the mandible is seen. The lateral surface displays marked striations and grooves directed anteroposteriorly, especially closer to the jugal suture.

4.3.7 | Prefrontals

These are paired, rhomboidal-shaped elements in dorsal view, with limited medial approximation that does not prevent the frontal-nasal contact. The prefrontals are bound by the frontals posteromedially, the nasals anteriorly, the lacrimals ventrolaterally and the palatines and pterygoids ventrally. Along their lateral margins, which contribute to the anterodorsal border of the orbits, the prefrontals have a ventrally deflected surface for the attachment of the anterior palpebrals, forming an elliptical surface that extends into the nasals. Ventrally, the prefrontals are marked by lateromedially broad, and anteroposteriorly flattened pillars, clearly visible through the orbits. Their surface curve outward, reaching the medial surface of the orbital rim (Figure 5 c₁ and c₃). As the prefrontal pillars descend to contact the pterygoid anterior projection and the palatines, they seem to narrow into laminar processes, but their distal ends are still mostly embedded in sediment, hindering a full description. The olfactory bulb passage is located dorsomedially at the contact with the ventral surface of the frontal, displaying a rounded outline. Ornamentation is only present on its dorsal surface and, contrasting with adult forms, lacks deep grooves.

4.3.8 | Frontal

The frontal of IFSP-VTP/PALEO 0003, as most of its skull roof, is poorly preserved. Its dorsal surface is mostly eroded, in addition to being fragmented at lateral regions bordering the orbits. It consists of a trapezoidal element in dorsal view, contacting the parietal posteriorly along a transverse suture, the prefrontals anterolaterally and the nasals anteriorly (Figures 2 and 5 c₁ and c₃). The anterodorsal region is better preserved, bearing a somewhat sharp sagittal crest bound on both sides by anteroposteriorly long depressions. The crest tapers forward, failing to reach the frontal-nasal contact. Anteriorly, the frontal has a slender process that is laterally constricted by the prefrontals, reaching the nasals only at a single point. Ventrally, the frontal has medially inclined surfaces that

meet at the longitudinal plane to form the concavity for the passage of the olfactory bulb. The internal structure, as revealed by CT data, is marked by lateral and medial recesses, the volume of which in relation to cortical bone seem to be ontogenetically conditioned, with diminishing pneumatic openings being replaced by cortical bone (see dos Santos et al., 2021).

4.3.9 | Postorbital

The postorbital is a major element of the skull roof, bounding the supratemporal fenestra anterolaterally as well as forming the dorsal margins of the infratemporal fenestra. It is part of a complex arrangement of bones involving the skull roof, temporal region and the basicranium, contacting the frontal anteromedially, parietal posteromedially, squamosal posterolaterally, jugal anteroventrally, quadratojugal posteroventrally, and laterosphenoid anteromedially. Due to the poor preservation of the skull roof, the dorsal surface of the postorbital is mostly damaged, lacking the temporal bar and the original surface texture. What is preserved of the postorbital has a quadrangular shape in dorsal view, with a straight medial border, a concave anterior margin, part of the posterior orbital rim, and a sharp lateral concavity that delineates a triangular infratemporal fenestra. Dorsally, it has an L-like shape, marked by a dorsoventrally compressed medial process. A descending anterior process contributes to the postorbital bar, with a more elliptical cross section at its encounter with the jugal. There is also a laminar posterior process that is overlapped by the quadratojugal alongside the posterior edge of the infratemporal fenestra. The poorly preserved supratemporal region reveals a fully open fenestra, although proportionally smaller in comparison to that of adult individuals, with verticalized walls and initial development of surrounding supratemporal fossae. No significant ornamentation was observed. The anterior insertion surface for the posterior palpebral was not preserved on either side.

4.3.10 | Lacrimal

The lacrimals are lateromedially compressed, laterally concave and vertically oriented elements with a quadrangular outline in lateral view. They are located on the posterolateral face of the rostrum, contacting the maxilla anteriorly, nasals and prefrontals dorsally, frontal medially, and jugals ventrally (Figures 2 and 5). Their anterior contact with the maxilla is convex in lateral view, slightly anterodorsally inclined, whereas ventrally they possess a straight, horizontal contact with the jugals, extending posteriorly along a tapering process.

Posteriorly, the lacrimals have a curved/concave margin that makes up the anterior rim of the orbit. A posterolateral view reveals that the dorsal region is medially deflect in respect to the ventral one, thus resulting in its contact with the prefrontal pillars. In addition to the nasals and the prefrontals, the attachment surface for the anterior palpebral is also formed by the lacrimals. These constitute an auxiliary support surface that forms a dorsal platform. Despite the fact that a lacrimal canal is not visible externally, the CT data seem to indicate a posterodorsal emergence, with the main duct extending anteroventrally along its length. The external surface lacks ornamentation, although the infraorbital crest reaches the lacrimal anteroventrally.

4.3.11 | Palatine

These comprise paired bones of the palate that meet medially along the sagittal plane to form a single tube-like, anteroposteriorly long element. They contact the maxilla anteriorly, the pterygoids dorsally (composing the nasopharyngeal tract) and the ectopterygoids posterolaterally (Figures 2 and 5). Laterally, their surfaces are concave and slope ventromedially, creating shallow fossae bounding the medial edge of the suborbital fenestrae. In ventral view, the palatines become transversely expanded posteriorly, bifurcating to meet the ectopterygoids and forming a straight posterior margin that overhangs the choanal septum as it enters the tract. These lateral processes together form a triangular area ventrally, bound laterally by a relief change near the palatine lateral surface. This region bears a relatively large pneumatic foramen at the medial plane. In cross section, the palatines are crescent-shaped, composing the bottom half of the nasopharyngeal tract. Pneumatic cavities also mark the palatines close to their contact with the maxillae anteriorly. Superficially, the palatines are mostly smooth, not displaying any ornamentation or muscle scars.

4.3.12 | Ectopterygoid-ptyergoid complex

The pterygoid wings are the major components of the posterior palatal surface and encircle the proportionally large and rhomboidal choanae typical of *Baurusuchinae* (Darlim, Carvalho, et al., 2021; Darlim, Montefeltro, & Langer, 2021), forming their posterolateral margins (Figure 5 d₂). Together, the ectopterygoid and pterygoid form large, triangular, wing-like structures surrounding the secondary nares that taper lateroventrally. These are dorsoventrally flat but transversely wide, tangentially contacting the medial surface of the angular, close to its

torose margin. This set of elements was probably forced into an almost horizontal configuration due to dorsoventral compression of the cranium. In life, it would have had a more verticalized disposition, with a ventrolateral orientation, as seen in specimens that were not submitted to such distortion.

The ectopterygoid Is formed by an ascending, laterally flattened process that culminates into an elliptical platform that sutures it to both the jugal and the maxilla, and also a narrow, tubiform, ventral projection that composes the pterygoid plate, thus sharing a long suture with the pterygoids. It also has a medial projection that meets the palatines along an almost anteroposteriorly-oriented contact. These delimit the posterior margin of the suborbital fenestra. In palatal view, the ectopterygoid displays thickened anterior margins and a marked concavity bearing minute neurovascular foramina, contributing to the large perichoanal fossa encompassing the pterygoid plate. The pterygoids are the larger elements of the set, compose the choanae lateroposteriorly, the choanal septum itself and enclose a significant portion of the posterior nasopharyngeal tract. They contact the palatines and the ectopterygoids anteriorly, the prefrontals dorsally through their paramedial descending processes, the laterosphenoids posterodorsally, the basisphenoid posteroventrally and the quadrates posterolaterally. There is also a minor contact with the basioccipital close to quadrates. CT images reveal that, anteromedially, the pterygoid dorsal nasopharyngeal cap forms a duct-like, dorsally convex arch, bound ventrally by the palatines, that reach the nasal passages (Figure 5 d₁). This anterior process tapers to a point as it enters the aforementioned cavity.

A transverse cross section (Figure 5 d₃) shows a tall but laterally thin septum, attached to the dorsal surface of the duct, that emerges anteriorly and has an extensive length, eventually emerging on the choanae as a thick rod that bisects the internal nares. The choanal opening itself displays thin bone walls (perichoanal lamina) surrounding the septum that possibly enclosed the air flow, directing it into the pharynx. The pterygoid wings are distinctly concave ventrally, forming a wide perichoanal fossa. Their posterior edge is straight but curves markedly as the pterygoid narrows to meet the basisphenoid. This contact is roughly v-shaped in palatal view.

The pterygoid lateral margin and distal end bear textures that might correlate with musculature attachments. For instance, when seen in lateral aspect the pterygoid buttress displays a shallow circular, dorsolaterally facing depression with porous surface that might correspond to its contact with *cartilage transiliens* (ct) in life (Holliday et al., 2013; Iordansky, 2000). Ventral to this, there are longitudinal marks that may indicate the passage of *M. intramandibularis* (mIRA) toward the mandibular adductor fossa, as inferred due to its attachment on the ct sesamoid (Tsai & Holliday, 2011). Dorsally, the pterygoid

forms a wide concavity with a mostly smooth surface with only minor striations related to *M. pterygoideus dorsalis* (mPTd). Ventrally, on its distal cojoined tip with the ectopterygoid, conspicuous deeper sulci indicate the origin site for *M. pterygoideus ventralis* (mPTv).

4.3.13 | Basisphenoid

It corresponds to a wedge-shaped element of the posteroventral portion of the basicranium, located between pterygoids anteriorly and the basioccipital posteriorly. Its anterior ventral surface shares a strong depression with the posteroventral process of the pterygoids, with which it shares a v-like suture (Figures 2 and 5). Within this depression, anterior but at the same dorsoventral level of the median eustachian foramen, there is an additional large foramen, roughly at the limit between these two bones. Due to the mentioned depression, the anteroventral surface of the basisphenoid slopes anteriorly, but posteriorly, a subquadratic crest-like feature is present at its border with the basioccipital. The posterolateral basisphenoid projections also bear shallow depressions and reach the quadrate along a narrow contact. In terms of surface texture, the basisphenoid is mostly smooth, lacking sculpturing and/or muscle striations. Given the poor preservation of the dorsal portion of the basisphenoid, nor the endocranium floor, cultriform process or vascular/nerve canals could be identified, even with the aid of CT imagery.

4.3.14 | Basioccipital

This element occupies the occipital region of the skull as well as the ventral portion of the basicranium, contacting both otoccipitals dorsolaterally, quadrates ventrolaterally, the basisphenoid ventroanteriorly and, possibly, the prootic internally. It is an anteroposteriorly thin, but lateromedially expanded bone, with a roughly triangular shape in occipital view. Dorsally, it narrows and then thickens posteriorly to form its part of the occipital condyle, a robust, rounded process additionally formed by ventromedial projections of the exo/otoccipitals, while ventrally it becomes increasingly transversely expanded, culminating in a fan-like process with an anteriorly convex contact with the basisphenoid (Figure 5b).

The occipital condyle is posteroventrally directed, roughly rounded, and marked by a vertical sagittal sulcus. Just ventral to the occipital condyle, three diverging crests emerge: two adjacent lateral elements, thicker and ventrolaterally inclined, and a medial one, sharper and vertically oriented. They bound lateral depressions which occupy large areas of the wide ventral process of

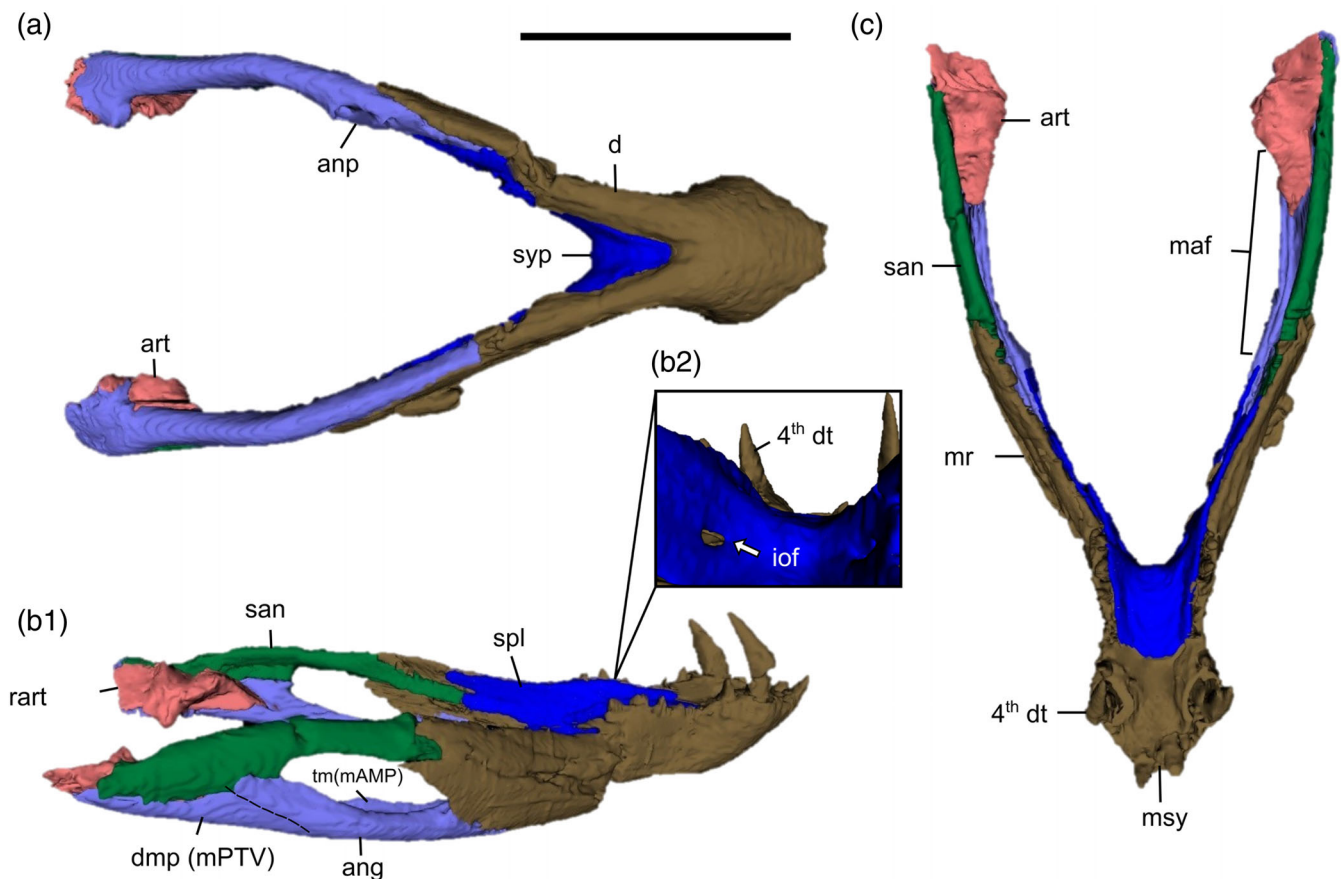


FIGURE 6 Digital model of the mandibles of IFSP-VTP/PALEO 003 in (a) ventral, (b1) dorsolateral, and (c) dorsal views. (b2) is a detailed image of the mandibular ramus medial wall, formed by the splenials, and its elliptical oral intramandibular foramen (iof). ang, angular; anp, angular pathology; art, articular bone; d, dentary; dmp, depression for insertion of *M. pterygoideus*; maf, mandibular adductor fossa; mr, mandibular ramus; msy, mandibular symphysis; san, surangular; spl, splenials; syp, symphyseal peg; 4th dt, fourth hypertrophied dentary tooth. Scale bar = 5 cm.

the basioccipital. These bear 2 mins neurovascular foramina near the midline, slightly ventral to the condyle and overhung by it. Each crest leads up to the basioccipital ventral border, where two conspicuous and rounded basal tubera emerge, making up the thickened margins surrounding the lateral and medial eustachian tubes. Three foramina are placed at the boundary between the basioccipital and basisphenoid, including elliptical lateral ones and a larger circular opening at the sagittal line. The ventral view exposes long sutures between these two basicranium elements, creating a sulcus where the eustachian tubes are located. The basioccipital external surface is mostly smooth with the noticeable exception of the basal tubera, that bear clear striations.

4.3.15 | Skull roof and occiput

As previously mentioned, in addition to the dorsoventral compression that substantially affected the occipital

region, flattening its components, the skull roof has also been exposed to weathering. The posterior end of the frontal, along with the parietal, the postorbitals and squamosals are all badly damaged, with almost all their dorsal surfaces obliterated. Fortunately, the rough outline of the left supratemporal fenestra is preserved, revealing a triangular shape, marked by somewhat rounded vertexes. One of the latter points medially, and no visible supratemporal fossae are preserved. Additionally, it is possible to notice that the fenestrae were relatively small in comparison to the skull roof area, not nearly as developed as in adult individuals, in which it becomes transversely wide, resulting in the narrowing of the parietals. Temporal bars have also collapsed, blocking a proper view of the otic cavity. The inner ear anatomy was successfully recovered with the use of CT scanning, and detailed in Dumont Jr et al. (2020). As a result of the dorsoventral compression, evidenced by the elliptical outline of the *foramen magnum*, and subsequent erosion, the supraoccipital and exoccipitals are poorly preserved, represented only by fragments.

4.3.16 | Dentary and splenials

The anterior and symphyseal regions of the mandible are composed by the dentary anterolaterally and the splenial posteromedially. Both elements contact one another anteriorly, but also the angular and surangular posteriorly (Figure 6a–c). In ventral view, the mandibular symphysis has a by rhomboidal-like shape, expanding transversely at mid length following the hypertrophied fourth dentary tooth and then tapering into a blunt anterior edge. Posterior to the fourth enlarged alveolus, the dentary has a marked lateral compression, resulting in concavities that occlude lingual to the second and third maxillary teeth. The splenials make up about a third of the total symphyseal length posteriorly, forming a v-like anterior process as both counterparts meet along the sagittal plane to contact the dentaries, diverging from the longitudinal plane posteriorly, assuming a verticalized and mediolaterally compressed aspect. Lateral to the medial suture, low-relief longitudinal crests develop close to its contact with the dentary ventrally, located within a wider triangular depression that reaches up to mid length. The sagittal suture of the symphysis is visibly thickened posteriorly, generating a conspicuous symphyseal protuberance which is surrounded by shallow depressions. It is noteworthy that its anterior symphyseal surface slopes into an oblique angle with respect to the horizontal plane, differing from the verticalized condition observed in mature semaphoronts.

In lateral view, the dentary has a somewhat rectangular shape, where the dorsolateral and ventrolateral margins are parallel to one another, ventrally forming a wedge-like contact with the splenials and the angular anterior process. Posterolaterally, the dentary becomes a thin vertical wall, slightly overlapping both angular and surangular, and forming the acute anterior edge of the mandibular fenestra. These elements together delimit the meckelian canal, the dentary laterally, and the splenials medially. The splenials, just posterior to the symphyseal protuberance, bear relatively large and elliptical anterior intermandibular foramina (*foramen intermandibularis oralis—fio*) (Figure 6 b₂). These face slightly dorsally and are responsible for the local emergence of the mandibular nerve (V_3). The ornamentation is more developed and clustered on the lateroventral surfaces of the mandibular symphysis, consisting of randomly distributed vermiform sulci. Laterally and posterolaterally, the dentary also displays less noticeable longitudinal sulci.

4.3.17 | Angular

The angular composes the ventroposterior region of the mandibles, making up more than half of their ventral

length (12 cm of a total of 22 cm, 54%). It is an anteroposteriorly elongated, but lateromedially narrow tubular-like bone with a convex outer surface and a concave medial one, forming a wide/open arch. Its cross section shows a characteristic U-shape, where a longitudinal sulcus, anteriorly contributing to the meckelian canal, is bound by medial and lateral walls/laminae. Anteriorly, in ventral view, it is pinched to a point between the splenial and dentary, but posteriorly it becomes increasingly wide and dorsoventrally flat, forming a platform to receive the articular bone. In lateral view, it also contacts to the surangular posterolaterally along a roughly rectilinear suture that follows the tapering of both elements, reaching the retroarticular process posteriorly. The angular makes up the ventral border of the external mandibular fenestra, where it has a laminar dorsal process posteriorly (more robust in adult forms).

Midway along the mandibular adductor fossa, the medial wall of the angular becomes conspicuously taller than its lateral counterpart, giving rise to a noticeable protuberance (torose margin sensu Nascimento & Zaher, 2010). This process takes the form of a thickened wall and topologically seems to have functioned as an attachment surface area for mandibular adductor musculature, most likely mAMP, which would cover most of the external mandibular fenestra (Figure 6 b₁, but also see discussion). A shallow, tear-drop-shaped depression for the lateral insertion of mPTv is present close to the ventral margin of the mandibular fenestra, an intriguing baurusuchid feature not seen in other notosuchians, except for *Araripesuchus* (Sellers et al., 2022). Yet, it is much less developed in IFSP-VTP/PALEO 0003 than in adult forms. Deep carving grooves and pits can be seen on the anterolateral surface of the angular, whereas most of its remaining surface is smooth and ornament-free.

4.3.18 | Surangular

Located at the posterior end of the mandibular ramus, the surangular comprises an anteroposteriorly long but mediolaterally compressed element that forms most of the external mandibular fenestra dorsal edge. It contacts the dentary and the splenial anterolaterally and anteromedially, respectively, the angular posteroventrally and the articular posteromedially (Figure 6a,b). The surangular is marked by an anterior narrowing process, fitting between the dentary and the splenial, forming a longitudinal sulcus where the mandibular branch of the trigeminal nerve (V_3) would fit, and advancing anterodorsally through the meckelian canal. Along its mid-length, this element bulges faintly outward, and is markedly concave ventrally, forming the dorsoposterior outline of the mandibular fenestra, with no visible fossa.

Posteriorly, it shows a tall but narrow process that bounds the articular bone laterally, composing the lateral portion of the mandibular glenoid fossa. This process also further extends posteriorly, tapering in parallel with the angular to contribute to the retroarticular process. The contact between these two elements is straight, reaching the posterior margin of the articular. The surangular mediadorsal surface is smooth and slightly depressed, serving as the attachment area for mAMES that extended from the quadratojugal concave ventral margin to the coronoid eminence (Figure 6 b₁). The latter forms a thickening on the surangular's anterior end, displaying a vertical medial wall adjacent to the pterygoid buttress, and consequently, the *cartilago transiliens* (ct). This surface likely served as an attachment facet for both mAMEM and mAMEP, but there is no visible muscle scarring like those of large adults such as in the *B. salgadoensis* holotype (MPMA-62-0001-02). Overall, the bone's surface is smooth externally, with the noticeable exception of the posterior margin of the mandibular fenestra parallel striations where the mAMP likely bulged.

4.3.19 | Articular

Both left and right articulars are well-preserved, and despite partially obscured by the articulation with the cranium, were reconstructed with the use of CT imagery. They contact the surangular laterally and the angular ventrally. The latter forming a wide platform onto which the articular rests upon. Overall, in dorsal view, the articular has a triangular outline, with an acute, tapering anterior process, wedged into the medial angular sulcus, and a wide retroarticular process posteriorly (Figure 6b,c). The glenoid fossa is located somewhat at the articular middle section, having its deepest concavity laterally (for the reception of the quadrate lateral hemicondyle). The medial concavity is limited by a thickened and raised margin, followed by a vertical medial wall. In medial view, it is possible to observe two distinct transverse crests that bound the glenoid fossa anteriorly and posteriorly, substantially limiting any fore-and-aft jaw movement. The anterior process slopes anteriorly as the element narrows, whereas posteriorly the articular contribution to the retroarticular process forms a wide and dorsoventrally flat sheet-like projection. This region is medioventrally inclined in occipital view. The ventromedial edge of the retroarticular process bears muscle insertion marks for mPTv.

4.3.20 | Palpebrals

The specimen preserves a partial right anterior element and a complete set of left palpebrals. It follows

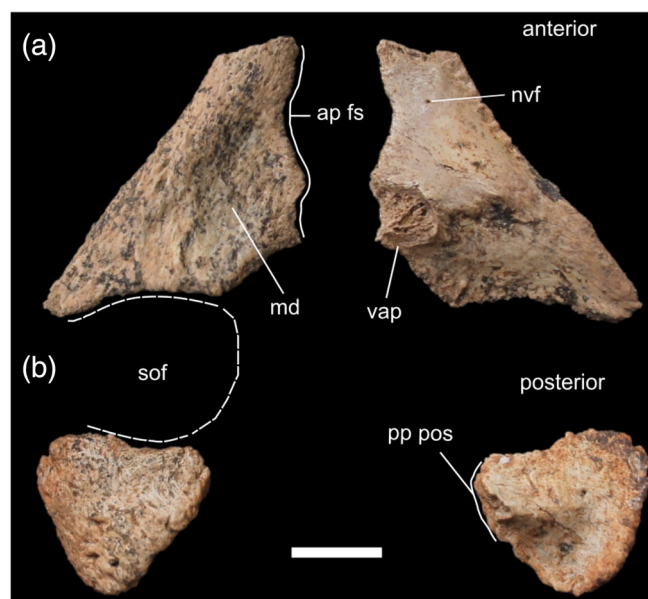


FIGURE 7 Anterior (a) and posterior (b) palpebrals of IFSP-VTP/PALEO 0003 in dorsal (left) and ventral (right) views. ap fs, anterior palpebral frontal suture; md, medial depression; nvf, neurovascular foramen; pp pos, posterior palpebral postorbital suture; sof, supraorbital fenestra; vap, ventral articular process. Scale bar = 1 cm.

the plesiomorphic crocodylomorph pattern of having two, anteroposterior articulating palpebrals, above each orbit, as seen in protosuchids (Colbert et al., 1951; Dollman et al., 2019), and also notosuchians like *Araripesuchus* and *Simosuchus* (Kley et al., 2010; Turner, 2006). As typical of baurusuchids, the anterior palpebral is substantially larger than the posterior, and both come into contact at discrete points medially and laterally, forming a large elliptical supraorbital fenestra (Carvalho et al., 2005; Nesbitt et al., 2012).

The anterior palpebral has a triangular outline in both dorsal and ventral views, tapering to a point and projecting posterolaterally at the horizontal plane above the eye socket (Figure 7a). Its lateral border is obliquely inclined with respect to the rostral-occipital length, whereas the posterior edge is mostly orthogonal to it and distinctively concave at the posterior palpebral margin. Dorsally, the anterior palpebral has a large shallow depression that encompasses most of its posteromedial area. It articulated with and was sutured to a lateral and elliptical facet formed marginally by the nasal, but mostly the prefrontal and frontal, where its medioventral process would fit.

The posterior palpebral, a small and triangular element, attached to an anterolaterally facing facet on the postorbital, protruding its lateral tip toward the anterior element (Figure 7b). This disposition, along with a visible concavity on its anterior margin, contributed to the

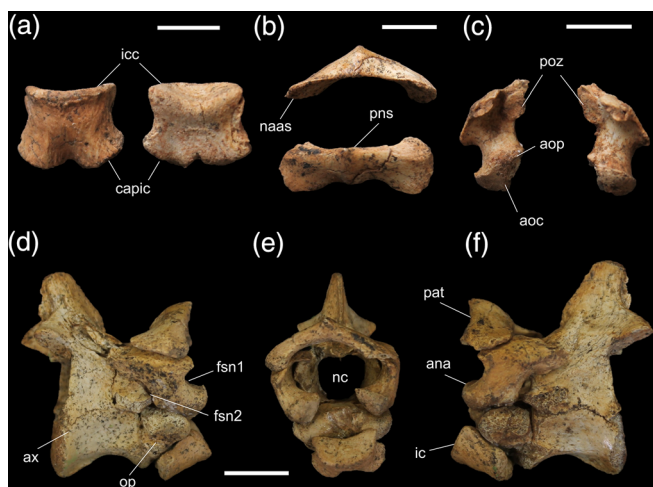


FIGURE 8 Atlas-axis complex of IFSP-VTP/PALEO-0003. (a) Intercentrum in ventral and dorsal views; (b) proatlas, highlighting posterior and ventral views; (c) right and left axial neural arches, respectively; (d–f) Complete articulated complex in right lateral, frontal and left lateral perspectives. ax, axis vertebra; ana, axial neural arch; aoc, articular surface for the occipital condyle; aop, articular surface for odontoid process; capic, intercentrum capitular process; fsn1, spinal nerve foramen; fsn2, spinal nerve foramen 2; ic, intercentrum; icc, intercentrum cotyle; naas, articular surface for the neural arches; nc, neural canal; op, odontoid process; pat, proatlas; poz, postzygapophysis; pns, proatlas neural spine. Scale bars = 1 cm.

formation of the supraorbital fenestra. Both palpebrals are substantially more sculptured when compared with the rest of the dermatocranium, bearing clear striations and sulci, as well as neurovascular foramina. Their ventral surfaces, however, are mostly smooth.

4.4 | Axial skeleton

4.4.1 | Atlas-axis complex

IFSP-VTP/PALEO 0003 possesses the best preserved and most complete baurusuchid atlas-axis complex found to date, including a proatlas with no substantial damage, both atlantal neural arches, intercentrum, odontoid process, which is fully sutured to the anterior articular surface of the axis, and, finally, the axis, with only minor signs of wear around the margins of the anterior and posterior articular surfaces (Figure 8). Its well-developed proatlas bridges the dorsal surfaces of the atlantal neural arches, and, along with *B. albertoi* and *C. dinizi* (Carvalho et al., 2011; Nascimento & Zaher, 2010), differs from notosuchians like *Simosuchus clarki*, that show no signs of having possessed such an element (Georgi & Krause, 2010).

The proatlas has an open v-like shape in both anterior and posterior views, and a straighter outline in dorsal view, being significantly wider (≈ 28 mm) than antero-posteriorly long (≈ 5 mm), as well as dorsoventrally flat. It is marked by two laterally-projecting processes that are cojoined dorsally, at an angle of roughly 120° as seen in anterior or posterior views (Figure 8b). A major feature is a medial ridge that extends dorsally along a posteroventrally inclined slope, thus forming a sharp, anteriorly placed apical portion. In dorsal view, the lateral processes maintain a semi constant length up to their middle portions, where each expand anteroposteriorly and also mediolaterally, forming a widespread projection with rounded outer margins. Ventrally, these form roughly circular articular surfaces for the contact with corresponding surfaces of the planar process of the atlantal neural arches. Additionally, the dorsal surface of these lateral processes display transverse, low relief crests that are anteriorly-shifted. These converge medially into the apical portion of the medial ridge and divide the proatlas outer surface in two distinct anteroposterior areas. The bone extends little anteriorly, but posteriorly forms a ventrally projecting triangular vertical wall, the ventral margin of which forms a medial knob and laterally merges into the edges of the articular processes. The element mostly lacks sculpturing, being smooth throughout its surface, except for the dorsolateral margins of the articular processes that show a rougher texture.

The atlas lies ventral to the proatlas, composed of an intercentrum and left/right neural arches, in addition to the odontoid process, firmly fixed to the axis. The intercentrum morphology is in line with the general pattern seen in other extant and extinct crocodylomorphs (e.g., Georgi & Krause, 2010; Vieira et al., 2016), including baurusuchids (Cotts et al., 2017; Nascimento & Zaher, 2010). It corresponds to a quadratic element in dorsal or ventral views, markedly broader than long, with a concave dorsal surface and a convex ventral one (Figure 8a). The atlas dorsal concavity slopes posteroventrally and provides a contact area for the odontoid process, whereas anteriorly it has a crescent-shaped, concave articular surface for the occipital condyle (*fossa condyloidea* sensu Georgi & Krause, 2010). Posteriorly, the intercentrum bifurcates into two posterolaterally-oriented semicircular processes for the articulation of the first pair of uncapitate cervical ribs (which are not preserved). These rib facets are slightly offset in relation to the anterior condyle, most likely due to its posterior contact with the odontoid process. There are moderately developed lateral constrictions that result in a concave lateral margin and a visible depression. Posteriorly, a trough is seen between the atlantal rib facets, reaching the mid length antero-posteriorly along the intercentrum. The bone lacks

major ornamentations, presenting only minor, shallow striations.

Dorsal to the intercentrum, the neural arches are separate paired elements, distinct due to their laterally curved, c-shaped outline in anterior/posterior views and t-like shape in lateral or medial aspects (Figure 8b). These are formed by a dorsal, horizontal laminar process and the anteroventrally-projecting pedicles (Figure 8c). The former is an anteroposteriorly elongated but dorsoventrally flattened laminar shelf that dorsally displays a shallow articular surface for the attachment of the proatlas and posteroventrally houses the postzygapophyses. Ventromedially, the postzygapophyses are visible as ovoid, low relief, mostly laterally facing surfaces. The horizontal laminar process also extends further posteriorly to meet the prespinal region of the axis in a tight fit. In lateral view, as it articulates with the axis, the concave posterior edge of the neural arch forms a vertically elliptical foramen with the anterior margin of the axial neural arch, as noted in previous works (Georgi & Krause, 2010; Pol, 2005), it represents the passage of the second cervical nerve (Figure 8d–f). Similarly, the foramen concave anterior border functions as passage for the first cervical nerve. The pedicles are projected anteroventrally by a laterally compressed process and display two articular areas set roughly at 45° from one another. Anteriorly, the neural arch contribution to the cotyle receives the occipital condyle, being an anteromedially directed half-moon-shaped surface, whereas posteriorly a triangular area forms the articular surface for the odontoid process. Despite the presence of a medial lamina emerging from the horizontal process, with clear ventrally inclining ends, the neural arches do not seem to meet along the sagittal plane, and no preserved bony processes appear to bridge this gap.

The axis (Figure 8d–f) presents a trapezoidal centrum in lateral view, marked by a lateromedial compression that generates elliptical depressions on its surface, a common feature throughout the axial skeleton of notosuchians (Pol, 2005). Ventrally, a conspicuous concavity is seen, divided by a prominent sagittal keel, which anteriorly and posteriorly transition into ventral expansions, the latter being more pronounced than the former. Additionally, centroparapophyseal laminae occur lateroventrally, running along the centrum and expanding anteriorly into the parapophyses. These face mostly ventrally. Firmly sutured to the anterior cotyle of the centrum, the odontoid process is characterized by a triangular profile in lateral view and a concave, half-moon-shaped outline in anterior view. The process is transversely expanded, having two anterolateral projections with horizontal platforms where the neural arches articulate. It is also marked by an anteriorly projecting medial ridge that fits the medial sulcus of the occipital

condyle, likely limiting lateral movements of the skull. Ventrally the odontoid process is slightly convex for the reception of the intercentrum.

The atlas-axis complex articulates with two pairs of cervical ribs, the anteriormost being unicapitate and contacting the lateroventral atlantal rib facet of the intercentrum. The posterior one is bicapitate attaching to two facets on the lateral surface of the odontoid process. These processes are separated by a depression. Parapophyses seem to contribute with the atlantal rib facet, whereas there is no sign of the diapophyses playing a similar role regarding the axial ribs. The axial neural arch is distinctly tall, with slight lateral concavities, and extends the entire length of the centrum. It is visibly not fully fused with the centrum, having a partially open neurocentral suture. The pedicles are transversely expanded and retain portions where the surface texture in contact with the centrum is relatively smooth. In anterior or posterior views, the neural canal is rounded and bears an interesting feature also present on posterior cervical vertebrae, that is, a longitudinal sulcus on the ventral wall of the neural canal. This sulcus has a rectangular cross section and extends medially along the canal.

Prezygapophyses are elliptical in shape, vertically positioned, and anterolaterally facing. A low spinozygapophyseal lamina is present, laterally bounds the prespinal lamina of the neural spine. The latter tapers ventrally, failing to reach the prespinal fossa. Differing from its anterior counterparts, the postzygapophyses are ventrolaterally inclined and bears a spinopostzygapophyseal lamina. This lamina, despite partial damage, can be determined to have been anteroposteriorly more stretched than the anterior spinal lamina. The neural spine is a laterally compressed, posterodorsally inclined projection with a rectangular profile in lateral view. Moreover, its anteroposterior length decreases dorsally.

4.4.2 | Remaining pre-sacral vertebrae

The remaining cervical and dorsal vertebrae are articulated and exposed in right lateral view. Consistent with the specimen's age at the time of death as estimated by previous histological work, both cervical and dorsal vertebrae show only partially closed neurocentral sutures (Brochu, 1996), with clear signs of the onset of fusion, but not fully sutured (Figure 9a,b).

The third cervical vertebra has a rectangular centrum, being longer than it is tall or wide, with a concave ventral facet and ventral keel. Due to the ventral concavity, the keel thickens anteriorly and posteriorly into small protrusions, despite maintaining a constant width along most of its length. The anterior protrusion is slightly more

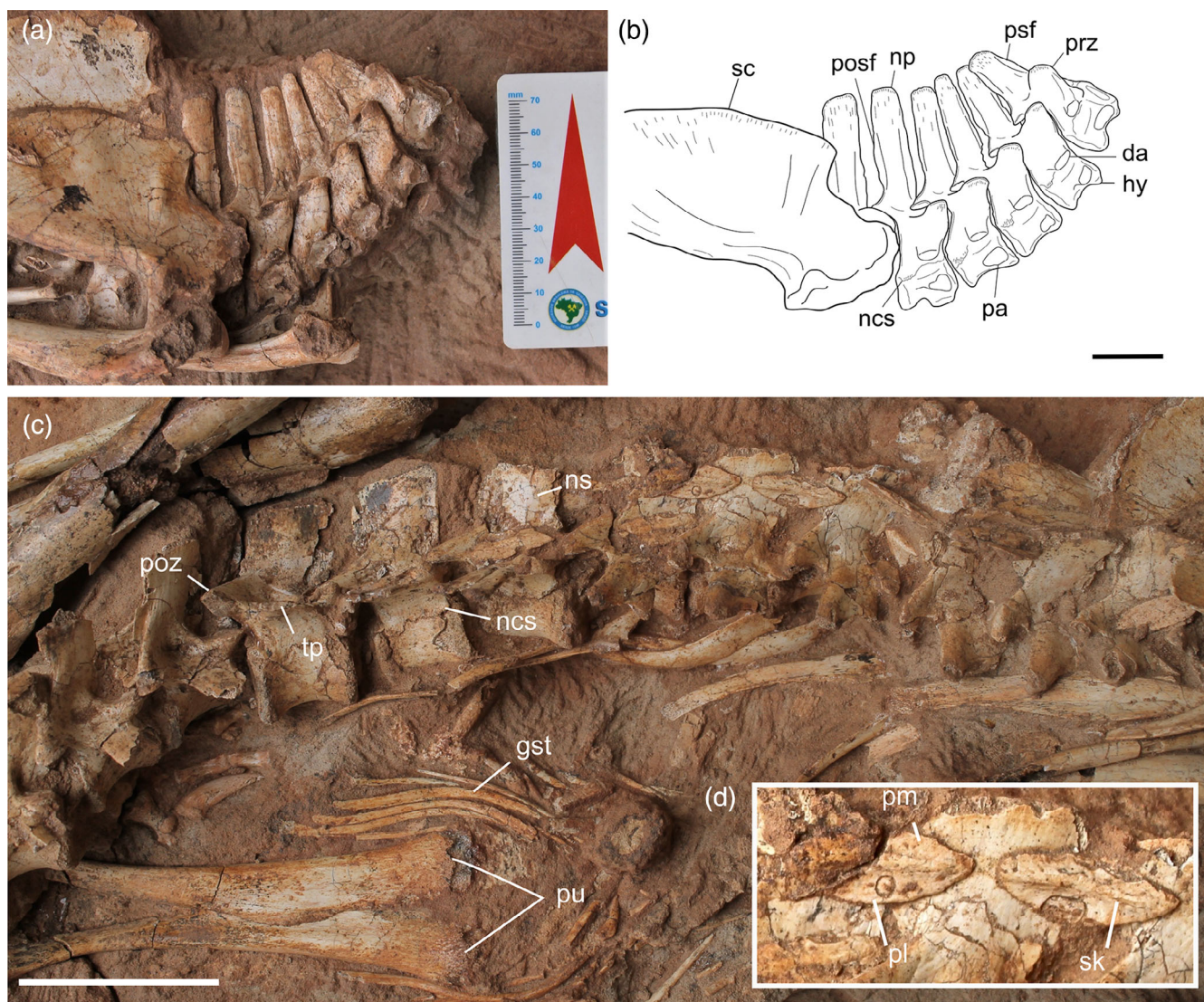


FIGURE 9 Axial skeleton of IFSP-VTP/PALEO 0003. Image of cervical series in (a) right lateral view, (b) with line interpretation. (c) Complete dorsal series in dorsolateral view. Pubes and gastralia can be seen in the lower left corner. (d) Close up of a sequence of thin, non-imbricated, and poorly sculptured dorsal osteoderms. dia, diapophysis; hy, hypapophysis; pa, parapophysis; pl, *pars laterale*; pm, *pars mediale*; poz, postzygapophyses; prz, prezygapophysis; ncs, neurocentral suture; ns, neural spine; sk, sagittal keel. Scale bar (a, b) = 1 cm, (c) = 5 cm.

prominent, forming a bulge-like hypapophysis. The mediolateral compression of the centrum, a pattern that persists onto posterior vertebrae, produces a visible horizontal ovate depression on its lateral surface, bound anteriorly and posteriorly by the raised margins of the cotyles. Parapophyses are anterolaterally placed on the lateral facet of the centrum, close to its ventral limit, and display an elongated elliptical profile with a horizontal major axis. They are significantly larger than its counterparts on more posterior vertebrae, occupying half the length of the centrum (Figure 9a,b). The neural arch is taller than long, slightly anteriorly inclined in lateral view, mediolaterally compressed and extends along the entire centrum. Prezygapophyses and diapophyses are connected by a robust lamina,

which is not as conspicuous on posterior vertebrae. The articular surface of the diapophyses are rounded and point ventrolaterally. The prezygapophyses form a more acute angle, roughly 45°, than the postzygapophyses, that are closer to the horizontal plane. Posteriorly, the neural arch shows a slight lateral compression for the accommodation of the prezygapophyses of succeeding vertebra. The neural canal is large, with a circular cross section and a featureless, smooth inner surface. It is bound laterally by transversely expanded pedicles.

As expected, the neural spines form a lateromedially flattened vertical projection, having a rectangular shape with a rounded dorsal tip in lateral view, but much shorter than on posterior elements. It is somewhat centrally

positioned on the neural arch and bound laterally at its base by shallow depressions that extend anteroposteriorly between pre- and postzygapophyses, most likely corresponding to the attachment site for *Mm. interarticularis* (Tsuihiji, 2005). The neural spine is also marked by pre-spinal and postspinal laminae, the former tapering into an anterior depression between prezygapophyses and the latter bisecting the postspinal fossa (pf). Additionally, there are well-defined prezygapophyseal and postzygapophyseal laminae that ascend and merge into the neural spine, extending parallel to the prespinal and postspinal laminae.

Cervical vertebrae four and five differ from the preceding elements by having anteroposteriorly shorter centra, thus more quadratic in lateral view, as well as more pronounced ventral keels. Anteriorly, these keels develop a low relief ventral projection treated here as hypapophyses. The articular surface of the parapophyses undergo a significant change in form, reducing their length anteroposteriorly and expanding dorsoventrally, assuming an inverted D-like shape. Diapophyses become flatter and start to shift posteriorly, but still retain a posteroventral orientation, bordering the neurocentral suture. Here both zygapophyses are more horizontal and, most importantly, anteriorly start to exhibit a clear prezygapophyseal bulge ventral to the articular facet, which might be related to *M. longissimus* group (Tsuihiji, 2007). Neural spines are placed posteriorly, their posterior edge now roughly parallel to the posterior cotyle. Furthermore, these become distinctly elongated with forward-inclining distal ends.

The sixth and seventh cervical vertebrae have marginally longer centra and also deeper, and more noticeable lateral depressions, which are bound dorsally by the diapophysis and the neurocentral suture and ventrally by the parapophysis. The latter increases the capitular articular area, with the same outline as in the more anterior elements. Ventrally, the centra have high longitudinal keels that transition anteriorly to rectangular-like hypapophyses in lateral view. Diapophyses continue to become more dorsoventrally compressed, assuming increasingly more dorsal positions on the neural arch, with their articular facets more posteriorly facing. Posterior cervical vertebrae also show a tendency to exhibit taller, anteroposteriorly shorter neural arches and more dorsally projecting prezygapophyses. These are also distinguished by the presence of clear dorsoventral parallel muscle striations on the outer edges of their prezygapophyses, absent on anterior vertebrae. Neural spines, in addition to becoming taller up to the eighth cervical, have substantially larger prespinal and postspinal laminae, that increase their superficial areas up to the middle section of the spine, giving it a convex aspect laterally but tapering dorsally. This is also seen in modern crocodylians and seems to represent increasing attachment surfaces for the

intervertebral *Mm. interspinales* (Tsuihiji, 2007; Vieira et al., 2016).

The last cervical vertebra follows the general pattern described previously in *B. albertoi* (Nascimento & Zaher, 2010), where the parapophyses have a kidney-like shape in lateral view, differing sharply from anterior ones. It also has a markedly tall and anteroposteriorly more stretched neural spine with squarish dorsal ends in lateral view. The centrum is similar to the previous ones of the series regarding its anteroposterior length and typical lateral compression. Unfortunately, further details on this vertebra could not be properly assessed because the scapula obscures most of its morphology.

4.4.3 | Dorsal vertebrae

Comprised of 15 vertebrae, the dorsal series is mostly articulated, except for posterior lumbar vertebrae, where centrum cotyles do not seem to come into contact with one another. These elements are preserved in a similar fashion to the cervical vertebrae, exposed in right lateral view (Figure 9c). Despite partial concealment by the right scapula, it is still possible to discern the general morphology of the first two dorsal vertebrae. Their centra have a squarish profile in lateral view, anteroposteriorly longer than tall or wide, as well as characteristic kidney-like parapophyses. The dorsal migration of the latter along the dorsal series is noticeable as its dorsal margin surpassed the neurocentral suture, partially reaching the lateral surface of the pedicles. The diapophysis is at the same plane as the zygapophysis on the second dorsal vertebra but is not confluent with them, with a laterally facing concavity separating these structures. Zygapophyses have elliptical articular surfaces, and are still inclined on a steep angle, but increasingly become horizontalized on posterior elements. As in cervical vertebrae, neural spines are tall, laterally flattened and anteroposteriorly short.

Posteriorly, the series is marked by anteroposteriorly stretched and laterally compressed centra, assuming a classic spool-like shape (Pol, 2005), with smooth and concave lateral and ventral surfaces. Parapophyses have fully migrated to the neural arch, being integrated with the diapophyses into the transverse process, where a small lateral concavity separates the two. Despite still being somewhat ventromedially placed on anterior dorsal vertebrae, the parapophyses gradually shift dorsolaterally, eventually reaching the same level as the diapophyses. Neural arches become stretched anteroposteriorly, fitting the length of the centra.

Mid and posterior dorsal vertebrae also have medio-laterally flattened and rectangular neural spines in lateral view, as well as robust spinopostzygapophyseal laminae,

that merge into the spinal body, attenuating as these laminae extend anterodorsally on the neural spine lateral facet. Well-developed postspinal fossae are also present, bisected by a conspicuous vertical postspinal lamina. Zygapophyseal articular facets face dorsally anteriorly and ventrally posteriorly, roughly parallel to the horizontal plane.

4.4.4 | Sacral vertebrae

The specimen possesses three sacral vertebrae, a common character for notosuchians (Martinelli et al., 2018; Nascimento & Zaher, 2010), but unlike extant crocodylians, which only have two (Ristevski, 2019; Vieira et al., 2016). Unfortunately, the neural arches and spines display substantial erosional damage, almost completely obliterating the superficial features of the second/middle element.

All sacral vertebrae are characterized by spool-shaped centra, wide and horizontally stretched neural arches, as well as robust, laterodorsally projecting sacral ribs. Confirming the skeletal immaturity of the specimen, the latter had not fully fused to the ilium at the time of the animal's death. The first two sacrals attach at a more anterior position with respect to the third, that is posteriorly-shifted toward the end of the postacetabular process. The first sacral vertebra generally resembles the lumbar elements, with elliptical zygapophyseal facets set at a roughly 45° inclination and anteriorly-shifted neural spines with prominent prespinal laminae. Its ribs emerge anterolaterally and have posteromedially inclined attachment surfaces that conform to the medial wall of the preacetabular process, resulting in a triangular shape in dorsal view.

The middle element has the largest and more robust set of sacral ribs, bearing an hourglass shape with markedly concave anterior and posterior margins. The sacral ribs attach to a more ventromedial position in the vertebra, compared to the anterior vertebra. The attachment/sutural expansion is much longer than in the remaining sacrals, encompassing a wider area of the iliac medial surface. The third sacral vertebra shares a similar, more slender rib morphology with the first element, except that these are more posteriorly inclined.

4.4.5 | Ribs

Out of eight cervical vertebrae, only two right side ribs have been preserved, whereas the dorsal series is mostly complete and semi-articulated, excluding the terminal lumbar vertebrae, which lack ribs. The cervical ribs have the recurrent plow-shaped form observed in other archosaurs (Romer, 1956), with an anteroposteriorly stretched

shaft orthogonal to bifurcating articular processes. The tuberculum is more dorsally positioned than the capitulum, both being of similar length and roughly aligned. The latter is slightly thicker and displays a larger articular facet. Posteriorly, the tubercular process is additionally connected to the shaft by a visible lamina that extends along its surface dorsally. The capitular process is slightly inset in relation to the medial margin, where an ill-developed longitudinal flange is present. Externally, the outer margin of the shaft is mostly straight, with only minor undulations, whereas medially it is marked by a strong, channel-like concavity. The shaft extends substantially further posteriorly than anteriorly, with both parts tapering to a point at their ends.

Naturally, dorsal rib morphology changes as the parapophyses migrate dorsally toward the transverse process, thus shifting the position of the costovertebral articulation. Capitula and tubercula gradually start to emerge and bifurcate roughly out of the same plane, with the processes of the former longer and more robust than those of the latter. Shafts become substantially more elongate, shifting from an anteroposterior orientation to a more posteroventral position. These are comprised of dorsoventrally stretched but lateromedially compressed projections that bow outward at mid length. As the series progresses, the articular processes become less projected, the incisure that separates the capitulum and tuberculum decreases, and eventually both assume a cojoined aspect posteriorly. The shafts of anterior dorsal ribs are very characteristic, due to their greater size and the presence of a large, anterior semi-lunate lamina that taper distally. Posterior elements have shorter and more strongly bowed shafts, culminating at the rod-like last rib.

4.5 | Forelimb and pectoral girdle

4.5.1 | Scapula

Both left and right elements of the pectoral girdle are preserved, yet only right side components could be thoroughly described given that the left counterparts are totally or partially covered by the cervical vertebrae and the right girdle. The dorsal outer edge of the scapular blade has been damaged, lacking portions of its posterior and anterodorsal regions, whereas its ventral margin has minor erosional loss on the coracoidal and glenoid surfaces. The scapular blade has also been partially perforated by a dorsal vertebra neural spine, evidence of taphonomic compression. In general terms, the scapula is a dorsoventrally tall, but lateromedially flat component of the pectoral girdle, with three major anatomical portions: the fan-shaped, anteroposteriorly expanded

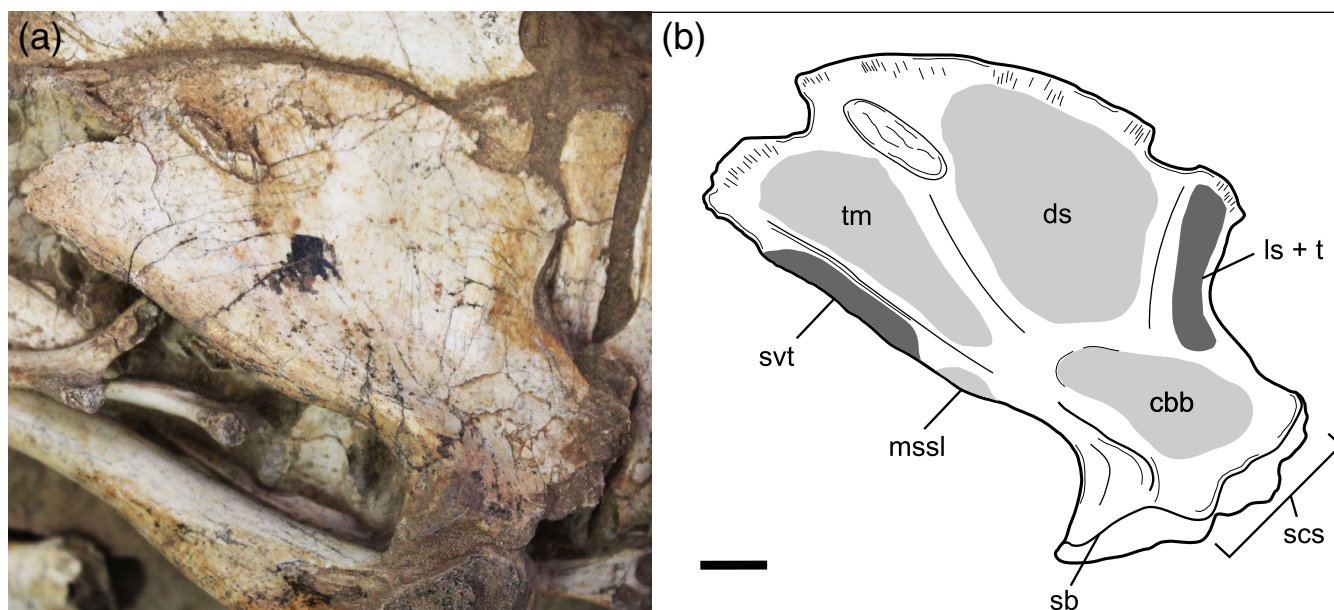


FIGURE 10 Left scapula in lateral view (a) and schematic drawing with inferred muscle origination (light gray) and insertion (dark gray) areas. cbb, *M. coracobrachialis brevis*; ds, *M. deltoideus scapularis*; ls + t, *M. levator scapulae* and *M. trapezius*; mssl, medial scapulosternal ligament; sb, scapular buttress; scs, scapulocoracoid suture; svt, *M. serratus ventralis thoracis*; tm, *M. teres major*. Scale bar = 1 cm.

scapular blade, marked by a conspicuous rounded dorsal edge; the short and anteroposteriorly constricted scapular shaft; and the ventral base, characterized anteriorly by the scapulocoracoid suture (scs), as well as the glenoid fossa and the scapular buttress (sb) (Figure 10).

In right lateral view, the scapular blade is posteriorly-shifted in respect to its base, resulting in an obliquely-oriented bone. The blade displays a straight posterior margin whereas the anterior is markedly concave, especially at the transition toward the shaft. Its broad, lateral surface displays three major depressions, separated by anterior and median ridges, with muscle scars on the dorsal edge of the blade in each of these regions.

The anteriormost sulcus is a slightly curved, dorso-ventrally elongated, and thin depression, bound anteriorly by the edge of the scapular blade and posteriorly by the low relief anterior ridge (ar). It is thus inferred to have been the insertion area for the trapezoidal muscle, as well as for *M. levator scapulae*. Posterior to the latter is a large trapezoidal depression where *M. deltoideus scapularis* originates, bound posteriorly by the median ridge, and followed by the slanted and triangular-shaped depression for *M. teres major* (Figure 10b). The slightly deflected posterior margin is marked by the insertion of *M. serratus ventralis thoracis* (svt) dorsally and the origin region of the medial scapulosternal ligament ventrally (mssl). The scapular shaft and ventral base are marked by a deep excavation which is topologically consistent with the origination of *M. coracobrachialis brevis*.

4.5.2 | Coracoid

The coracoid composes the lower half of the shoulder girdle, contributing to the glenoid fossa (Figure 11a–d). Dorsally, it is marked by a robust and blocky epiphysis, with a large semicircular depression on its lateral side perforated by a prominent coracoid foramen (cf), located close to the eroded glenoid facet. The latter depression represents the origin site of *M. supracoracoideus* (sc). The irregular suture/synchondrosis edge with the scapula is found dorsally, bound posteriorly by the posterolaterally sloping glenoid surface. From its articulation with the scapula, the coracoid was posteroventrally inclined in life. The shaft is elongated, somewhat laterally compressed, and visibly outwardly arched, with concave anterior and posterior margins. Just ventral to the glenoid's pendulous facet, a deep fossa served as the attachment site for the medial scapulosternal ligament.

Distally, along the posterior margin of the shaft, a sulcus, similar to the insertion for *M. costocoracoideus superficialis* in extant and fossil crocodyliforms (Meers, 2003; Sertich & Groenke, 2010) is seen. Midway along this same surface, the coracoid origin site for *triceps* muscle bundles is present as a small circular rugosity. The distal fan-shaped expansion bears vertical muscle scarring on its medial side, corresponding to origin of *M. coracobrachialis brevis* ventralis that inserts on the proximal end of the humerus.

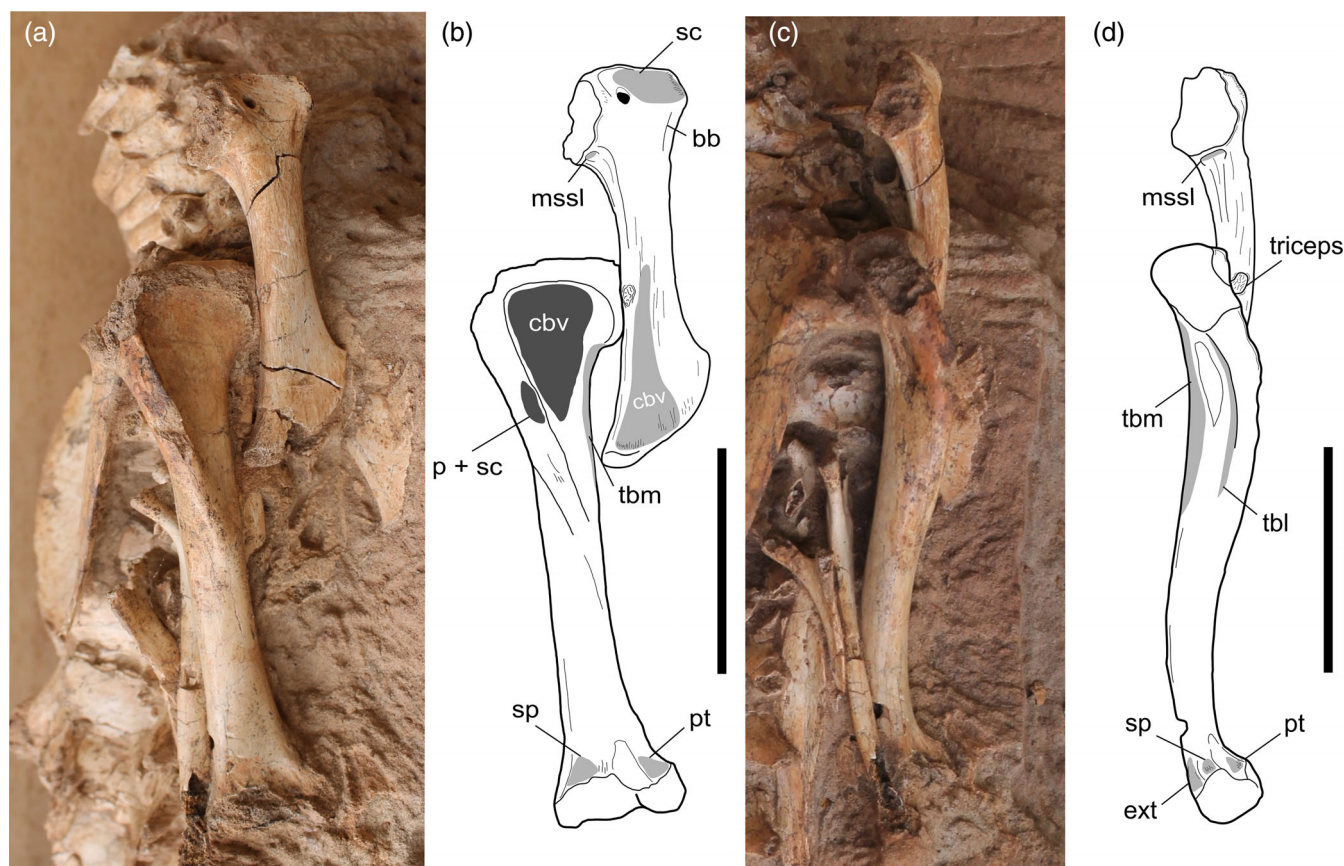


FIGURE 11 Right humerus and coracoid with myological interpretations of origination (light gray), and insertion sites (dark gray) based on osteological correlates. Humerus in (a, b) anterolateral and coracoid in (c, d) ventrolateral view. bb, *M. biceps branchii*; ext, distal extensors; mssl, medial scapulosternal ligament; p + sc, *M. pectoralis* and *M. supracoracoideus*; pt, *M. pronator teres*; tbl, *M. triceps branchii caput laterale*; tbm, *M. triceps branchii caput mediale*; sc, *M. supracoracoideus*; sp, *M. supinator*. Scale bar = 5 cm.

4.5.3 | Stylopodium (humerus)

The humerus is an elongate element, marked by a transversely expanded, anteroposteriorly flattened proximal end, a straight shaft in anterior view, and prominent distal condyles, with little rotation between proximal/distal ends and the shaft (Figure 11a–d). In lateral or medial views, the proximal articulation curves posteriorly, whereas the distal portion bends anteriorly, seemingly giving the distal condyles an anterior projection. The proximal end is characterized by a wide/broad, trapezoidal outline in anterior or posterior views, possessing distinct medial and lateral tubercles adjacent to the medial glenohumeral condyle. The articular condyle is straight and horizontalized, extending considerably posteriorly, whereas the medial tubercle has a pronounced rounded margin and the lateral one a sharper, lateroventrally inclining edge. There seems to be no clear depressions separating the glenohumeral condyle from lateral and medial tubercles anteriorly, forming a somewhat continuous humeral proximal surface.

Anteriorly, the proximal end presents a large triangular-shaped depression with a rounded dorsal margin for the insertion of *M. coracobrachialis brevis ventralis* (cbv; Figure 11b). This is limited dorsally by the glenoid protuberance and laterally by the deltopectoral crest, along with muscle scars on its medial edge, where the *Triceps brevis medialis* (tbm) would originate, extending distally along the shaft. The pectoral crest emerges lateroventrally from the lateral humeral protuberance, reaching a maximum width at its mid length, where an anterolateral insertion area is found for both *M. pectoralis* and *M. supracoracoideus* (p + sc), then tapering distally as it integrates into the shaft. Its distal portion is medially-shifted and extensive, so that the pectoral crest extends roughly half the total humeral length. Its proximolateral surface has, dorsal to the pectoralis and coracoideus, two successive, circular depressions: the smaller one likely *M. deltoideus scapularis* (ds) and a larger more elliptical one, with vertical striations interpreted as scars of *M. deltoideus scapularis* (dc). Ventral to those depressions, with a more posterolateral position in relation to

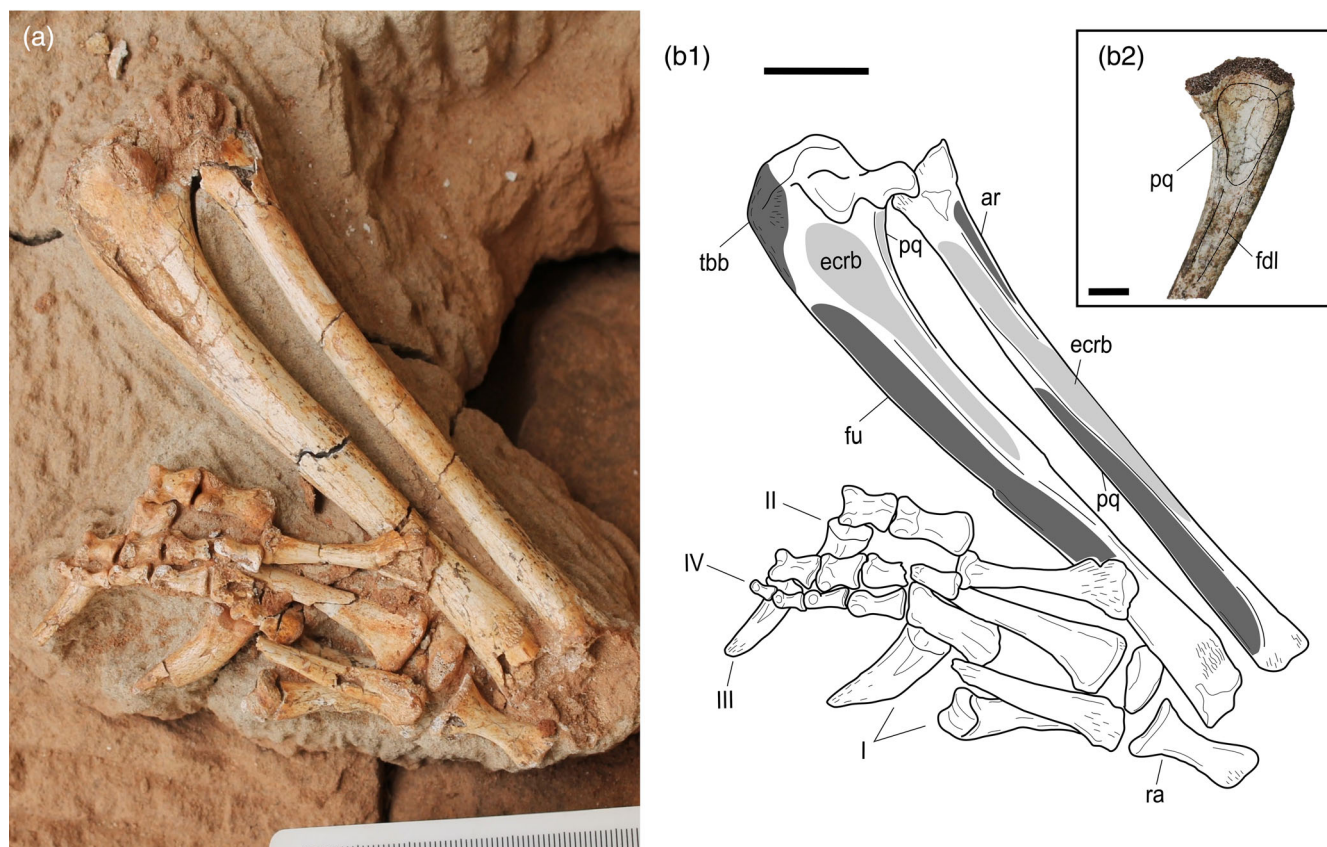


FIGURE 12 Right ulna and radius in lateral view with myological interpretations of origination (light gray) and insertion sites (dark gray), as well as all preserved autopodium elements. (a, b1) photograph with line interpretation and (b2) detail of medial facet of ulnar proximal epiphysis. ar, anterior ridge; ecrb, *M. extensor carpi radialis brevis*; fdl, *M. flexor digitorum longus*; fu, *M. flexor ulnaris*; pq, *M. pronator quadratus*; tbb, *M. triceps branchii*. Scale bars: b1 = 2 cm; b2 = 1 cm.

the deltoid crest, there is a large negative relief area, roughly vertical, and limited medially by the *Triceps brevis cranialis* crest, that possibly marks the origin of *humero-radialis*.

Due to the preserved position of the right humerus, the depression for *M. scapulohumeralis* cannot be clearly distinguished, though its presence is inferred by the presence of the laterally preceding crest occupied by the *Triceps brevis*. Lateromedially, there is a small vertical crest medial to the pectoral crest which might be a marker for *Triceps brevis cranialis*. The distal condyles are transversely expanded and markedly asymmetrical in both anterior and posterior views, where the lateral radial condyle is substantially larger than the medial ulnar condyle. These are separated by a narrow trough that extends into the anterior region. Additionally, just proximal to the condyles (anteriorly), a wide depression forms, separating lateral and medial ramifications. In anterior view, the radial condyle is lateromedially wide and elliptical in shape, whereas the ulnar is more rounded. The medial and lateral views reveal an anterior extension of the articular surfaces and a somewhat limited backward

movement between stylopodium and zygapodium as the condylar area is not developed posteriorly. Muscle scars in the form of vertical and oblique striations indicate origin sites for *M. pronator teres* proximal to the ulnar condyle and *M. supinator* above the radial articular surface. The *supinator* attachment seems to be separated from the extensor group by a vertical change in surface relief, giving rise to a more verticalized origin area for the latter (Figure 11c,d).

4.5.4 | Zygapodium (ulna and radius)

This portion of the forelimb is mostly complete on the right side with both the ulna and radius well-preserved and articulated, whereas left side elements are missing (Figure 12a,b). Their shafts are marked by a few longitudinal but mainly transverse fractures. The distal ends of both elements are not preserved due to a fracture that also damaged the carpals. The ulna is an elongated and laterally flattened element, with a convex lateral surface and a concave medial one, resulting in a noticeable medial bend

of the shaft. The element is considerably anteroposteriorly and transversely thicker proximally than distally, mostly owing to the development of the humeral and radial articular surfaces in addition to the olecranon process.

The proximal glenoid facet is marked by a semi-lunate anterior surface with two distinct lobes, a lateral and a medial one, for the articulation of the humeral condyles. Additionally, distal to these lobes, there is a slightly ventrally deflected edge where the proximal head of the radius would rest. Laterally, the most prominent humeral articular facet covers the outer surface and is more proximodistally developed than the medial one. In lateral view, it is possible to observe a partial erosion of the olecranon process, which does not extend substantially posterior to the proximal articular region. Its posteroventral margin is somewhat rounded and bears muscle insertion marks for *M. triceps branchii* (tbb), while proximally the olecranon process is a mediolaterally compressed expansion, roughly aligned with the ulnar major axis.

The shaft displays an anterior, low relief ridge that tapers distally and most likely limited the extension of *M. pronator quadratus* (pq) onto the dorsolateral facet of the humerus. A lateral aspect reveals an additional longitudinal ridge, extending mostly along the mid-section of the shaft, as well as a similarly oriented sulcus closer to the proximal metaphysis. Ventral to the glenoid articular facet, in lateral view, the ulna bears a shallow depression that extends distally and is consistent with the origin area of *M. extensor carpi radialis brevis* (ecrb). Extending parallel to the longitudinal sulcus, and ventral to it, yet another elongated depression is observed, here interpreted as the insertion area for *M. flexor ulnaris* (fu), due to its proximodistal position.

A medial view of the proximal end of the ulna reveals additional muscle attachment sites (Figure 12 b₂), including a large, triangular depression, encompassing the medial surface of the olecranon process, followed distally by a narrow sulcus that extends the length of the shaft. These represent *M. pronator quadratus* (pq) and *M. flexor digitorum longus* (fdl), respectively.

The radius is a straight, gracile, and elongated bone, the shaft of which retains a somewhat constant thickness throughout its length. A slight ventrolateral flexure of the proximal portion is present but does not propagate distally. The entire bone shows a slight anteroposterior compression. Its proximal and distal articular regions, although not fully preserved, lacking the articular facets, are marked by clear mediolateral expansions, and bear visible striations for muscle attachments.

The shaft bears an anterior ridge that emerges anterolaterally on the proximal process and then shifts anteriorly, and also a sinuous, lateral ridge which becomes visible on the proximal portion of the shaft and then

gradually curves dorsally/anteriorly as it approaches the distal end of the bone. The area in-between ridges delimitates the origin of *M. extensor carpi radialis brevis* (ecrb), whereas dorsally the anterior ridge marks the lateral boundaries of *M. supinator*, which extends anteriorly. Ventral to the lateral edge, and located mostly ventrally along the shaft, there is the radial attachment of *M. pronator teres*. Unfortunately, the medial facet of the bone could not be described due to the surrounding matrix and fragility that prevented further preparation.

4.5.5 | Autopodium

The specimen preserves an almost complete and semi-articulated right manus, including proximal carpals (ulnar and pisiform), except for the radiale, likely lost to the erosional fracture surrounding this region. The manus is exposed in palmar view (Figure 12a,b), owing to a strong taphonomic outward inflection, which also partially disarticulated and dislocated metacarpals II and V, whereas MC I, III and IV remain in close association with their respective phalanges. The phalangeal formula is 2-3-4-4-? and based on previously published work by Nascimento and Zaher (2010), which established a phalangeal formula of 2-3-4-4-3 for *B. albertoi*, and given the lack of digit V phalanges in the current specimen, we infer that they are missing, due to a fragmented MC V.

Generally, the metacarpals of IFSP-VTP/PALEO 0003 have mediolaterally expanded proximal ends that are slightly dorsoventrally compressed, with marked articulation edges where the adjacent element would rest. The shafts of MC I and II are markedly robust, with others becoming longer and more gracile laterally in the series, MC IV being the longest. Distally they display well-developed and rounded trochleae whose articular edges extend ventrally. These and the phalanges, with the exception of the distal ones, bear circular pits on the lateral surface of their trochleae, an attachment site for interosseous muscle group (Meers, 2003). The shafts of MC I and II display concave lateral margins, contrasting more rectilinear medial ones, as well as slight lateral inflection of their distal ends. The trochleae of MC III and IV are also well-developed but have a straighter orientation. Their shafts become narrower at mid length, gradually thickening again toward the distal end. The phalanges of digits I and II are sturdier and proximodistally shorter, with distinctly concave ventral surfaces and well-developed trochleae marked by deeper intercondylar fossae. Lateromedially compressed, claw-like ungual phalanges of decreasing sizes are present only on digits I, II, and III, a recurrent condition among fossil crocodylians and modern crocodylians (Colbert et al.,

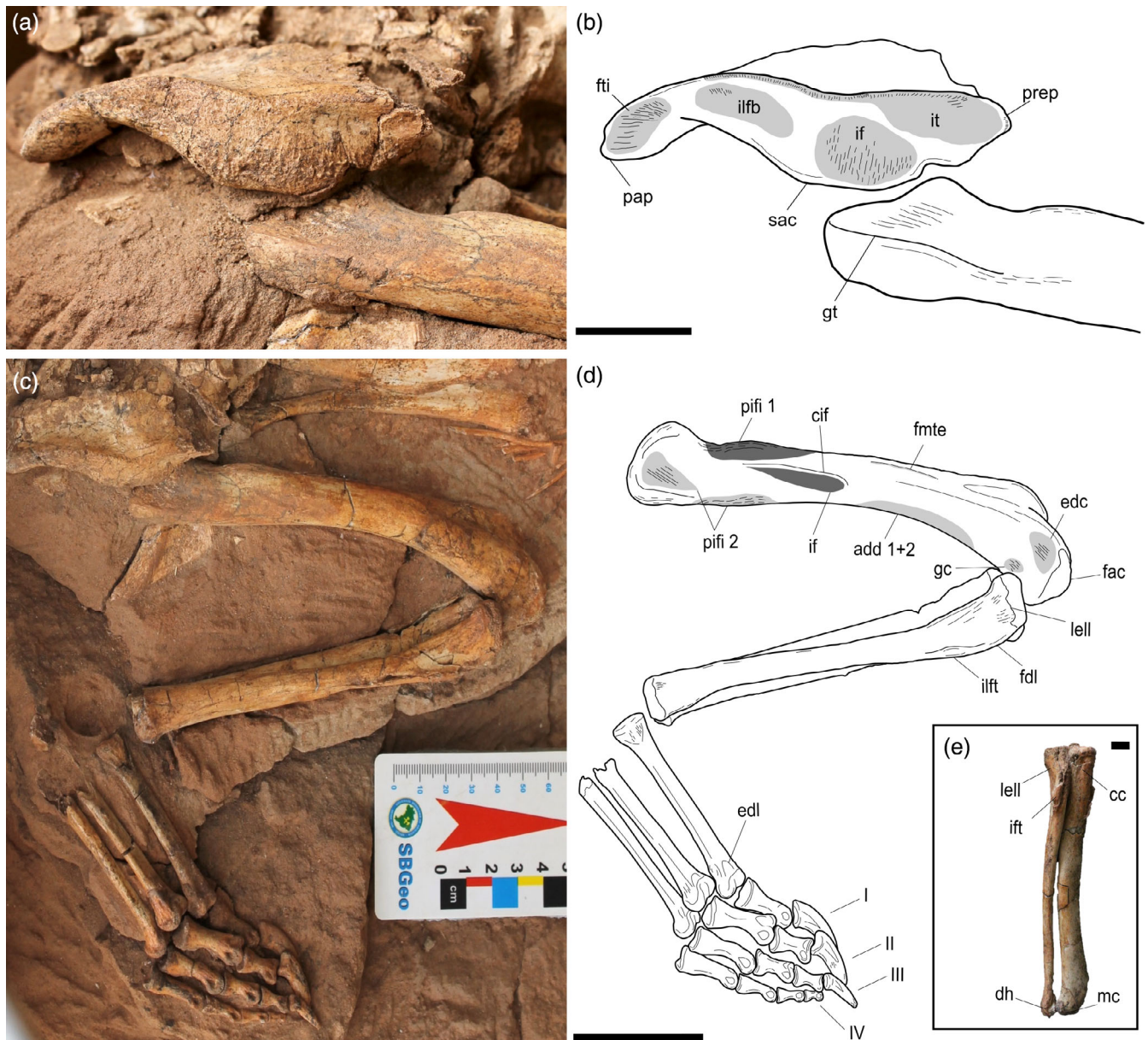


FIGURE 13 Pelvic girdle and articulated hind limb of IFSP-VTP/PALEO 0003. Ilium in right lateral view (a) and inferred muscle origins (light gray) based on textural/osteological correlates (b). (c, d) Right hind limb in lateral view and line interpretation of muscle insertions (dark gray) and origins (light gray). (e) Tibia and fibula in anterior view. add 1 + 2, *M. adductor femoris* 1 and 2; cc, cnemial crest; cif, crest for the insertion of *M. iliofemoralis*; dh, distal hook of fibula; edl, *M. extensor digitorum longus*; fac, fibular articular facet of the femur; fdl, *M. flexor digitorum longus*; fmte, *M. femorotibialis externus*; fti, *M. flexor tibialis internus fascia*; gc, *M. gastrocnemius*; gt, great trochanter; if, *M. iliofemoralis*; ift, *M. iliofemoralis* trochanter; iflb, *M. iliofibularis*; it, *M. iliotibialis*; lell, external lateral ligament; pap, precetabular process; prep, postacetabular process; pifi 1, *M. puboischiofemoralis internus* 1; pifi 2, *M. puboischiofemoralis internus* 2; sac, supracetabular crest. Note ventrally inclined supracetabular crest and possible abduction of femur. Scale bar (a, b) = 2 cm; (c, d) = 5 cm and (e) = 1.

1951; Grigg, 2015; Nascimento & Zaher, 2010; Sertich & Groenke, 2010). These articulated with their proximal phalanges in a slightly laterally inclined manner and bear triangular lateral neurovascular sulci. Digit IV displays a series of four morphologically similar phalanges that diminish in size distally. These are characterized by tapering, less developed thochleae.

4.6 | Hind limb and pelvic girdle

All elements of the pelvic girdle are present and relatively well-preserved, despite the visible dorsoventral compression to which the entire set was submitted. Both ilia are medially sutured to two sacral vertebrae, through their transversely expanded ribs. Ischia were laterally

deflected to the right side due to taphonomic forces, but their proximal ends are properly connected with the ilia, enclosing the acetabulum, to which both femora are articulated. The pubes were also preserved close to their life position, anteroposteriorly-oriented and meeting along their medial edge.

4.6.1 | Ilium

The ilium morphology is unique due to the short, anteriorly tapering preacetabular process, a strong ventral deflection of the supracetabular process and an anteroposteriorly developed, postacetabular process, that makes up more than half the length of the entire element (Figure 13a,b). In anterior/posterior view, the acetabular wall is medially set in respect to the acetabular roof, thus resulting in an inverted L-like shape. These features generate a sigmoidal shape in lateral view, where the ventral border of the iliac blade is sharply convex anteriorly, while acutely concave posteriorly, along the postacetabular process. The dorsal margin follows the opposite concavity/convexity pattern. In dorsal view, the ilia are also marked by a substantial latero-medial expansion, resulting in highly developed acetabular roof, that laterally obscures and overhangs the deeply inset acetabular wall, which could not be observed due to the articulated femora. This gives the ilia a somewhat trapezoidal shape dorsally. As mentioned previously, the preacetabular process tapers toward the anterior end, but reaches roughly the same level as the anterior margin of the first sacral prezygapophyses. It is medially accompanied by a similar anterior projection, thus creating an anteriorly concave margin.

Dorsally, the iliac blade has a conspicuous depression that extends its length and is bound laterally by the thickened edge of the supracetabular crest. The lateral surface of the latter bulges outward, especially directly above the acetabulum, and possesses a few osteological cues for muscle insertions/originations. The lateral view reveals a dorsal margin marked by continuous local rugosities which seem to merge anteriorly with the laterally depressed preacetabular process, which bears vertical and longitudinal striations. Together, these likely marked the origin of *M. iliotibialis* (it—Figure 13). The highest rugosity density consisting of vertical sulci and striations may be found on the surface of the supracetabular crest, which is consistent with the insertion of *M. iliofemoralis* (if), given similar configurations in extinct and extant pseudosuchians (Liparini & Schultz, 2013; Romer, 1923). These are followed posteriorly, along the transition toward the postacetabular process, by fewer rugosities and a shallow and somewhat oblique elliptical depression where *M. iliofibularis* (ilfb) would originate. The postacetabular

process has a clear posteroventral deflection on its posteriormost end, forming a lateroventral surface with oblique muscle scars, the site where *M. flexor tibialis internus fascia* (fti) would attach. It is here inferred that the inset nature of the acetabular wall and the verticality of the supracetabular crest would strongly hinder the abduction of the femur, thus constantly forcing a “pillar-erect” parasagittal gait (Bates & Schachner, 2011), where most of the weight of region would rest on the proximal end of the femur, mostly limiting it to fore-and-aft movements.

4.6.2 | Pubis

These are the anteriormost elements of the pelvic girdle and both sides are preserved in their full extent. The pubic bones are exceptionally elongated, reaching the same level as the tenth dorsal vertebra anteriorly, and have two distinct broader portions separated by a long shaft (Figure 9c). The posterior pubic head (ph) is transversely narrow and has a vertical articular surface that attaches to the pubic pedicle of the ischium, whereas anteriorly the tubular shaft becomes wider as it reaches the distal pubic blade (pb), forming a tabular-like dorso-ventrally flattened anterior end, with a squared margin in dorsal view. There is a clear rotation between these two regions of the pubis, as recognized in other baurusuchids (Godoy et al., 2016), with the shaft transitioning from a dorsomedial orientation posteriorly to a horizontal disposition anteriorly.

In dorsal view, the pubis is clearly bent medially, generating laterally oblique ends as well as a medial pubic symphyseal margin (psm) at mid length, where counterparts come into contact. This region is characterized by the development of a pronounced medial lamina, with a shallow elliptical depression on its dorsal surface. The shaft surface is mostly smooth, whereas the pubic blade displays anteroposterior striations and muscle insertion marks on its distalmost edge. Once this surface would have faced medially in life, it is thus interpreted as insertion scars for *M. pubioischiofemoralis externus* 1 (PIFE 1 sensu Romer, 1923).

4.6.3 | Ischium

Owing to the way the pelvic girdle was preserved, the left ischium is not available for description as it is still embedded in the surrounding sandstone. The right element, although visible, is partially obstructed by the right femur, precluding a more detailed description of its proximal region. The ischium follows the general shape seen in crocodyliforms (Colbert et al., 1951; Pol et al., 2012; Romer, 1923;

Vieira et al., 2016), with a quadrangular, mediolaterally compressed iliac blade (ib) with strongly and slightly concave posterior and anterior edges, respectively.

In lateral view, the iliac blade bears a conspicuous proximodistal ridge close to the posterior border but separated from it by a similarly shaped groove. Anterior to it, a large, depressed surface is seen, comprising most of the lateral surface of the iliac blade. Additionally, there is a posteroventrally tapering process, which gives the blade an anteriorly inclining aspect in lateral view. Although muscle insertions left less conspicuous markings on the ischium compared to adult forms, there are clear muscle scars for the Adductor muscle 1 on the anteroventral edge of the blade, and similar striations on the anteroventral and posteroventral regions of the iliac ridge, possibly for *M. puboischiofemoralis* 3 (PIFE 3) and Adductor 2.

4.6.4 | Stylopodium (femur)

The specimen preserves both left and right femora (Figure 13c,d), but the left element is mostly unavailable for description, due to its poor state of preservation. The right femur is exposed in anterolateral view, still articulated with the pelvic girdle. It is a slender and elongate bone, slightly longer than the tibia and fibula, with a somewhat straight shaft, an only marginally expanded proximal ends with a medially inturned femoral head, and a transversely expanded condylar distal end (Figure 13c,d). The proximal end is only slightly thicker than the shaft and mediolaterally flattened, bearing a circular lateral depression. Within this depression there are proximodistal striations marking the attachment of *M. puboischiofemoralis internus* (pifi 2), which extends posterodistally to the great trochanter. Posterolaterally, the great trochanter forms a raised proximodistal crest with shallow depressions and striations posteriorly and anterolaterally to it, where *M. puboischiofemoralis externus* (pife) and the aforementioned second extension of *M. puboischiofemoralis internus* (pifi 2) would attach (Klinkhamer et al., 2017; Romer, 1923).

Anterolaterally, the proximal portion of the shaft bears an undeveloped anterior flange (af), where longitudinal muscle scars for the anterior extension of *M. puboischiofemoralis* would attach (pifi 1). Although mostly straight, the diaphysis is also slightly anteriorly curved, generating a concave posterior surface and an anterior convex one, but substantially less so than the more sigmoidal eusuchian condition (Romer, 1956).

In anterolateral view, the proximal shaft bears an elongated and shallow tear-drop shaped depression, anteriorly bound by an oblique and low crest, near the anterior flange. These represent, respectively, the insertion site for *M. iliofemoralis* (if) and its auxiliary fixation

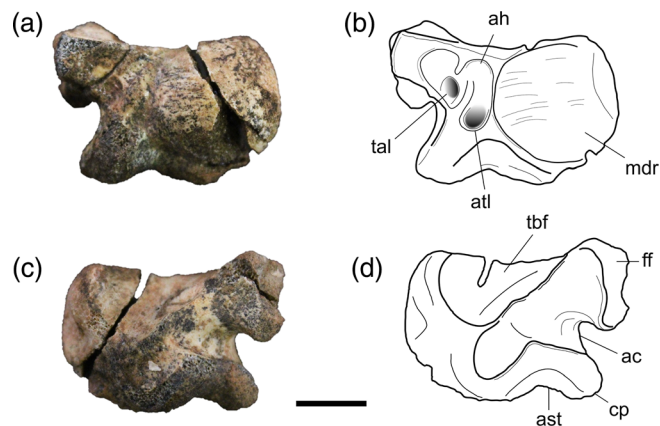


FIGURE 14 Right astragalus and corresponding line interpretation in anterior (a) and posterior (b) views. ac, articulation channel; ah, anterior hollow; ast, astragalular trochlea; atl, astragalular tarsale ligament pit; cp, calcaneal peg; ff, fibular facet; mdr, medial distal roller; tal, tibial-astragalular ligament pit; tbf, tibial articular facet. Scale bar = 1 cm.

crest (cif). Anteriorly, along the distal half of the shaft, the femorotibialis ridge (ftr) extends as a thin crest on its anterior convexity, limited distally by the intercondylar fossa (if). In the opposite concavity, the posterior adductors attach (add 1 + 2, Romer, 1923; or *M. adductor femoris* sensu Sertich & Groenke, 2010), having originated on the ischium. Distally, the shaft and both lateral and medial condyles rotate outward at about 90°. The distal end is formed by the mediolaterally expanded condyles, which posteroventrally bear the tibial articular surfaces. The lateral condyle is visibly larger, more ventrally developed and forward leaning than the medial one and both are separated anteriorly by an intercondylar fossa, emerging on the distal end of the shaft and then becoming increasingly deeper and wider ventrally. The ventrolateral margin of the lateral condyle possesses a crescent-shaped fibular condyle. Proximal to it, clear markings for the origin of *M. gastrocnemius* (gc) and *M. extensor digitorum communis* (edc) are present.

4.6.5 | Zeugopodium (tibia, fibula, astragalus)

Tibiae and fibulae are preserved on both sides (Figure 13d,e). The tibia is robust and thick with a much-expanded proximal end and a roughly circular cross section of the diaphysis. Proximally, the articular surface is somewhat triangular and flattened, accommodating both distal femoral condyles in a hinge-like articulation. Just anterior to the proximal articular surface, there is a low relief cnemial crest (*quadriceps*

femoris insertion). The tibial shaft arches outward/laterally along its middle portion, resulting in the confluence of both tibia and fibula proximally, whereas distally there is a clear gap between the two.

Distally, the tibia has wide lateral and medial condyles which articulate with the proximal tarsals, mostly the astragalus. The medial condyle contacts the fibula, whereas the lateral one extends further distally, also being laterally inclined, creating an oblique articular surface. The tibia articulates laterally with the fibula, a gracile and elongate bone distinguished by a mediolateral compression along its length in addition to a posteriorly curved and anteroposteriorly stretched proximal epiphysis. Its shaft is mostly straight, maintaining a constant thickness, and culminates into a distal expansion, bearing the tarsal articular surface distally as well as the distal hook medially that extends to contact the medial tibial condyle.

A depression and vertical striations on the lateral surface of proximal end correspond to the attachment of the long external lateral ligament (*lell*), while anterop proximally the *iliofibularis* trochanter (*ilft*) has as a thickened and swollen crest. Medial to the latter, a depression for *flexor digitorum longus* is visible.

A single right astragalus is the only well-preserved proximal tarsal element, although an oblique fracture affects the medial distal roller. In both anterior and posterior views, the astragalus has an hourglass-like shape, wider than tall but also anteroposteriorly narrow, with distinct concave dorsal and ventral margins (Figure 14). Dorsally, the astragalus is marked by the v-shaped tibial articular facet (*tbf*), where a larger and posteriorly extending depression receives the tibial medial condyle, and the laterodorsal and elongate shallow elliptical fossa, the lateral one. These facets are somewhat orthogonal to one another and delimited medially by the astragal fossa.

Anteromedially, the astragalus is dominated by a large, semicircular surface that bulges outward, the medial distal roller, where the first metatarsal articulates. By contrast, the lateral end bifurcates into a fibular articular facet dorsally, and the calcaneal peg ventrally. The latter fits into the calcaneal socket at the astragalus-calcaneum interface.

A visible anterior hollow is seen anterolaterally, defined by a shallow triangular depression which is bisected by a conspicuous crest. The medial fossa corresponds to the astragalus-tarsale ligament attachment (*atl*), at the same time as the rounded lateral one represents the tibial astragalus ligament pit (*tal*). Posterolaterally, between the fibular articular facet and the calcaneal peg, the astragalus articulation channel (*ac*) forms a deep sulcus, bounded ventrally by the astragalus trochlea.

4.6.6 | Autopodium

The right pes is articulated and mostly complete, only missing the fourth metatarsal, the proximal articular ends of MT II and III, and the smaller MT V (Figure 13c,d). Noticeably, these were preserved with shafts parallel and near one another, with minimum spread, and at an oblique angle to the plane formed by phalanges. The metatarsals are similar and share a common morphology comprised of an elongated and dorsoventrally compressed, with proximally and distally expanded ends, and a straight shaft with a uniform thickness and elliptical cross-section. Their proximodistal lengths increase, with MT I being the shortest and MT III the longest. The latter, consequently, also yields the longest digit. Distally, they bear transversely wide and strongly rounded trochleae with shallow intercondylar sulci. The distal part of the shaft, just proximal to the articular end, bears conspicuous semicircular depressions.

The trochlear articular surfaces ascend anterodorsally toward the distal metaphysis, possibly allowing for increased dorsiflexion/hyperextension of the metatarsophalangeal joint, as evidenced by manual articulation (Figure 13). This feature is present on all three preserved metatarsals. The pedal phalangeal formula, not encompassing the fifth digit is: 2-3-4-4. The proximal phalanges of digits I and II are visibly more robust and stouter than the more lateral ones. They display well-developed proximal concavities for articulation with the metatarsals, straight dorsal surfaces, and strongly concave ventral ones, giving them an arch-like aspect. Deep lateral and medial pits for ligament insertions are present on all preserved phalanges. Distal phalanges decrease in size preserving their general morphology, and digits I, II and III terminate in laterally compressed claw-like unguis, which articulate with a noticeable lateral inclination. Similarly, digit IV contains four sequential phalanges that diminish in size.

4.7 | Osteoderms

The two parallel sagittal rows of osteoderms typical of baurusuchids are poorly preserved and only three individual right side plates were found associated with the skeleton. However, these are sequential, and rest upon the neural spines of the thirteenth and fourteenth dorsal vertebrae, respectively, suggesting preservation close to their position in life.

The osteoderms of IFSP-VTP/PALEO-0003 are elliptical and symmetrical in superficial view, substantially anteroposteriorly longer than wide, with convex lateral and medial margins and a tapering anterior articular

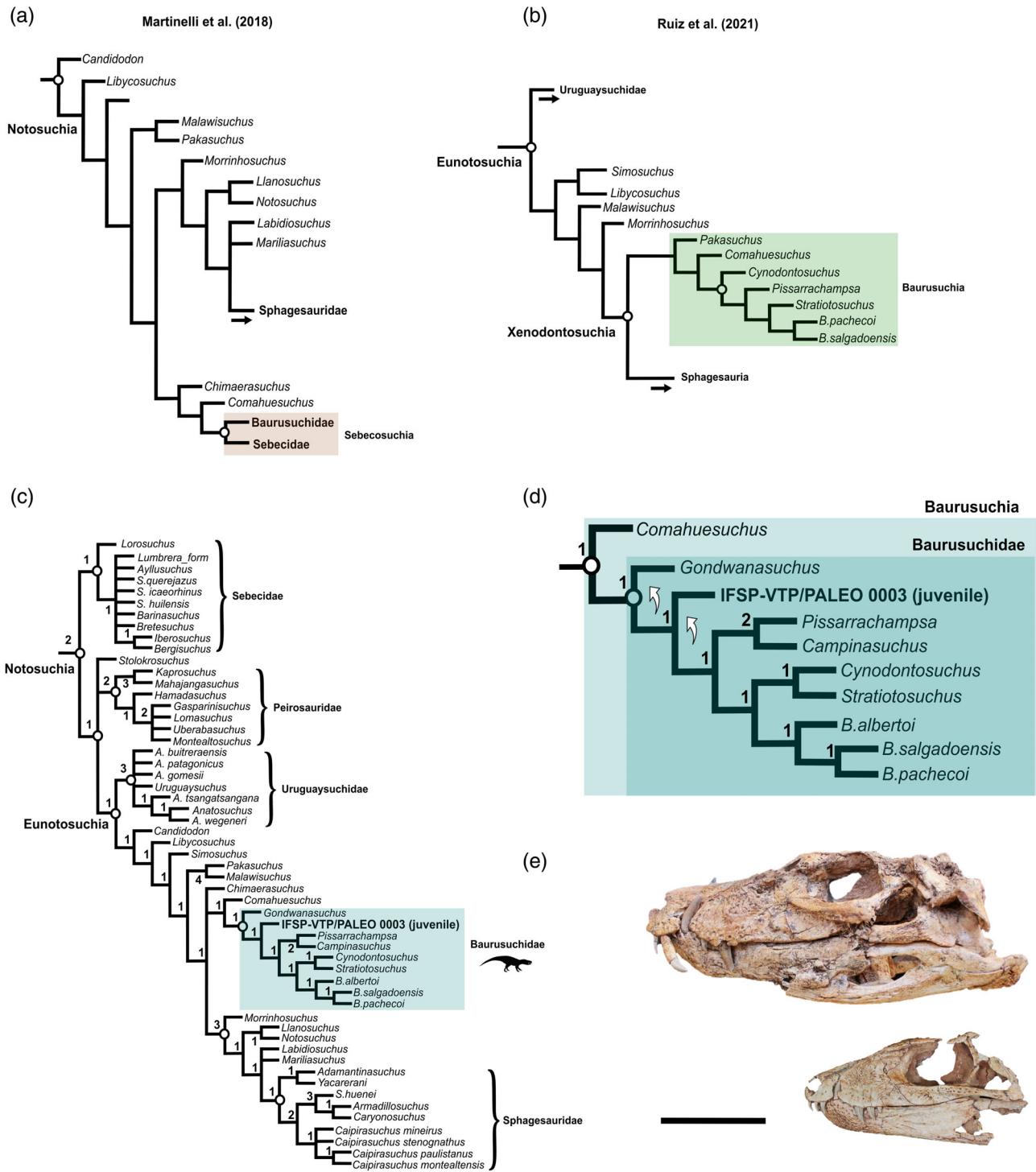


FIGURE 15 Topologies by previous works and results of phylogenetic analysis. (a) Phylogeny adapted from Martinelli et al. (2018) showing the recovery of Sebecosuchia. (b) Phylogeny from Ruiz et al. (2021) with Baurusuchia as sister clade to Sphagesauria (c) Strict consensus tree of 5568 MPTs obtained as a working hypothesis. The neosuchian branch within mesoeucrocodylia is not shown. Bremer supports are shown for each node. (d) Detailed internal relationships of Baurusuchidae, showing the tendency of both IFSP-VTP/PALEO 0003 and *Gondwanasuchus* to emerge as basal terminals. (e) Skulls shown in left lateral view to highlight size differential. Scale bar = 5 cm.

surface (Figure 9d). There is also a slightly medially-shifted longitudinal keel (lk) that reaches the posterior end but fails to invade the anterior one. Consequently, the marginally inset position of the keel creates a larger

area of the *pars laterale* in respect to the *pars mediale*. The keel itself is low, not rising substantially above the overall external surface. These osteoderms also lack the thickness/robustness and dorsal deflection of the anterior

and posterior ends observed in adult forms, being instead mostly flat and dorsoventrally thin, almost sheet-like. Sculpturing patterns of pits and sulci are also absent and/or nascent. Despite not being imbricated, the presence of a *facies articularis externa* indicates that they might have been so in life, or, perhaps, gained progressively increasing imbrication as the animal grew. No suture marks were observed on the medial edge of the osteoderms, pointing to a looser parallel arrangement at this life stage.

4.8 | Phylogenetic systematics

An initial unpruned analysis that included all 115 taxa resulted in a poorly resolved topology with undetermined relationships between major notosuchian clades (see supplementary information). Following the procedures of Martinelli et al. (2018) and subsequent work (Cunha & Santucci, 2020), a set of five unstable taxa were pruned from the following attempt (*Pehuenquesuchus enderi*, *Neuquensuchus universitas*, *Microsuchus schilleri*, *Pabhowehshi pakistanensis*, and *Coringasuchus anisodontis*),

yielding a much improved phylogeny, with the strict consensus of a total of 5568 MPTs with 1729 steps, presented in Figure 15c,d.

As expected, it recovers the main dichotomy within Mesoeucrocodylia, composed of Neosuchia, a mainly semi-aquatic lineage, and the terrestrial and ecologically diverse Notosuchians. Nevertheless, the relationships of major notosuchian clades have changed significantly from previous works (Figure 15a) (Fiorelli et al., 2016; Martinelli et al., 2018; Pol et al., 2012). The monophyly of Sebecosuchia, originally erected by Colbert et al., 1946 to encompass superficially similar oreinirostral and ziphodont forms, *Sebecus icaeorhinus* and *B. pachecoi*, is no longer supported, and sebecids emerge as the earliest branching notosuchian clade. This implies a substantial ghost lineage, in spite of recent finds of Cretaceous materials with likely sebecid affinities (Rabi & Sebők, 2015; Sellés et al., 2020). Sebecidae was found as sister to a clade including Peirosauridae (excluding *Stolokrosuchus*) and a new clade uniting Uruguaysuchidae and a larger group containing the so-called “advanced notosuchians” (sensu Pol, 2005) plus Baurusuchidae.

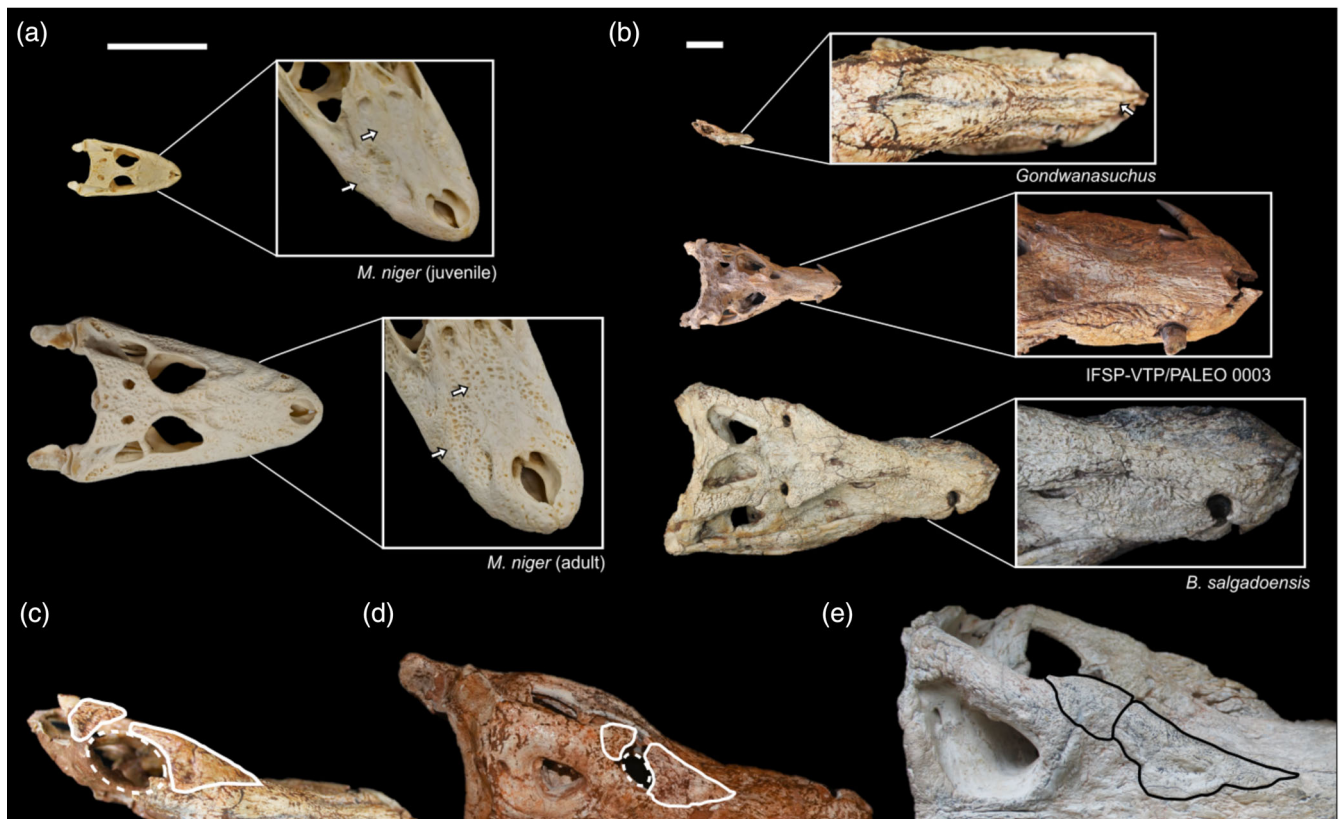


FIGURE 16 Ontogenetic development of dermal bone ornamentation in *Melanosuchus niger* and Baurusuchidae. (a) Juvenile and adult *M. niger* showing increasingly sculptured rostra. (b) Rostral sculpturing development in *Gondwanasuchus*, IFSP-VTP/PALEO 0003 and the *B. salgadoensis* holotype. Note the size differential and unfused nasals in *Gondwanasuchus scabrosus*. (c–e) Levels of fusion between palpebrals in different baurusuchid semaphoronts. (d) A juvenile *Pissarrachampsia sera* (Godoy et al., 2018). Scale bars, a = 10 cm, b = 5 cm.

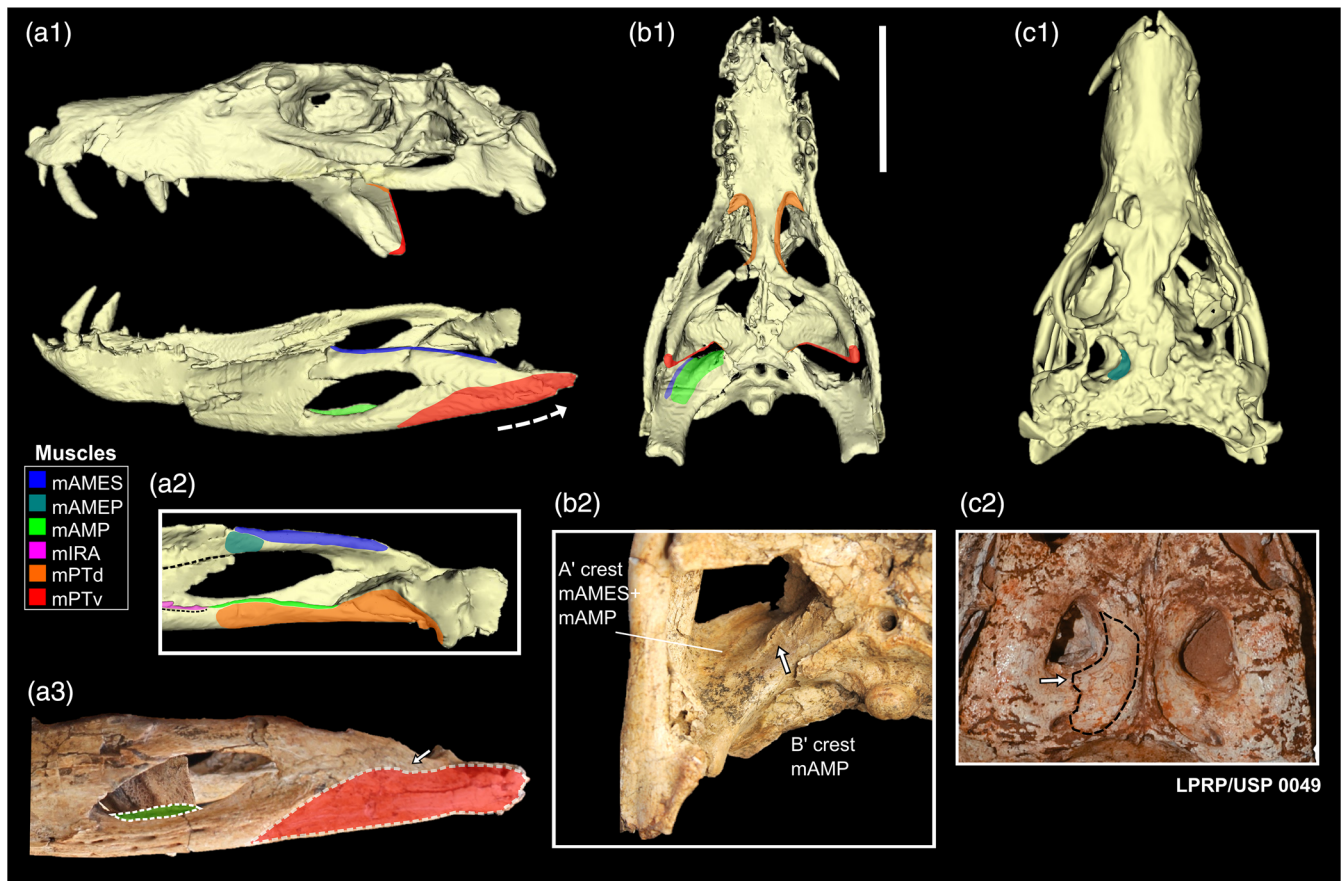


FIGURE 17 Digital reconstruction of adductor musculature for IFSP-VTP/PALEO 0003 in lateral, medial, palatal, and dorsal views (a1, a2, b1, and c1). An annotated photograph of its left posterior mandibular ramus and quadrate aponeurosis are also shown (a3 and b2). A *Pissarrachampsia* juvenile, LRP/USP 0049, is shown to highlight the origination site for mAMEP in the dorsotemporal fossa (c2). mAMES, *M. adductor mandibularis externus superficialis*; mAMEP, *M. adductor mandibularis externus profundus*; mAMP, *M. adductor mandibularis posterior*; mIRA, *M. intramandibularis*; mPTd, *M. pterygoideus dorsalis*; mPTv, *M. pterygoideus ventralis*. Scale bar a1-b1-c1 = 5 cm.

Although there is some uncertainty regarding the position of *Chimaerasuchus*, the internal relations of Sphagesauridae and related forms are similar to previous works. *Comahuesuchus*, an enigmatic taxon known from a fragmentary skull (Martinelli, 2003), is recovered as closely related to Baurusuchidae. The latter, in accordance to recent baurusuchid-focused phylogenies (Darlim, Montefeltro, & Langer, 2021; Godoy et al., 2014; Montefeltro et al., 2011) is comprised of *Pissarrachampsinae* and *Baurusuchinae*, with the noticeable difference of *Cynodontosuchus*, which was found as the sister taxon to *Stratiotosuchus*. The newly codified specimens, IFSP-VTP/PALEO-0003 and *G. scabrosus*, sit sequentially as the earliest branching baurusuchids.

5 | DISCUSSION

The skull of IFSP-VTP/PALEO-0003 differs considerably from adult individuals, in terms of proportion,

ornamentation and development of individual bones (Figures 16, 17, and 18). Comparisons with other baurusuchid semaphoronts (Table 1) resulted in the identification of several osteological characters, mostly cranial, that reveal substantial morphological shifts along ontogeny.

These may be divided into characters relating to: (1) dermatocranium development and (2) hypertrophy of jaw adductors. As with modern and fossil crocodyli-forms (Drumheller et al., 2021; Salas-Gismondi et al., 2015; Staniewicz et al., 2018; Tucker et al., 1996), as well as other archosaurian lineages (Frederickson et al., 2020; Holtz, 2021), ontogeny plays an important role in the trophic structures of communities. Given its inferred position as top predator, based on anatomical, biomechanical, and tentative geochemical evidence (Cardia et al., 2018; Montefeltro et al., 2020; Riff & Kellner, 2011), it is important to assess the predatory capabilities of immature baurusuchid specimens in order to better understand their paleoecology, as well as

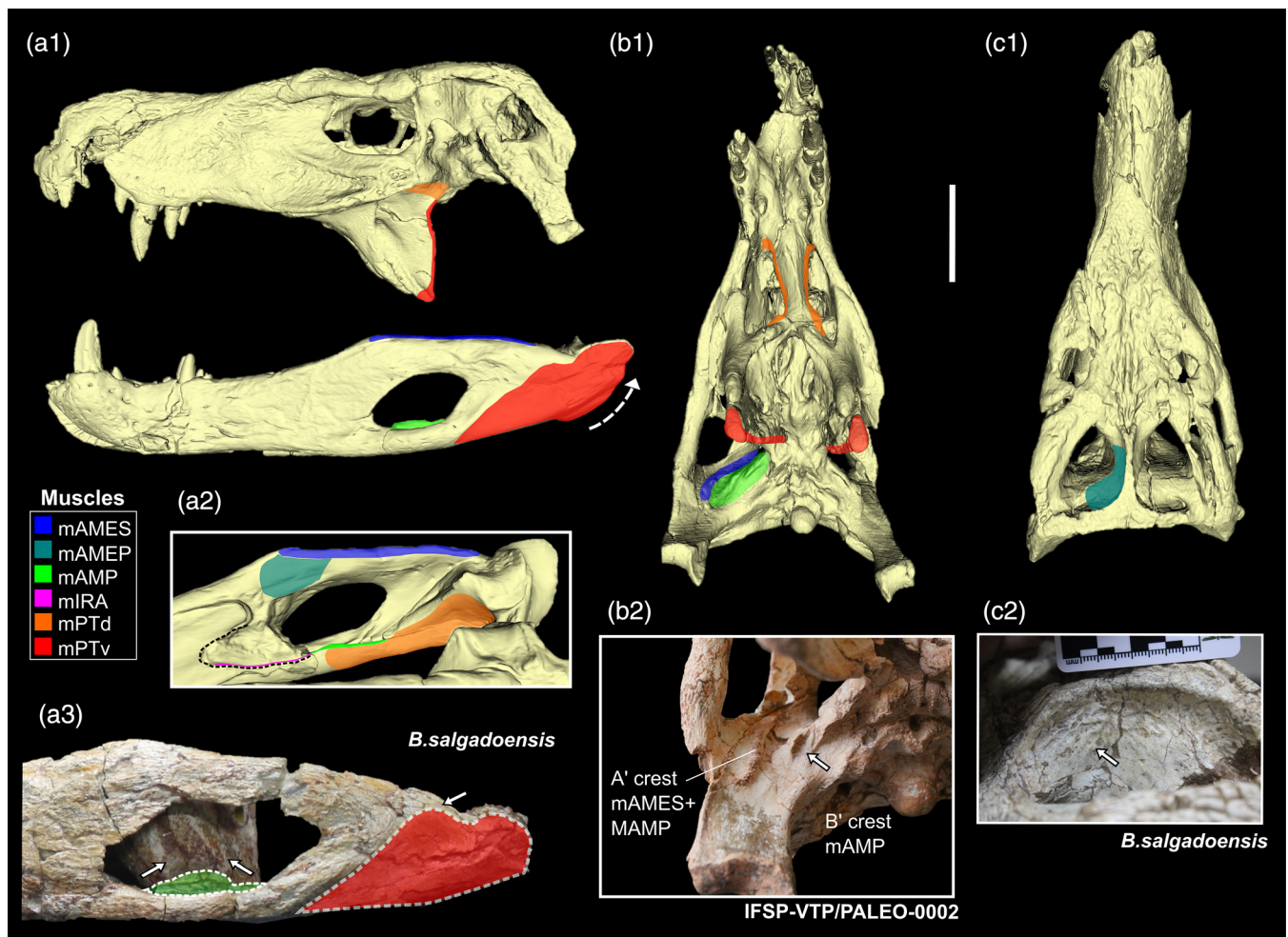


FIGURE 18 Digital adductor musculature reconstruction for FEF-PV-R-1/9, and adult baurusuchid in lateral, medial, palatal, and dorsal views (a1, a2, b1, and c1). Both *B. salgadoensis* (a3 and c2) and IFSP-VTP/PALEO 0002 (b2) are shown to highlight origination and insertion sites. mAMES, *M. adductor mandibularis externus superficialis*; mAMEP, *M. adductor mandibularis externus profundus*; mAMP, *M. adductor mandibularis posterior*; mIRA, *M. intramandibularis*; mPTd, *M. pterygoideus dorsalis*; mPTv, *M. pterygoideus ventralis*. Scale bar a1-b1-c1 = 5 cm.

critically assess previously proposed trophic relations in the Bauru Basin (Godoy et al., 2014; Klock et al., 2022).

5.1 | Dermatocranium development

In both extant and fossil crocodylians, post-hatching growth is characterized by substantial development of the sculpturing of dermatocranium bones (de Buffrénil et al., 2015; Grigg, 2015), which have been used to assess growth stages (Griffin et al., 2021). Juveniles, such as IFSP-VTP/PALEO-0003, in line with what is observed in immature modern crocodylians, (Figure 16), show only incipient ornamentation with respect to larger specimens.

Sculpturing is concentrated on the rostral region, mostly on the nasal and dorsolateral surfaces of the maxilla, marked by shallow and incipient vermiform grooves,

whereas other regions retain smoother external surfaces. Ornamentation on much larger and skeletally mature baurusuchid specimens, on the other hand, such as MPMA 62-0001-02 and DGM 1477-R (Carvalho et al., 2005; Riff, 2003; Riff & Kellner, 2011), encompasses the entire cranium, with the noticeable exception of the quadrate, which is part of the splanchnocranium. Also, the ornamentation occurs as a network of more densely concentrated grooves and pits, also heavily concentrated on skull roof elements, that may obliterate or complicate the identification of sutures, resulting in a more robust overall aspect of the skull. As in IFSP-VTP/PALEO-0003, incipient/absent ornamentation is also observed in both LPRP/USP 0049, a *P. sera* juvenile (Godoy et al., 2018), and *G. scabrosus*, the smallest known baurusuchid.

The mandibles seem to closely follow the pattern above, where juveniles like IFSP-VTP/PALEO-0003 and

LPRP/USP 049, in addition to *G. scabrosus*, possess symphyseal sculpturing marked by pitting, but mostly smooth lateral surfaces of mandible, whereas in adults ornamentation is expanded to these areas, reaching the anterior border of the external mandibular fenestrae (emf) and the lateral surface of the surangular in the holotype of *B. salgadoensis*.

As previously hinted by dos Santos et al. (2021), IFSP-VTP/PALEO-0003 displays a more clearly visible and high-relief sagittal crests on the dorsal surface of the frontal compared to adult forms, where this feature becomes proportionately less raised with respect to surrounding surfaces, especially assuming the form of a wide frontal depression (Carvalho et al., 2005; Price, 1945; Riff, 2003).

The development of dense sculpturing adjacent to the crest might obscure this structure. This general pattern is present in members of *Baurusuchus* and *Aphaurosuchus escharafacies* (Darlim, Carvalho, et al., 2021; Darlim, Montefeltro, & Langer, 2021), but not in *A. sordidus* (Godoy et al., 2014) and *P. sera* (Montefeltro et al., 2011, Figure 3b). Additionally, the immature specimens IFSP-VTP/PALEO-0003 and LPRP/USP 0049 also share a protruding infraorbital crest that overhangs the anterior ramus of the jugal. Such crest may get reabsorbed into the jugal lateral surface as the animal matured, resulting in a less distinct, but still noticeable crest that, together with the development of the ventral margin of the jugal, resulted in the fan-shaped lateral depression shared by mature baurusuchids (Godoy et al., 2014).

Finally, juvenile individuals display slender, less ornamented palpebrals that form proportionally larger elliptical supraorbital fenestrae. Comparisons with mature individuals reveals the gradual closure of such opening, with gradual fusing occurring along the lateral margin of the frontal (Figure 16c–e). Instead, mature specimens generally have reduced supraorbital openings, in the shape of ellipses with a lateromedially-oriented major axis. Curiously, *S. maxhechti* Campos (2001), which bears the largest baurusuchid skull ever found, have palpebrals fully fused to one another, completely closing these fenestrae. Together, it seems likely that the ontogenetic series start with relatively large circular openings, reaching a smaller elliptical phase in adulthood as palpebrals become more robust, and eventually culminating in total closure in older individuals.

5.2 | Hypertrophy of jaw adductors

Considering the nature of preservation of most vertebrate fossil remains, myological reconstructions and comparisons are commonly achieved by the observation of

osteological correlates of muscle origins and insertions in the form of surface textures, like muscle scarring and crest-like features (Bona & Desojo, 2011). These crests and tuberosities, in the context of extant homologies, are thus inferred to have marked where the known crocodylian jaw musculature aponeurosis and tendons inserted (Iordansky, 1964; Iordansky, 2000).

Overall, the osteological correlates for jaw adductor musculature present in IFSP-VTP/PALEO-0003 closely follow the living crocodylian architecture (Bona & Desojo, 2011; Iordansky, 2000; Schumacher, 1973; van Drongelen & Dullemeijer, 1982), despite differences in positioning and size, that are mostly attributable to the different rostrum shapes (Sellers et al., 2022). In addition, IFSP-VTP/PALEO 0003 exhibits significant size and development deviations from the condition in adult baurusuchids (Figures 17 and 18). Considering the ecological relevance of bite force and the ontogenetic shifts in muscle arrangement in modern crocodylians (Erickson et al., 2003; Gignac & Erickson, 2016; Sellers et al., 2017), the description of such changes in Baurusuchidae is important to better understand their post-hatching ecology.

In agreement with the findings of Gignac & Erickson, 2016 and Sellers et al. (2022), the ontogenetic hypertrophy and lateral insertion of mPTv seemed to also have played a similar role in the bite force of the altirostral baurusuchids. In IFSP-VTP/PALEO-0003 and LPRP/USP 049, the distal ends of pterygoids and ectopterygoids are roughly subequal, both contributing to form the origin area for mPTv, whereas in adults the ectopterygoid fails to reach the distal tip of the pterygoid, and the pterygoid aponeurosis is dominated by the distal pterygoid flange (Figures 17a,b and 18a,b). As expected, based on modern crocodylian cranial mandibular myology (Bona & Desojo, 2011), the mPTv would envelop the angular ventral edge as it reached for its lateral surface, where it inserted to a depression that bounds the external mandibular fenestra (dmp, depression for the insertion of mPTv).

Medium-sized and large adults reveal that this teardrop-shaped depression not only gets larger area but also substantially deeper as the mPTV enlarged with growth (Figures 17 and 18 a₁–a₃). Its shallowness and limited posterodorsal reach in IFSP-VTP/PALEO-0003, marginally extending above the angular-surangular suture, contrasts with the much deeper and broader depression of adults, that extends almost to the dorsal edge of the surangular (Figure 18 a₃, white arrow). It is bound by an oblique crest that borders the posterior margin of the external mandibular fenestra that also develops further, going from a low relief feature to a thick protuberance or crest, limiting the mPTv anteriorly.

There is also evidence for pennate muscle fibers in the form of parallel striations that rapidly shift to an oblique

orientation on the posterolateral surface of the angular, reaching the retroarticular process in lateral view. These striations, marking the growth of the ventral *M. Pterygoideus*, are lacking in the juveniles IFSP-VTP/PALEO-0003 and LPRP/USP 049, and may attest to an increasing reliance on bite-force as the animals grew, as the pennate configuration yields larger cross sections and muscle forces and, consequently, enhanced tensions (Gignac & Erickson, 2016; Holliday et al., 2022; Sellers et al., 2017; Sellers et al., 2022).

Also, the dorsal surfaces of the pterygoid wings in juveniles are mostly smooth and featureless, whereas larger specimens have numerous thin parallel sulci that pervade this surface extending anteriorly into the closed caviconchal fossa, as in modern crocodylians (Holliday et al., 2013; Witmer, 1997). These represent osteological evidence of the passage and development of the mPTd in adult, a muscle responsible for most of the total bite-force in pseudosuchians (Sellers et al., 2022).

Also, in juveniles like IFSP-VTP/PALEO 0003, the retroarticular processes (Figures 17 and 18 a₁–a₃) are laminar, more rectangular, and anteroposteriorly longer, forming a shallow angle to the horizontal plane, resulting in a straight profile that extends much further back.

Adults develop comparably shorter, deeper, and more robust paddle-shaped retroarticular processes. Their lateral flanges are more vertically oriented and dorsally ascending, with a rounded posterior margin, further expanding, and reorienting the retroarticular aponeurosis where the mPTv partially attaches to (Figure 18 a₁). The medial flange of the retroarticular process somewhat maintains its orientation to the horizontal plane, with a sharp, oblique lamina that connects its posterior end to the medial margin. In this area, a ventromedial pendant protuberance becomes more robust and pronounced, further projecting toward the sagittal plane as an orthogonal process, that both increases the attachment area of mPTd and limits in posterior reach (Figures 17 and 18 a₂).

In its ventral portion, IFSP-VTP/PALEO-0003 displays a medially curving elongate crest extending parallel and close to the quadrate-quadratojugal ventromedial contact, bordering the infratemporal fenestra. Somewhat oblique to the latter, an additional, but substantially thicker and high-relief crest is found, bordering the contact between the quadrate and the basioccipital, and fitting the quadrate shape as it bends toward the sagittal plane in ventral view (Figures 17 and 18 b₁–b₂). Considering their position on the ventral surface of the quadrate's distal process, they are inferred as homologous to the crests described by Iordansky (1964, 2000) for modern crocodylians that support tendons A and B, respectively. These comprised and were encompassed by the quadrate aponeurosis, which could be divided into lateral and medial sheets (van Drongelen & Dullemeijer, 1982). The lateral edge

of the A' crest would be the origin site of most of mAMES, whereas external portions of mAMP would attach to its medial border, with its deepest bundles emerging from the anteromedial margin of B' crest (Holliday & Witmer, 2007; Iordansky, 1964; van Drongelen & Dullemeijer, 1982).

There is substantial development in terms of relief and thickness of both these adductor crests during ontogeny, as observed in *M. niger* ontogenetic. A' crest gains relief above the quadrate surface, becoming more pronounced and rugose, whereas B' crest becomes more robust, slightly sinuous, and anteriorly developing into a hook-like projection with medially concave and laterally convex facets (Figure 18 b₂). Similar features on B'-crest were only found in the largest of *M. niger* specimens, such as UF Herp 5600.

Corresponding changes were also observed on the insertion sites of the aforementioned muscle groups. mAMP ventrally attaches to the angular bone, covering most of the emf, and attaching on the lateral surface of the medial process of the angular (torose margin sensu Darlim, Carvalho, et al., 2021; Darlim, Montefeltro, & Langer, 2021; Nascimento & Zaher, 2010), and inserting within the meckelian groove, anteriorly bound by mIRA (*M. intermandibularis*) (Figures 17 and 18 a₂). The latter enters the meckelian canal itself attaching to its medial wall at the intramandibular aponeurosis (Bona & Desojo, 2011; Iordansky, 2000).

The medial process of the angular varies from an undeveloped, more rectilinear shape in IFSP-VTP/PALEO-0003 and LPRP/USP 0049, to a dorsally ascending, thickened, and torose aspect in adult specimens (Figures 17 and 18 a₃), reflecting the development of mAMP. Curiously, as notosuchians lack a coronoid bone (Bona et al., 2022), which in crown crocodylians is partially responsible for the attachment of both mAMP and mIRA and the closure of the caudal intermandibular foramen (FIC; Holliday et al., 2013; Sellers et al., 2022, Appendix A), we hypothesize that such enlargement of the angular medial process through ontogeny evolved as a compensatory structure for larger adductor attachment in Baurusuchidae.

Also related to the development of the A' crest and *M. adductor mandibulae externus* group, the origin sites of the deepest bundles are not preserved in IFSP-VTP/PALEO-0003, the surangular ontogenetically gains dorsoventral depth and a more raised coronoid prominence (Figures 17 and 18 a₁–a₃). The mAMES inserts dorsomedially on the surangular and is limited by the posteroven-tral projection of the quadratojugal posteriorly and the coronoid prominence anteriorly, above the emf in lateral view. A medial view comparison reveals a shorter coronoid prominence with a smoother medial surface in IFSP-VTP/PALEO-0003, thus a proportionally smaller insertion areas for both mAMEM and mAMEP compared to larger

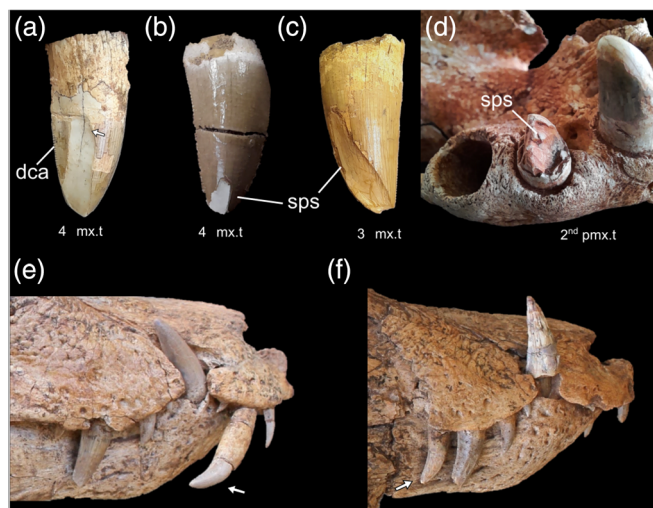


FIGURE 19 Patterns of tooth wear in Baurusuchidae. (a–d) Adults repeatedly preserve spalled enamel surfaces resulting from tooth-prey contact, similar to some tyrannosaurs, while a smaller juvenile such as IFSP-VTP/PALEO 0003 (d, e) replaced teeth with little to no damage. dca, distal carina; sps, spalled surface. Not to scale.

specimens (Figures 17 and 18 a₂). This area increase is accompanied in skeletally mature individuals by conspicuous anteroposterior muscles scarring at these sites.

The lack of a coronoid bone results in an anteriorly open-ended mandibular adductor fossa, marked by the absence of a FIC, not constrained by ossifications (Bona et al., 2022). The mandibular adductor fossa anterior margins are formed by the surangular dorsally, the dentary anteromedially and the angular ventrally, producing a rounded profile. This is somewhat anteriorly tapered in IFSP-VTP/PALEO-0003 but dorsoventrally expanded in larger specimens (Figures 17 and 18 a₂).

Unfortunately, the poor preservation of the dorsotemporal fenestra and basicranium elements, such as laterosphenoid, in IFSP-VTP/PALEO 0003 hinders comparisons of the origin sites for deep and external adductors like mPST and mAMEM. Still, the holotype of *B. salgadoensis*, consists of a large adult skull (ROL = 43 cm) that displays substantial muscle scarring in the form of a network of irregular anastomosed pits and vertical striations on the lateral wall of the parietal, within the dorsotemporal fossae (Figure 18 c₂). Considering the pennation of its dorsal portion with respect to the ventral one, they are here interpreted to represent the cross section of individual bundles of mAMEP as it inserted on the parietal walls (Holliday et al., 2022).

The fact that smaller skulls lack such features (such as LPRP/USP 049, Figures 17 and 18 c1, c2), points to the increased development of such muscle throughout life and perhaps greater reliance on its functions for mature



FIGURE 20 Paleart by Felipe Alves Elias, depicting distinct foraging strategies for juveniles and adults. On the foreground, IFSP-VTP/PALEO 0003, with its undeveloped cranial adductors, chases after a beetle, while a dominant adult starts consuming a small sphagesaurid.

individuals. Moreover, the absence of additional muscle correlates outside of the parietal lateral surfaces and dorsotemporal fossae supports the Holliday et al. (2020) model for supratemporal fenestra function, where mAMEP would be the only adductor to reach the dorsotemporal fossa, whereas the frontoparietal fossa would house vasculature, fatty tissues and serve a thermoregulatory role.

Size and wear discrepancies between the exposed teeth of IFSP-VTP/PALEO-0003 and adult specimens are also revealing. None of the premaxillary and maxillary teeth of IFSP-VTP/PALEO 0003 display wear facets and/or apical spalled surfaces which were found in adult specimens collected at the same site (Figure 19a–d). The third premaxillary tooth, in fact, despite showing minimal wear, was preserved as it was being pushed down by a replacement tooth (Figure 19e,f, white arrows), exposing a long root projecting ventrolaterally. The spalled surfaces of baurusuchid teeth are remarkably similar to those of large tyrannosaurids exhibit due to flaking from tooth and food contact (Schubert & Ungar, 2005). The osteophagy, which likely caused the observed wear, is also corroborated in tyrannosaurs by abundant bone fragments found in coprolites, puncture marks and bite force modeling (Chin et al., 1998; Chin et al., 2003; Erickson & Olson, 1996; Gignac & Erickson, 2017; Rayfield, 2004). Similarly, in addition to tooth flaking, rare stomach contents showed *Aplestosuchus* to have consumed bone fragments of a small sphagesaurid (Godoy et al., 2014), and the recent analysis of coprolites assigned to Baurusuchidae, including x-ray diffraction, also points to osteophagy (de Oliveira et al., 2021), despite finite element modeling

indicating a weaker than expected bite force (Montefeltro et al., 2020).

In line with the ontogenetic niche shifts observed in modern crocodylians with increases in size and bite forces (Erickson et al., 2012; Gignac & Erickson, 2015; Gignac & Erickson 2016b; Tucker et al., 1996), also inferred for fossil crocodyliforms (Drumheller et al., 2021), and considering the presented differences between juveniles and adults, we suggest that baurusuchid semaphoronts of distinct ages and sizes occupied distinct trophic levels. Altogether, the considerable ontogenetic changes in cranial adductor muscles likely were reflected in bite forces, prey size and, possibly, shifting patterns of tooth wear (Erickson et al., 2003; Gignac & Erickson, 2016; Holliday et al., 2013).

We incorporate these aspects in the paleoart reconstruction below (Figure 20, by Felipe Alves Elias), which depicts IFSP-VTP/PALEO 0003 as a cursorial juvenile foraging on pliable prey, contrasting the consumption of small to medium-sized vertebrates by baurusuchid adults. The co-occurrence of different semaphoronts in the same area is based on the outcrops of Jales-SP and Fernandópolis-SP that, as previously mentioned, yield several nests, egg clutches, juveniles, and adults.

5.3 | Phylogenetics and ontogeny

The notosuchian internal relationships obtained here constitute one of the most divergent derived from the Pol et al. (2014) character matrix. Although sebecids as early diverging notosuchians seems strange in light of their abundance and diversity in Cenozoic terrestrial environments, especially in South America (Cidade et al., 2019), it underpins the possibility that their shared morphological characters with Baurusuchidae are homoplasies, questioning the status of Sebecosuchia (Colbert et al., 1946).

Larsson and Sues (2007), erected a clade uniting sebecids and peirosaurids, named Sebecia, which found some support among recently published studies (Pinheiro et al., 2021; Ruiz et al., 2021). The hypothesis does not support Sebecia, but there are some intriguing morphological similarities between the two clades, such as choanae anatomy, their anteroposteriorly thin pterygoid flanges, their upturned retroarticular processes, and, more strikingly, the shared configuration of their posterior mandibular rami (Carvalho et al., 2004; Powell et al., 2011, p. 356, fig. 3d), including: (1) a tear drop-shaped emf with a medially inset and acute posterior dentary process; (2) heavily sculptured and thick ventrolateral margin of angular; (3) bulged dorsolateral protuberance of surangular; (4) lack of lateral insertion of mPTv.

Furthermore, the oreinirostral and zipodont conditions employed to unite sebecids and baurusuchids are only

marginally similar. Baurusuchids display a more abrupt transition from their skull roofs to their rostra in dorsal view, and also a more rounded dorsal surface along the latter, resulting in a roughly c-shaped cross section, whereas sebecids generally display a more gradual transition and a distinct v-shaped profile (Colbert et al., 1946; Molnar, 2010). Sebecid teeth are also generally smaller and more numerous, contrasting with the reduced number of hypertrophied teeth observed in baurusuchids (Bravo et al., 2021; Colbert et al., 1946), with the noticeable exceptions of *Barinasuchus* and *Dentaneosuchus*, some of the largest terrestrial crocodyliforms found to date (Martin et al., 2022; Paolillo & Linares, 2007). Therefore, in the light of myological inferences presented here and elsewhere for *S. icaeorhinus* (Molnar, 2012), we find it plausible that these two forms had distinct ecologies, despite being considered top-tier terrestrial predators, and so could have arrived at superficially similar morphologies along different character transformation sequences.

Another interesting aspect of the phylogeny presented here is its convergence with the results of Ruiz et al. (2021) (Figure 15b,c), itself derived from previous revision and combination of several other matrices (Montefeltro et al., 2013). The clade Eunosuchia is recovered in detriment of the commonly found Ziphosuchia Ortega et al., 2000 (Martinelli et al., 2018; Pol et al., 2014). Likewise, eunosuchians are composed of Uruguaysuchidae, Sphagesauridae, and Baurusuchia, the latter two sharing a more recent common ancestor. Yet Xenodontosuchia, here does not exclude *Morrinhosuchus luziae* Iori & Carvalho, 2009, but does *Pakasuchus kapilimai* O'Connor et al., 2010.

The phylogenetic affinities of Baurusuchidae corroborates previous works, with its main Baurusuchinae/Pissarrachampsinae dichotomy (Darlim, Montefeltro, & Langer, 2021; Godoy et al., 2018; Montefeltro et al., 2011), with the exception *Cynodontosuchus rothi* Woodward, 1896, which emerges as a sister to *Stratiotosuchus* within Baurusuchinae. As previously mentioned, the main objective of the analysis was to codify the juvenile IFSP-VTP/PALEO-0003 in order to observe its systematic placement with respect to adult baurusuchids, testing the degree to which ontogeny affects the topology and the problems with including of juvenile specimens (Hennig, 1966; Sharma et al., 2017). As in Campione et al. (2013), we also sought to compare its placement with *G. scabrosus*, a putative juvenile and the smallest baurusuchid species known (Marinho et al., 2013). Our results show that both *G. scabrosus* and IFSP-VTP/PALEO-0003 were recovered as sequential terminal taxa at the base of Baurusuchidae, outside the Pissarrachampsinae/Baurusuchinae dichotomy.

Our study also allowed the identification of several differences between IFSP-VTP/PALEO-0003 and skeletally mature baurusuchids (details above), including

characters related to dermatocranium development and muscle aponeurosis and attachment sites, accumulating evidence for extensive ontogenetic changes in crocodyli-form lineages (Drumheller et al., 2021; Godoy et al., 2018; Watanabe & Slice, 2014).

The resulting systematic placement of IFSP-VTP/PALEO-0003 is in line with similar effects produced by the inclusion of juveniles in other archosaur phylogenies, whereby immature individuals of known taxa tend to fall outside their clades, like in Hadrosauridae and Tyrannosauridae (Campioni et al., 2013; Tsuihiji et al., 2011). This effect coupled with its size and morphology, hints to the immature state of the *G. scabrosus* holotype, highlighted by its characters with ontogenetic influence. Indeed, as recently seen for other taxa (Carr, 2020; Horner & Goodwin, 2006; Horner & Goodwin, 2009; Larson, 2013; Woodward et al., 2020), more time should be devoted toward the placement of a given specimens in ontogenetic context whenever possible.

5.4 | Implications for Baurusuchidae diversity

Although such revision is beyond the scope of this article, the ontogenetic characters discussed here can be applied to assess the validity of some baurusuchid species.

5.4.1 | *Stratiotosuchus maxhechti*

In the case of *S. maxhechti* (Campos, 2001). We hold that the rectangular outline of the orbits, the distorted external nares, the elliptical *foramen magnum*, together with a fragmented posterior palate, are indicators of dorsoventral taphonomic compression, indicating that the specimen was not preserved in its original form. Additionally, a supposedly unique character of *Stratiotosuchus*, the presence of only three premaxillary teeth (all other baurusuchids have four) (Riff & Kellner, 2011), could be explained by non-phylogenetic processes like the ontogenetic shifts in tooth count observed in modern crocodylids, where some individuals were found to lose premaxillary teeth (Brown et al., 2015). As mentioned above, *Stratiotosuchus* also lacks a supraorbital fenestra between palpebrals, which, as herein inferred, tends to reduce with increases in body size and dermal ornamentation. Whether its noticeable large size, in this proposed taphonomic and ontogenetic context, could challenge its validity is an open question. Further comparisons, long bone histology and application of geometric morphometrics might help resolving these questions.

5.4.2 | *Gondwanasuchus scabrosus*

Baurusuchid semaphoronts have been identified and described previously without the necessity of erecting new species (Geroto & Bertini, 2012; Godoy et al., 2018). The influence of ontogeny on their cranial anatomy, makes it possible to determine that the vast majority of baurusuchid name-bearing types were skeletally mature individuals, with the noticeable exception of *Gondwanasuchus*. This taxon consists of a partial skull, with a rostral-occipital length of just $\cong 12$ cm, just about one-third the average length of other holotypes, which range between 30 and 40 cm. In fact, it is substantially smaller even when compared with the currently described juvenile (20 cm).

Naturally, size alone would not suffice to assign a young age for the *G. scabrosus* holotype, as small-bodied forms could have existed, but the skull also lacks proportions, morphology, and sculpturing characteristics of adult individuals (Figure 15e and 16), sharing character states and positions with the most likely juvenile IFSP-VTP/PALEO 0003, and also sharing with it a more basal placement on the phylogeny. Most of the unique features of *Gondwanasuchus* may be reinterpreted as ontogenetic. For instance, both an overbite, where premaxillary teeth overhang the mandibular symphysis, and slender jugals can be found in the specimen described here and in LPRP/USP 0049. Indeed, the original diagnosis fails to demonstrate that *G. scabrosus* falls outside the range of morphological variation expected for the ontogenetic series of previously known baurusuchid species. It is here thus suggested that it should be further treated as a *nomem dubium*, given that it could not yet be firmly attributed to a semaphoront series of a previously described species. The discovery of further specimens may yield new information that allows for its placement into a firmly established species, most likely within the *Baurusuchus* genus, due to proximity to the sites where *B. Salgadoensis* and *B. albertoi* were collected. Comparisons with other known juveniles will also contribute to better constrain ontogenetic character variation within the clade.

Even though, the apicobasal sulci and ridges present on the teeth of *Gondwanasuchus* may be perceived as autapomorphic, seems not enough to sustain this taxon validity, considering that dental morphology varies substantially throughout ontogeny in other archosaur lineages (Therrien et al., 2021; Voris et al., 2021; Woodruff et al., 2018). Similar features are seen in juveniles of basal theropod *Coelophysis* (Buckley & Currie, 2014) and longitudinal enamel ridges were described to become less prominent with increasing tooth size in the neosuchian *Deltasuchus*, which was also suggested to have exhibited ontogenetic niche partitioning (Drumheller et al., 2021).

Apicobasal ridges are a common feature among taxa that fed in aquatic environments and could be related to the capture of pliable prey (McCurry et al., 2019). If longitudinally ridged crowns truly relate to development, they are another important indicator of ontogenetic niche partitioning in Baurusuchidae.

This question may be resolved in the future with the aid of modern tools such as mercury geochemistry and bite force estimates for juveniles (Cardia et al., 2018; Montefeltro et al., 2020). Ultimately, for the reasons expressed above, a thorough taxonomic revision of Baurusuchidae is necessary. All holotypes must be examined not only for atypical and ontogenetic features, but also their diagnoses must be revised in search for the influences of taphonomic deformation in their autapomorphies.

6 | CONCLUSIONS

We sought to better understand baurusuchid ontogeny by providing an osteomyological description of the most complete baurusuchid juvenile known to date, deepening our knowledge of the group's anatomy. Comparisons with adult baurusuchids and other taxa allowed the identification of several ontogenetic anatomical shifts, including the degree of sculpturing of dermal bones, the development of origin and attachment sites of mandibular adductor musculature, as well as distinct tooth wear patterns that could work as a framework to fit other crocodyliform specimens in their post-hatching developmental context.

A phylogenetic analysis including both the new semaphoront and the small baurusuchid *G. scabrosus* found both to represent early diverging baurusuchids, with the latter as the basalmost within the clade. This shift toward the base of the clade was also seen in other phylogenies which include immature individuals. In the light of the ontogenetic characters described here, their dimensions and phylogenetic placement, we conclude that *G. scabrosus* most likely constituted an immature individual, perhaps younger than IFSP-VTP/PALEO-0003 at the time of death, whereas the exceptionally large *Stratiotosuchus* exhibits signs of being an older individual. Consequently, we propose the former should be considered as a *nomem dubium* and suggest that a future taxonomic revision for Baurusuchidae should account for both ontogenetic and taphonomic sources of morphological variation in order to improve the stability of proposed taxonomic units.

AUTHOR CONTRIBUTIONS

Daniel Martins dos Santos: Writing – original draft; writing – review and editing; visualization; methodology;

software; validation; investigation; conceptualization; data curation; formal analysis. **Joyce Celerino de Carvalho:** Writing – review and editing; conceptualization; methodology; visualization. **Carlos Eduardo Maia de Oliveira:** Conceptualization; methodology; visualization; writing – review and editing; funding acquisition. **Marco Brandalise de Andrade:** Conceptualization; methodology; visualization; writing – review and editing; funding acquisition. **Rodrigo Miloni Santucci:** Conceptualization; methodology; visualization; writing – review and editing; funding acquisition; project administration; supervision.

ACKNOWLEDGMENTS

This study was financed in part by the Coordenação de Aperfeiçoamento de Pessoal de Nível Superior—Brasil (CAPES)—Finance Code 001. The authors would like to thank the Brazilian funding agencies CAPES and CNPq, for the financial support of DMS and the sponsoring of this project. The authors would also like to extend their gratitude to Dr. Julia Klaczko and Dr. Angele Martins of the Zoology Department of the University of Brasília, who kindly provided materials to support anatomical descriptions and comparisons.

CONFLICT OF INTEREST STATEMENT

The authors declare no conflicts of interest.

ORCID

Daniel Martins dos Santos  <https://orcid.org/0009-0008-9716-8753>

REFERENCES

- Amorim, P., Moraes, T., Silva, J., & Pedrini, H. (2015). InVesalius: An interactive rendering framework for health care support. In G. Bebis, R. Boyle, B. Parvin, D. Koracin, I. Pavlidis, R. Feris, T. McGraw, M. Elendt, R. Kopper, E. Ragan, et al. (Eds.), *Advances in visual computing* (pp. 45–54). Springer International Publishing. https://doi.org/10.1007/978-3-319-27857-5_5
- Arai, M., & Fernandes, L. A. (2023). Lower Campanian palynoflora from the Araçatuba formation (Bauru group), southeastern Brazil. *Cretaceous Research*, 150, 105586. <https://doi.org/10.1016/j.cretres.2023.105586>
- Assis, L. C. (2016). Semaphoronts: The elements of biological systematics. In *The future of phylogenetic systematics: The legacy of Willi Hennig* (pp. 213–229). Cambridge University Press.
- Bates, K., & Schachner, E. (2011). Disparity and convergence in bipedal archosaur locomotion. *Journal of the Royal Society Interface*, 9, 1339–1353. <https://doi.org/10.1098/rsif.2011.0687>
- Batezelli, A. (2010). Arcabouço tectono-estratigráfico e evolução das Bacias Caiuá e Bauru no Sudeste brasileiro. *Revista Brasileira de Geociências*, 40(2), 265–285.
- Batezelli, A., Perinotto, J. D. J., Etchebehere, M. D. C., Fulfaro, V. J., & Saad, A. R. (1999). Redefinição litoestratigráfica da unidade Araçatuba e da sua extensão regional na

- Bacia Bauru, Estado de São Paulo, Brasil. *Simpósio Sobre o Cretáceo do Brasil*, 5, 195–200.
- Benton, M. J., & James, C. (1988). Archosaur phylogeny and the relationships of the Crocodylia. In *The phylogeny and classification of the tetrapods, Volume I: Amphibians, reptiles, birds* (Vol. 1, pp. 295–338). Clarendon Press.
- Bertini, R. J. (1993). *Paleobiologia do Grupo Bauru, Cretáceo Superior continental da Bacia do Paraná, com ênfase em sua fauna de amniotas*. Universidade Federal do Rio de Janeiro.
- Bona, P., & Desojo, J. B. (2011). Osteology and cranial musculature of *Caiman latirostris* (Crocodylia: Alligatoridae). *Journal of Morphology*, 272(7), 780–795. <https://doi.org/10.1002/jmor.10894>
- Bona, P., Fernandez Blanco, M. V., Ezcurrea, M. D., von Baczko, M. B., Desojo, J. B., & Pol, D. (2022). On the homology of crocodylian post-dentary bones and their macroevolution throughout Pseudosuchia. *The Anatomical Record*, 305(10), 2980–3001. <https://doi.org/10.1002/ar.24873>
- Bravo, G. G., Pol, D., & García-López, D. A. (2021). A new sebecid mesoeucrocodylian from the Paleocene of northwestern Argentina. *Journal of Vertebrate Paleontology*, 41(3), e1979020. <https://doi.org/10.1080/02724634.2021.1979020>
- Brochu, C. A. (1996). Closure of neurocentral sutures during crocodylian ontogeny: Implications for maturity assessment in fossil archosaurs. *Journal of Vertebrate Paleontology*, 16(1), 49–62. <https://doi.org/10.1080/02724634.1996.10011283>
- Brown, C. M., VanBuren, C. S., Larson, D. W., Brink, K. S., Campione, N. E., Vavrek, M. J., & Evans, D. C. (2015). Tooth counts through growth in diapsid reptiles: Implications for interpreting individual and size-related variation in the fossil record. *Journal of Anatomy*, 226(4), 322–333.
- Buckley, L. G., & Currie, P. J. (2014). *Analysis of intraspecific and ontogenetic variation in the dentition of Coelophysis bauri (late Triassic), and implications for the systematics of isolated theropod teeth: Bulletin 63*. New Mexico Museum of Natural History and Science.
- Campione, N. E., Brink, K. S., Freedman, E. A., McGarrity, C. T., & Evans, D. C. (2013). ‘Glishades ericksoni’, an indeterminate juvenile hadrosaurid from the two medicine formation of Montana: Implications for hadrosauroid diversity in the latest cretaceous (Campanian-Maastrichtian) of western North America. *Palaeobiodiversity and Palaeoenvironments*, 93(1), 65–75. <https://doi.org/10.1007/s12549-012-0097-1>
- Campos, D. A. (2001). *Short note on a new Baurusuchidae (Crocodyliformes, Metasuchia) from the upper cretaceous of Brazil*. Museu Nacional.
- Cardia, F. M. S., Santucci, R. M., Bernardi, J. V. E., de Andrade, M. B., & de Oliveira, C. E. M. (2018). Mercury concentrations in terrestrial fossil vertebrates from the Bauru group (upper cretaceous), Brazil and implications for vertebrate paleontology. *Journal of South American Earth Sciences*, 86, 15–22. <https://doi.org/10.1016/j.jsames.2018.06.006>
- Carr, T. D. (2020). A high-resolution growth series of *Tyrannosaurus rex* obtained from multiple lines of evidence. *PeerJ*, 8, e9192. <https://doi.org/10.7717/peerj.9192>
- Carvalho, I. d. S., Arruda Campos, A. d. C., & Henrique Nobre, P. (2005). *Baurusuchus salgadoensis*, a new Crocodylomorpha from the Bauru Basin (cretaceous), Brazil. *Gondwana Research*, 8(1), 11–30. [https://doi.org/10.1016/S1342-937X\(05\)70259-8](https://doi.org/10.1016/S1342-937X(05)70259-8)
- Carvalho, I. d. S., Borges Ribeiro, L. C., & Avilla, L. d. S. (2004). *Uberasuchus terrificus* sp. nov., a new Crocodylomorpha from the Bauru Basin (upper cretaceous, Brazil). *Gondwana Research*, 7(4), 975–1002. [https://doi.org/10.1016/S1342-937X\(05\)71079-0](https://doi.org/10.1016/S1342-937X(05)71079-0)
- Carvalho, I. D. S., Teixeira, V. D. P. A., Ferraz, M. L. D. F., Ribeiro, L. C. B., Martinelli, A. G., Neto, F. M., Sertich, J. J. W., Cunha, G. C., Cunha, I. C., & Ferraz, P. F. (2011). *Campinasuchus dinizi* gen. et sp. nov., a new late cretaceous baurusuchid (Crocodyliformes) from the Bauru Basin, Brazil. *Zootaxa*, 2871(1), 19–42. <https://doi.org/10.11646/zootaxa.2871.1.2>
- Castro, M. C., Goin, F. J., Ortiz-Jaureguizar, E., Vieytes, E. C., Tsukui, K., Ramezani, J., Batezelli, A., Marsola, J. C. A., & Langer, M. C. (2018). A late cretaceous mammal from Brazil and the first radioisotopic age for the Bauru group. *Royal Society Open Science*, 5(5), 180482. <https://doi.org/10.1098/rsos.180482>
- Chin, K., Eberth, D. A., Schweitzer, M. H., Rando, T. A., Sloboda, W. J., & Horner, J. R. (2003). Remarkable preservation of undigested muscle tissue within a late cretaceous tyrannosaurid coprolite from Alberta, Canada. *Palaios*, 18(3), 286–294.
- Chin, K., Tokaryk, T. T., Erickson, G. M., & Calk, L. C. (1998). A king-sized theropod coprolite. *Nature*, 393(6686), 680–682. <https://doi.org/10.1038/31461>
- Cidade, G. M., Fortier, D., & Hsiou, A. S. (2019). The crocodylomorph fauna of the Cenozoic of South America and its evolutionary history: A review. *Journal of South American Earth Sciences*, 90, 392–411. <https://doi.org/10.1016/j.jsames.2018.12.026>
- Colbert, E. H., Mook, C. C., & Brown, B. (1951). The ancestral crocodylian *Protosuchus*. *Bulletin of the AMNH*, 97, 3 Retrieved from <https://digitallibrary.amnh.org/handle/2246/413>
- Colbert, E. H., Simpson, G. G., & Williams, C. S. (1946). Expedition (1930–1931) SP. 1946. Sebecus, representative of a peculiar suborder of fossil Crocodylia from Patagonia. *Bulletin of the AMNH*, 87, 4 Retrieved from <https://digitallibrary.amnh.org/handle/2246/394>
- Cotts, L., Pinheiro, A. E. P., da Silva, M. T., de Souza, C. I., & Di Dario, F. (2017). Postcranial skeleton of *Campinasuchus dinizi* (Crocodyliformes, Baurusuchidae) from the upper cretaceous of Brazil, with comments on the ontogeny and ecomorphology of the species. *Cretaceous Research*, 70, 163–188. <https://doi.org/10.1016/j.cretres.2016.11.003>
- Cunha, G. O., Santucci, R. M., de Andrade, M. B., & de Oliveira, C. E. M. (2020). Description and phylogenetic relationships of a large-bodied sphagesaurid notosuchian from the upper cretaceous Adamantina formation, Bauru group, São Paulo, southeastern Brazil. *Cretaceous Research*, 106, 104259. <https://doi.org/10.1016/j.cretres.2019.104259>
- Darlim, G., Carvalho, I. d. S., Tavares, S. A. S., & Langer, M. C. (2021). A new *Pissarrachampsinae* specimen from the Bauru Basin, Brazil, adds data to the understanding of the Baurusuchidae (Mesoeucrocodylia, Notosuchia) distribution in the late cretaceous of South America. *Cretaceous Research*, 128, 104969. <https://doi.org/10.1016/j.cretres.2021.104969>
- Darlim, G., Montefeltro, F. C., & Langer, M. C. (2021). 3D skull modelling and description of a new baurusuchid (Crocodyliformes, Mesoeucrocodylia) from the late cretaceous (Bauru Basin) of Brazil. *Journal of Anatomy*, 239, 622–662. <https://doi.org/10.1111/joa.13442>
- de Buffrénil, V., Clarac, F., Fau, M., Martin, S., Martin, B., Pellé, E., & Laurin, M. (2015). Differentiation and growth of bone ornamentation in vertebrates: A comparative histological

- study among the Crocodylomorpha. *Journal of Morphology*, 276(4), 425–445. <https://doi.org/10.1002/jmor.20351>
- de Oliveira, F. A., Santucci, R. M., de Oliveira, C. E. M., & de Andrade, M. B. (2021). Morphological and compositional analyses of coprolites from the upper cretaceous Bauru group reveal dietary habits of notosuchian fauna. *Lethaia*, 54, 664–686. <https://doi.org/10.1111/let.12431>
- de Souza, G. A., Soares, M. B., Weinschütz, L. C., Wilner, E., Lopes, R. T., de Araújo, O. M. O., & Kellner, A. W. A. (2021). The first edentulous ceratosaur from South America. *Scientific Reports*, 11(1), 22281. <https://doi.org/10.1038/s41598-021-01312-4>
- Dias, A. N. C., Chemale, F., Candeiro, C. R. A., Lana, C. C., Guadagnin, F., & Sales, A. S. W. (2021). Unraveling multiple tectonic events and source areas in the intracratonic Bauru Basin through combined zircon geo and thermochronological studies. *Journal of South American Earth Sciences*, 106, 103061. <https://doi.org/10.1016/j.jsames.2020.103061>
- Dias-Brito, D., Musachio, E. A., Castro, J. C., Maranhão, M. S. A. S., Suarez, J. M., & Rodrigues, R. (2001). Bauru group: A continental cretaceous unit in Brazil—Concepts based on micropaleontological, oxygen isotope and stratigraphic data. *Revue de Paléobiologie*, 20(1), 245–304.
- Dollman, K. N., Viglietti, P. A., & Choiniere, J. N. (2019). A new specimen of *Orthosuchus stormbergi* (Nash 1968) and a review of the distribution of southern African lower Jurassic crocodylomorphs. *Historical Biology*, 31(5), 653–664. <https://doi.org/10.1080/08912963.2017.1387110>
- dos Santos, D., Santucci, R., Andrade, M., & Oliveira, C. E. M. (2021). A baurusuchid yearling (Mesoeucrocodylia, Crocodyliformes), from the Adamantina formation, Bauru group, upper cretaceous of Brazil. *Historical Biology*, 34(11), 2137–2151. <https://doi.org/10.1080/08912963.2021.2001807>
- Drumheller, S. K., Adams, T. L., Maddox, H., & Noto, C. R. (2021). Expanded sampling across ontogeny in *Deltasuchus motherali* (Neosuchia, Crocodyliformes): Revealing Ecomorphological niche partitioning and Appalachian endemism in Cenomanian Crocodyliforms. *Elements of Paleontology*, 1–68. <https://doi.org/10.1017/9781009042024>
- Dumont, M. V., Jr., Santucci, R. M., de Andrade, M. B., & de Oliveira, C. E. M. (2020). Paleoneurology of *Baurusuchus* (Crocodyliformes: Baurusuchidae), ontogenetic variation, brain size, and sensorial implications. *The Anatomical Record*, 305, 2670–2694. <https://doi.org/10.1002/ar.24567>
- Erickson, G. M., Gignac, P. M., Steppan, S. J., Lappin, A. K., Vliet, K. A., Brueggen, J. D., Inouye, B. D., Kledzik, D., & Webb, G. J. W. (2012). Insights into the ecology and evolutionary success of crocodylians revealed through bite-force and tooth-pressure experimentation. *PLoS One*, 7(3), e31781. <https://doi.org/10.1371/journal.pone.0031781>
- Erickson, G. M., Lappin, A. K., & Vliet, K. A. (2003). The ontogeny of bite-force performance in American alligator (*Alligator mississippiensis*). *Journal of Zoology*, 260(3), 317–327. <https://doi.org/10.1017/S0952836903003819>
- Erickson, G. M., & Olson, K. H. (1996). Bite marks attributable to *Tyrannosaurus rex*: Preliminary description and implications. *Journal of Vertebrate Paleontology*, 16(1), 175–178.
- Fernandes, L. A. (2004). Mapa litoestratigráfico da parte oriental da Bacia Bauru (PR, SP, MG), escala 1: 1.000. 000. *Boletim Paranaense de Geociências*, 55, 53–66.
- Fernandes, L. A., & Coimbra, A. M. (1996). A Bacia Bauru (Cretáceo Superior, Brasil). *Anais da Academia Brasileira de Ciências*, 68(2), 195–206.
- Fiorelli, L. E., Leardi, J. M., Hechenleitner, E. M., Pol, D., Basilici, G., & Grellet-Tinner, G. (2016). A new late cretaceous crocodyliform from the western margin of Gondwana (La Rioja Province, Argentina). *Cretaceous Research*, 60, 194–209. <https://doi.org/10.1016/j.cretres.2015.12.003>
- Fonseca, P. H. M., Martinelli, A. G., da Silva, M. T., Ribeiro, L. C. B., Schultz, C. L., & Soares, M. B. (2020). Morphology of the endocranial cavities of *Campinasuchus dinizi* (Crocodyliformes: Baurusuchidae) from the upper cretaceous of Brazil. *Geobios*, 58, 1–16. <https://doi.org/10.1016/j.geobios.2019.11.001>
- Frederickson, J. A., Engel, M. H., & Cifelli, R. L. (2020). Ontogenetic dietary shifts in *Deinonychus antirrhopus* (Theropoda; Dromaeosauridae): Insights into the ecology and social behavior of raptorial dinosaurs through stable isotope analysis. *Palaeogeography, Palaeoclimatology, Palaeoecology*, 552, 109780. <https://doi.org/10.1016/j.palaeo.2020.109780>
- Gasparini, Z. B. (1971). Los Notosuchia de Cretácico de America del Sur como un nuevo infraorden de los Mesosuchia (Crocodylia). *Ameghiniana*, 8(2), 83–103.
- Gasparini, Z. B. (1972). Los Sebecosuchia (Crocodylia) del territorio argentino. Consideraciones Sobre Su “Status” taxonómico. *Ameghiniana*, 9(1), 23–34.
- Georgi, J. A., & Krause, D. W. (2010). Postcranial axial skeleton of *Simosuchus clarki* (Crocodyliformes: Notosuchia) from the late cretaceous of Madagascar. *Journal of Vertebrate Paleontology*, 30-(suppl 1), 99–121. <https://doi.org/10.1080/02724634.2010.519172>
- Geroto, C. F. C., & Bertini, R. J. (2012). Descrição de um espécime juvenil de Baurusuchidae (Crocodyliformes: Mesoeucrocodylia) do Grupo Bauru (Neocretáceo): considerações preliminares sobre ontogenia. *Revista do Instituto Geológico*, 33(2), 13–29. <https://doi.org/10.5935/0100-929X.20120007>
- Gignac, P. M., & Erickson, G. M. (2015). Ontogenetic changes in dental form and tooth pressures facilitate developmental niche shifts in American alligators. *Journal of Zoology*, 295(2), 132–142. <https://doi.org/10.1111/jzo.12187>
- Gignac, P. M., & Erickson, G. M. (2016). Ontogenetic bite-force modeling of *Alligator mississippiensis*: Implications for dietary transitions in a large-bodied vertebrate and the evolution of crocodylian feeding. *Journal of Zoology*, 299(4), 229–238. <https://doi.org/10.1111/jzo.12349>
- Gignac, P. M., & Erickson, G. M. (2017). The biomechanics behind extreme osteophagy in *Tyrannosaurus rex*. *Scientific Reports*, 7(1), 2012. <https://doi.org/10.1038/s41598-017-02161-w>
- Godoy, P. L., Bronzati, M., Eltink, E., Marsola, J. C. d. A., Cidade, G. M., Langer, M. C., & Montefeltro, F. C. (2016). Postcranial anatomy of *Pissarrachampsia sera* (Crocodyliformes, Baurusuchidae) from the late cretaceous of Brazil: Insights on lifestyle and phylogenetic significance. *PeerJ*, 4, e2075. <https://doi.org/10.7717/peerj.2075>
- Godoy, P. L., Ferreira, G. S., Montefeltro, F. C., Nova, B. C. V., Butler, R. J., & Langer, M. C. (2018). Evidence for heterochrony in the cranial evolution of fossil crocodyliforms. *Palaeontology*, 61(4), 543–558. <https://doi.org/10.1111/pala.12354>
- Godoy, P. L., Montefeltro, F. C., Norell, M. A., & Langer, M. C. (2014). An additional Baurusuchid from the cretaceous of Brazil with evidence of interspecific predation among

- Crocodyliformes. *PLoS One*, 9(5), e97138. <https://doi.org/10.1371/journal.pone.0097138>
- Goldberg, K., & Garcia, A. J. V. (2000). Palaeobiogeography of the Bauru group, a dinosaur-bearing cretaceous unit, northeastern Parana Basin, Brazil. *Cretaceous Research*, 21(2), 241–254. <https://doi.org/10.1006/cres.2000.0207>
- Goloboff, P. A., Farris, J. S., & Nixon, K. C. (2008). TNT, a free program for phylogenetic analysis. *Cladistics*, 24(5), 774–786. <https://doi.org/10.1111/j.1096-0031.2008.00217.x>
- Gould, S. J. (1985). *Ontogeny and phylogeny*. Harvard University Press.
- Griffin, C. T., Stocker, M. R., Colleary, C., Stefanic, C. M., Lessner, E. J., Riegler, M., Formoso, K., Koeller, K., & Nesbitt, S. J. (2021). Assessing ontogenetic maturity in extinct saurian reptiles. *Biological Reviews*, 96(2), 470–525. <https://doi.org/10.1111/brv.12666>
- Grigg, G. (2015). *Biology and evolution of Crocodylians*. CSIRO Publishing.
- Hay, O. P. (1930). *Second bibliography and catalogue of the fossil vertebrata of North America*. Carnegie Institution of Washington.
- Hendrickx, C., Mateus, O., & Araujo, R. (2015). A proposed terminology of theropod teeth (Dinosauria, Saurischia). *Journal of Vertebrate Paleontology*, 35, e982797. <https://doi.org/10.1080/02724634.2015.982797>
- Hennig, W. (1966). *Phylogenetic systematics*. University of Illinois Press.
- Holliday, C. M., Porter, W. R., Vliet, K. A., & Witmer, L. M. (2020). The Frontoparietal fossa and dorsotemporal fenestra of archosaurs and their significance for interpretations of vascular and muscular anatomy in dinosaurs. *The Anatomical Record*, 303(4), 1060–1074. <https://doi.org/10.1002/ar.24218>
- Holliday, C. M., Sellers, K. C., Lessner, E. J., Middleton, K. M., Cranor, C., Verhulst, C. D., Lautenschlager, S., Bader, K., Brown, M. A., & Colbert, M. W. (2022). New frontiers in imaging, anatomy, and mechanics of crocodylian jaw muscles. *The Anatomical Record*, 305(10), 3016–3030. <https://doi.org/10.1002/ar.25011>
- Holliday, C. M., Tsai, H. P., Skiljan, R. J., George, I. D., & Pathan, S. (2013). A 3D interactive model and atlas of the jaw musculature of *Alligator mississippiensis*. *PLoS One* Retrieved from <https://journals.plos.org/plosone/article?id=10.1371/journal.pone.0062806>, 8, e62806.
- Holliday, C. M., & Witmer, L. M. (2007). Archosaur adductor chamber evolution: Integration of musculoskeletal and topological criteria in jaw muscle homology. *Journal of Morphology*, 268(6), 457–484. <https://doi.org/10.1002/jmor.10524>
- Holtz, T. R. (2021). Theropod guild structure and the tyrannosaurid niche assimilation hypothesis: Implications for predatory dinosaur macroecology and ontogeny in later late cretaceous Asia. *Canadian Journal of Earth Sciences*, 58(9), 778–795. <https://doi.org/10.1139/cjes-2020-0174>
- Horner, J. R., & Goodwin, M. B. (2006). Major cranial changes during *triceratops* ontogeny. *Proceedings of the Royal Society B: Biological Sciences*, 273(1602), 2757–2761. <https://doi.org/10.1098/rspb.2006.3643>
- Horner, J. R., & Goodwin, M. B. (2009). Extreme cranial ontogeny in the upper cretaceous dinosaur *Pachycephalosaurus*. *PLoS One*, 4(10), e7626. <https://doi.org/10.1371/journal.pone.0007626>
- Iordansky, N. N. (1964). The jaw muscles of the crocodiles and some relating structures of the crocodylian skull. *Anatomischer Anzeiger*, 115. Retrieved from <https://pubmed.ncbi.nlm.nih.gov/14327484/>, 256–280.
- Iordansky, N. N. (2000). Jaw muscles of the crocodiles: Structure, synonymy, and some implications on homology and functions. *Russian Journal of Herpetology*, 7(1), 41–50.
- Iori, F. V., & Carvalho, I. D. S. (2009). *Morrinhosuchus luziae*, um novo Crocodylomorpha Notosuchia da Bacia Bauru, Brasil. *Revista Brasileira de Geociências*, 39(4), 717–725. <https://doi.org/10.25249/0375-7536.2009394717725>
- Kellner, A. W. A., Weinschütz, L. C., Holgado, B., Bantim, R. a. M., & Sayão, J. M. (2019). A new toothless pterosaur (Pterodactyloidea) from southern Brazil with insights into the paleoecology of a cretaceous desert. *Anais da Academia Brasileira de Ciências*, 91, e20190768. <https://doi.org/10.1590/0001-3765201920190768>
- Kley, N. J., Sertich, J. J. W., Turner, A. H., Krause, D. W., O'Connor, P. M., & Georgi, J. A. (2010). Craniofacial morphology of *Simosuchus clarki* (Crocodyliformes: Notosuchia) from the late cretaceous of Madagascar. *Journal of Vertebrate Paleontology*, 30(suppl 1), 13–98. <https://doi.org/10.1080/02724634.2010.532674>
- Klinkhamer, A. J., Wilhite, D. R., White, M. A., & Wroe, S. (2017). Digital dissection and three-dimensional interactive models of limb musculature in the Australian estuarine crocodile (*Crocodylus porosus*). *PLoS One*, 12(4), e0175079. <https://doi.org/10.1371/journal.pone.0175079>
- Klock, C., Leuzinger, L., Santucci, R. M., Martinelli, A. G., Marconato, A., da Silva, M. T., Luz, Z., & Vennemann, T. (2022). A bone to pick: Stable isotope compositions as tracers of food sources and paleoecology for notosuchians in the Brazilian upper cretaceous Bauru group. *Cretaceous Research*, 131, 105113. <https://doi.org/10.1016/j.cretres.2021.105113>
- Larson, P. (2013). The case for *Nanotyrannus*. In *Tyrannosaurid paleobiology* (pp. 15–53). Indiana University Press.
- Larsson, H. C. E., & Sues, H.-D. (2007). Cranial osteology and phylogenetic relationships of *Hamadasuchus rebouli* (Crocodyliformes: Mesoeucrocodylia) from the cretaceous of Morocco. *Zoological Journal of the Linnean Society*, 149(4), 533–567. <https://doi.org/10.1111/j.1096-3642.2007.00271.x>
- Liparini, A., & Schultz, C. L. (2013). A reconstruction of the thigh musculature of the extinct pseudosuchian *Prestosuchus chiniquensis* from the *Dinodontosaurus* assemblage zone (middle Triassic epoch), Santa Maria 1 sequence, southern Brazil. *Geological Society*, 379(1), 441–468. <https://doi.org/10.1144/SP379.20>
- Manzig, P. C., Kellner, A. W. A., Weinschütz, L. C., Fragoso, C. E., Vega, C. S., Guimarães, G. B., Godoy, L. C., Liccardo, A., Ricetti, J. H. Z., & de Moura, C. C. (2014). Discovery of a rare pterosaur bone bed in a cretaceous desert with insights on ontogeny and behavior of flying reptiles. *PLoS One*, 9(8), e100005. <https://doi.org/10.1371/journal.pone.0100005>
- da Silva, M. T., Iori, F. V., Carvalho, I. d. S., & de Vasconcellos, F. M. (2013). *Gondwanasuchus scabrosus* gen. et sp. nov., a new terrestrial predatory crocodyliform (Mesoeucrocodylia: Baurusuchidae) from the late cretaceous Bauru Basin of Brazil. *Cretaceous Research*, 44, 104–111. <https://doi.org/10.1016/j.cretres.2013.03.010>
- Martin, J. E., Pochat-Cottilloux, Y., Laurent, Y., Perrier, V., Robert, E., & Antoine, P.-O. (2022). Anatomy and phylogeny of an exceptionally large sebecid (Crocodylomorpha) from the middle Eocene of southern France. *Journal of Vertebrate*

- Paleontology*, 42(4), e2193828. <https://doi.org/10.1080/02724634.2023.2193828>
- Martinelli, A. G. (2003). Comahuesuchus brachybuccalis (Archosauria, Crocodyliformes) from the late cretaceous of Rio Negro Province (Argentina). *Ameghiniana*, 40(4), 559–572.
- Martinelli, A. G., da Silva, M. T., Iori, F. V., & Ribeiro, L. C. B. (2018). The first *Caipirasuchus* (Mesoeucrocodylia, Notosuchia) from the late cretaceous of Minas Gerais, Brazil: New insights on sphagesaurid anatomy and taxonomy. *PeerJ*, 6, e5594. <https://doi.org/10.7717/peerj.5594>
- Martinelli, A. G., & Pais, D. F. (2008). A new baurusuchid crocodyliform (Archosauria) from the late cretaceous of Patagonia (Argentina). *Comptes Rendus Palevol*, 7(6), 371–381. <https://doi.org/10.1016/j.crpv.2008.05.002>
- Martins, K. C., Queiroz, M. V., Ruiz, J. V., Langer, M. C., & Montefeltro, F. C. (2023). A new Baurusuchidae (Notosuchia, Crocodyliformes) from the Adamantina formation (Bauru group, upper cretaceous), with a revised phylogenetic analysis of Baurusuchia. *Cretaceous Research*, 153, 105680. <https://doi.org/10.1016/j.cretres.2023.105680>
- McCurry, M. R., Evans, A. R., Fitzgerald, E. M. G., McHenry, C. R., Bevitt, J., & Pyenson, N. D. (2019). The repeated evolution of dental apicobasal ridges in aquatic-feeding mammals and reptiles. *Biological Journal of the Linnean Society*, 127(2), 245–259. <https://doi.org/10.1093/biolinnean/blz025>
- Meers, M. B. (2003). Crocodylian forelimb musculature and its relevance to Archosauria. *The Anatomical Record Part A*, 274A(2), 891–916. <https://doi.org/10.1002/ar.a.10097>
- Molnar, R. E. (2010). A new reconstruction of the skull of *Sebecus icaeorhinus* (Crocodyliformes: Sebecosuchia) from the Eocene of Argentina. *Brazilian Geographical Journal*, 1(2), 314–330.
- Molnar, R. E. (2012). Jaw musculature and jaw mechanics of *Sebecus icaeorhinus* Simpson, 1937 (Mesoeucrocodylia, Sebecosuchia). *Earth and Environmental Science Transactions of the Royal Society of Edinburgh*, 103(3–4), 501–519. <https://doi.org/10.1017/S1755691013000285>
- Montefeltro, F. C., Larsson, H. C. E., de França, M. A. G., & Langer, M. C. (2013). A new neosuchian with Asian affinities from the Jurassic of northeastern Brazil. *Die Naturwissenschaften*, 100(9), 835–841. <https://doi.org/10.1007/s00114-013-1083-9>
- Montefeltro, F. C., Larsson, H. C. E., & Langer, M. C. (2011). A new Baurusuchid (Crocodyliformes, Mesoeucrocodylia) from the late cretaceous of Brazil and the phylogeny of Baurusuchidae. *PLoS One*, 6(7), e21916. <https://doi.org/10.1371/journal.pone.0021916>
- Montefeltro, F. C., Lautenschlager, S., Godoy, P. L., Ferreira, G. S., & Butler, R. J. (2020). A unique predator in a unique ecosystem: Modelling the apex predator within a late cretaceous crocodyliform-dominated fauna from Brazil. *Journal of Anatomy*, 237(2), 323–333. <https://doi.org/10.1111/joa.13192>
- Nascimento, P. M. (2014). *Revisão da família Baurusuchidae e seu posicionamento filogenético dentro do clado Mesoeucrocodylia*. Universidade de São Paulo. <https://doi.org/10.11606/T.41.2014.tde-27082014-103842>
- Nascimento, P. M., & Zaher, H. (2010). A new species of *Baurusuchus* (Crocodyliformes, Mesoeucrocodylia) from the upper cretaceous of Brazil, with the first complete postcranial skeleton described for the family Baurusuchidae. *Papéis Avulsos de Zoologia*, 50(21), 323–361. <https://doi.org/10.1590/S0031-10492010002100001>
- Nesbitt, S. J., Turner, A. H., & Weinbaum, J. C. (2012). A survey of skeletal elements in the orbit of Pseudosuchia and the origin of the crocodylian palpebral. *Earth and Environmental Science Transactions of the Royal Society of Edinburgh*, 103(3–4), 365–381. <https://doi.org/10.1017/S1755691013000224>
- Nobre, P. H., & Carvalho, I. d. S. (2013). Postcranial skeleton of *Mariliasuchus amarali* Carvalho and Bertini, 1999 (Mesoeucrocodylia) from the Bauru Basin, upper Cretaceous of Brazil. *Ameghiniana*, 50(1), 98–113. <https://doi.org/10.5710/amgh.15.8.2012.500>
- O'Connor, P. M., Sertich, J. J. W., Stevens, N. J., Roberts, E. M., Gottfried, M. D., Hieronymus, T. L., Jinnah, Z. A., Ridgely, R., Ngasala, S. E., & Temba, J. (2010). The evolution of mammal-like crocodyliforms in the cretaceous period of Gondwana. *Nature*, 466(7307), 748–751. <https://doi.org/10.1038/nature09061>
- Oliveira, C. E. M., Santucci, R. M., Andrade, M. B., Fulfaro, V. J., Basílio, J. a. F., & Benton, M. J. (2011). Crocodylomorph eggs and eggshells from the Adamantina formation (Bauru group), Upper Cretaceous of Brazil. *Palaentology*, 54(2), 309–321. <https://doi.org/10.1111/j.1475-4983.2010.01028.x>
- Ortega, F., Gasparini, Z., Buscalioni, A. D., & Calvo, J. O. (2000). A new species of *Araripesuchus* (Crocodylomorpha, Mesoeucrocodylia) from the lower cretaceous of Patagonia (Argentina). *Journal of Vertebrate Paleontology*, 20(1), 57–76. [https://doi.org/10.1671/0272-4634\(2000\)020\[0057:ANSOAC\]2.0.CO;2](https://doi.org/10.1671/0272-4634(2000)020[0057:ANSOAC]2.0.CO;2)
- Otero, A., Cuff, A. R., Allen, V., Sumner-Rooney, L., Pol, D., & Hutchinson, J. R. (2019). Ontogenetic changes in the body plan of the sauropodomorph dinosaur *Mussaurus patagonicus* reveal shifts of locomotor stance during growth. *Scientific Reports*, 9(1), 7614. <https://doi.org/10.1038/s41598-019-44037-1>
- Paolillo, A., & Linares, O. J. (2007). Nuevos cocodrilos sebecosuchia del cenozoico suramericano (Mesosuchia: Crocodylia). *Paleobiologia Neotropical*, 3, 1–25.
- Pinheiro, A. E. P., Souza, L. G. D., Bandeira, K. L. N., Brum, A. S., Pereira, P. V. L. G. C., Castro, L. O. R. D., Ramos, R. R. C., & Simbras, F. M. (2021). The first notosuchian crocodyliform from the Araçatuba formation (Bauru group, Paraná Basin), and diversification of sphagesaurians. *Anais da Academia Brasileira de Ciências*, 93, e20201591. <https://doi.org/10.1590/0001-3765202120201591>
- Pol, D. (2005). Postcranial remains of *Notosuchus terrestris* Woodward (Archosauria: Crocodyliformes) from the upper cretaceous of Patagonia, Argentina. *Ameghiniana*, 42(1), 21–38.
- Pol, D., Lardi, J. M., Lecuona, A., & Krause, M. (2012). Postcranial anatomy of *Sebecus icaeorhinus* (Crocodyliformes, Sebecidae) from the Eocene of Patagonia. *Journal of Vertebrate Paleontology*, 32(2), 328–354. <https://doi.org/10.1080/02724634.2012.646833>
- Pol, D., Nascimento, P. M., Carvalho, A. B., Riccomini, C., Pires-Domingues, R. A., & Zaher, H. (2014). A new Notosuchian from the late cretaceous of Brazil and the phylogeny of advanced Notosuchians. *PLoS One*, 9(4), e93105. <https://doi.org/10.1371/journal.pone.0093105>
- Powell, J., Babot, J., García-López, D., Deraco, V., & Herrera, C. (2011). Eocene vertebrates of northwestern Argentina: Annotated list. In *Cenozoic Geology of the Central Andes of Argentina*. SCS Publisher.
- Price, (1945). A new reptile from the Cretaceous of Brazil. Rio de Janeiro, Departamento Nacional da Produção Mineral, Notas preliminares e estudos. *Boletim*, 25, 8.

- Rabi, M., & Sebök, N. (2015). A revised Eurogondwana model: Late cretaceous notosuchian crocodyliforms and other vertebrate taxa suggest the retention of episodic faunal links between Europe and Gondwana during most of the cretaceous. *Gondwana Research*, 28(3), 1197–1211. <https://doi.org/10.1016/j.gr.2014.09.015>
- Rayfield, E. J. (2004). Cranial mechanics and feeding in *Tyrannosaurus rex*. *Proceedings of the Royal Society of London Series B: Biological Sciences*, 271(1547), 1451–1459.
- Rieppel, O. (2003). Semaphoronts, cladograms and the roots of total evidence. *Biological Journal of the Linnean Society*, 80(1), 167–186. <https://doi.org/10.1046/j.1095-8312.2003.00228.x>
- Riff, D. (2003). Descrição morfológica do crânio e mandíbula de *Striatosuchus maxhechti* (Crocodylomorpha, Cretáceo Superior do Brasil) e seu posicionamento filogenético. Masters dissertation. Retrieved from <http://pantheon.ufrj.br/handle/11422/3437>
- Riff, D., & Kellner, A. W. A. (2011). Baurusuchid crocodyliforms as theropod mimics: Clues from the skull and appendicular morphology of *Striatosuchus maxhechti* (upper cretaceous of Brazil). *Zoological Journal of the Linnean Society*, 163(Suppl 1), S37–S56. <https://doi.org/10.1111/j.1096-3642.2011.00713.x>
- Ristevski, J. (2019). Crocodylia morphology. In J. Vonk & T. Shackelford (Eds.), *Encyclopedia of animal cognition and behavior* (pp. 1–22). Springer International Publishing. https://doi.org/10.1007/978-3-319-47829-6_955-2
- Romer, A. S. (1923). Crocodylian pelvic muscles and their avian and reptilian homologues. *Bulletin of the AMNH*, 48, 15 Retrieved from <https://digitallibrary.amnh.org/handle/2246/1307>
- Romer, A. S. (1956). *Osteology of the Reptiles*. University of Chicago Press.
- Ruiz, J. V., Bronzati, M., Ferreira, G. S., Martins, K. C., Queiroz, M. V., Langer, M. C., & Montefeltro, F. C. (2021). A new species of *Caipirasuchus* (Notosuchia, Sphagesauridae) from the late cretaceous of Brazil and the evolutionary history of Sphagesauria. *Journal of Systematic Palaeontology*, 19(4), 265–287. <https://doi.org/10.1080/14772019.2021.1888815>
- Salas-Gismondi, R., Flynn, J. J., Baby, P., Tejada-Lara, J. V., Wesselingh, F. P., & Antoine, P.-O. (2015). A Miocene hyperdiverse crocodylian community reveals peculiar trophic dynamics in proto-Amazonian mega-wetlands. *Proceedings of the Royal Society B: Biological Sciences*, 282(1804), 20142490. <https://doi.org/10.1098/rspb.2014.2490>
- Scannella, J. B., & Horner, J. R. (2010). *Torosaurus* marsh, 1891, is *triceratops* marsh, 1889 (Ceratopsidae: Chasmosaurinae): Synonymy through ontogeny. *Journal of Vertebrate Paleontology*, 30(4), 1157–1168. <https://doi.org/10.1080/02724634.2010.483632>
- Schubert, B. W., & Ungar, P. S. (2005). Wear facets and enamel spalling in tyrannosaurid dinosaurs. *Acta Palaeontologica Polonica*, 50(1), 93–99.
- Schumacher, G. H. (1973). The head muscles and hyolaryngeal skeleton of turtles and crocodylians. In *Biology of the reptilia. Volume 4 morphology D* (pp. 101–199). Academic Press.
- Sellers, K. C., Middleton, K. M., Davis, J. L., & Holliday, C. M. (2017). Ontogeny of bite force in a validated biomechanical model of the American alligator. *Journal of Experimental Biology*, 220(11), 2036–2046. <https://doi.org/10.1242/jeb.156281>
- Sellers, K. C., Nieto, M. N., Degrange, F. J., Pol, D., Clark, J. M., Middleton, K. M., & Holliday, C. M. (2022). The effects of skull flattening on suchian jaw muscle evolution. *The Anatomical Record*, 305(10), 2791–2822. <https://doi.org/10.1002/ar.24912>
- Sellés, A. G., Blanco, A., Vila, B., Marmi, J., López-Soriano, F. J., Llácer, S., Frigola, J., Canals, M., & Galobart, À. (2020). A small cretaceous crocodyliform in a dinosaur nesting ground and the origin of sebecids. *Scientific Reports*, 10(1), 15293. <https://doi.org/10.1038/s41598-020-71975-y>
- Sertich, J. J. W., & Groenke, J. R. (2010). Appendicular skeleton of *Simosuchus clarki* (Crocodyliformes: Notosuchia) from the late cretaceous of Madagascar. *Journal of Vertebrate Paleontology*, 30(suppl 1), 122–153. <https://doi.org/10.1080/02724634.2010.516902>
- Sharma, P. P., Clouse, R. M., & Wheeler, W. C. (2017). Hennig's semaphoront concept and the use of ontogenetic stages in phylogenetic reconstruction. *Cladistics*, 33(1), 93–108. <https://doi.org/10.1111/cla.12156>
- Soares, P. C., Landim, P. M. B., Fúlfaro, V. J., & Neto, A. F. S. (1980). Ensaio de caracterização estratigráfica do Cretáceo no Estado de São Paulo: Grupo Bauru. *Revista Brasileira de Geociências*, 10(3), 177–185.
- Staniewicz, A., Behler, N., Darmansyah, S., & Jones, G. (2018). Niche partitioning between juvenile sympatric crocodylians in Mesangat Lake, East Kalimantan, Indonesia. *The Raffles Bulletin of Zoology*, 66, 528–537.
- Tavares, S. A. S., Branco, F. R., Carvalho, I. d. S., & Maldanis, L. (2017). The morphofunctional design of Montealtosuchus arrudacamposi (Crocodyliformes, Upper Cretaceous) of the Bauru Basin, Brazil. *Cretaceous Research*, 79, 64–76. <https://doi.org/10.1016/j.cretres.2017.07.003>
- Therrien, F., Zelenitsky, D. K., Voris, J. T., & Tanaka, K. (2021). Mandibular force profiles and tooth morphology in growth series of *Albertosaurus sarcophagus* and *Gorgosaurus libratus* (Tyrannosauridae: Albertosaurinae) provide evidence for an ontogenetic dietary shift in tyrannosaurids. *Canadian Journal of Earth Sciences*, 58(9), 812–828. <https://doi.org/10.1139/cjes-2020-0177>
- Tsai, H. P., & Holliday, C. M. (2011). Ontogeny of the alligator Cartilago Transiliens and its significance for Sauropsid jaw muscle evolution. *PLoS One*, 6(9), e24935. <https://doi.org/10.1371/journal.pone.0024935>
- Tsuihiji, T. (2005). Homologies of the transversospinalis muscles in the anterior presacral region of Sauria (crown Diapsida). *Journal of Morphology*, 263(2), 151–178. <https://doi.org/10.1002/jmor.10294>
- Tsuihiji, T. (2007). Homologies of the longissimus, iliocostalis, and hypaxial muscles in the anterior presacral region of extant diapsida. *Journal of Morphology*, 268(11), 986–1020. <https://doi.org/10.1002/jmor.10565>
- Tsuihiji, T., Watabe, M., Tsogtbaatar, K., Tsubamoto, T., Barsbold, R., Suzuki, S., Lee, A. H., Ridgely, R. C., Kawahara, Y., & Witmer, L. M. (2011). Cranial osteology of a juvenile specimen of *Tarbosaurus bataar* (Theropoda, Tyrannosauridae) from the Nemegt formation (upper cretaceous) of Bugin Tsav, Mongolia. *Journal of Vertebrate Paleontology*, 31(3), 497–517. <https://doi.org/10.1080/02724634.2011.557116>
- Tucker, A. D., Limpus, C. J., McCallum, H. I., & McDonald, K. R. (1996). Ontogenetic dietary partitioning by *Crocodylus johnstoni* during the dry season. *Copeia*, 1996(4), 978–988. <https://doi.org/10.2307/1447661>
- Turner, A. H. (2006). Osteology and phylogeny of a new species of *Araripesuchus* (Crocodyliformes: Mesoeucrocodylia) from the

- late cretaceous of Madagascar. *Historical Biology*, 18(3), 255–369. <https://doi.org/10.1080/08912960500516112>
- van Drongelen, W., & Dullemeijer, P. (1982). The feeding apparatus of *Caiman crocodilus*: A functional-morphological study. *Anatomischer Anzeiger*, 151, 337–366.
- Vasconcellos, F. M., & Carvalho, I. S. (2010). Paleoichnological assemblage associated with *Baurusuchus salgadoensis* remains, a Baurusuchidae Mesoeucrocodylia from the Bauru Basin, Brazil (late cretaceous). *Bulletin of the New Mexico Museum of Natural History and Science*, 51, 227–237.
- Vieira, L. G., Lima, F. C., Mendonça, S. H. S. T., Menezes, L. T., Hirano, L. Q. L., & Santos, A. L. Q. (2018). Ontogeny of the postcranial axial skeleton of *Melanosuchus niger* (Crocodylia, Alligatoridae). *The Anatomical Record*, 301(4), 607–623. <https://doi.org/10.1002/ar.23722>
- Vieira, L. G., Santos, A. L. Q., Lima, F. C., Mendonça, S. H. S. T., Menezes, L. T., & Sebben, A. (2016). Osteologia de *Melanosuchus Niger* (Crocodylia: Alligatoridae) e a evidência evolutiva. *Pesquisa Veterinária Brasileira*, 36, 1025–1044. <https://doi.org/10.1590/S0100-736X2016001000018>
- Vieira, L. G., Santos, A. L. Q., Hirano, L. Q. L., Menezes-Reis, L. T., Mendonça, J. S., & Sebben, A. (2019). Ontogeny of the skull of the black Caiman (*Melanosuchus niger*) (Crocodylia: Alligatoridae). *Canadian Journal of Zoology*, 97(2), 142–155. <https://doi.org/10.1139/cjz-2018-0076>
- Voris, J. T., Zelenitsky, D. K., Therrien, F., Ridgely, R. C., Currie, P. J., & Witmer, L. M. (2021). Two exceptionally preserved juvenile specimens of *Gorgosaurus libratus* (Tyrannosauridae, Albertosaurinae) provide new insight into the timing of ontogenetic changes in tyrannosaurids. *Journal of Vertebrate Paleontology*, 41(6), e2041651. <https://doi.org/10.1080/02724634.2021.2041651>
- Watanabe, A., & Slice, D. E. (2014). The utility of cranial ontogeny for phylogenetic inference: A case study in crocodylians using geometric morphometrics. *Journal of Evolutionary Biology*, 27(6), 1078–1092. <https://doi.org/10.1111/jeb.12382>
- Whetstone, K. N., & Whybrow, P. J. (1983). A cursorial crocodylian from the Triassic of Lesotho (Basutoland) southern Africa. *Occasional Papers of the Museum of Natural History, the University of Kansas*, 106, 1–37.
- Wilson, J. A., Malkani, M. S., & Gingerich, P. D. (2001). New crocodyliform (Reptilia, Mesoeucrocodylia) from the upper cretaceous Pab formation of Vitakri, Balochistan (Pakistan). *Contributions from the Museum of Paleontology*, 30(12), 321–336.
- Witmer, L. M. (1997). The evolution of the Antorbital cavity of archosaurs: A study in soft-tissue reconstruction in the fossil record with an analysis of the function of Pneumaticity. *Journal of Vertebrate Paleontology*, 17(suppl 1), 1–76. <https://doi.org/10.1080/02724634.1997.10011027>
- Witmer, L. M., & Ridgely, R. C. (2008). The paranasal air sinuses of predatory and armored dinosaurs (Archosauria: Theropoda and Ankylosauria) and their contribution to cephalic structure. *The Anatomical Record*, 291(11), 1362–1388. <https://doi.org/10.1002/ar.20794>
- Woodruff, D. C., Carr, T. D., Storrs, G. W., Waskow, K., Scannella, J. B., Nordén, K. K., & Wilson, J. P. (2018). The smallest diplodocid skull reveals cranial ontogeny and growth-related dietary changes in the largest dinosaurs. *Scientific Reports*, 8(1), 1–12.
- Woodward, A. S. (1896). On two mesozoic crocodylians, *Notosuchus* (genus novum) and *Cynodontosuchus* (gen. Nov.) from the red sandstones of territory of Neuquén (Argentina). *Anales del Museo de La Plata, Série Paleontología*, 4, 1–20.
- Woodward, H. N., Tremaine, K., Williams, S. A., Zanno, L. E., Horner, J. R., & Myhrvold, N. (2020). Growing up *Tyrannosaurus rex*: Osteohistology refutes the pygmy “*Nanotyrannus*” and supports ontogenetic niche partitioning in juvenile *tyrannosaurus*. *Science Advances*, 6(1), eaax6250. <https://doi.org/10.1126/sciadv.aax6250>

SUPPORTING INFORMATION

Additional supporting information can be found online in the Supporting Information section at the end of this article.

How to cite this article: dos Santos, D. M., de Carvalho, J. C., de Oliveira, C. E. M., de Andrade, M. B., & Santucci, R. M. (2024). Cranial and postcranial anatomy of a juvenile baurusuchid (*Notosuchia*, *Crocodylomorpha*) and the taxonomical implications of ontogeny. *The Anatomical Record*, 1–46. <https://doi.org/10.1002/ar.25419>